



NTNU – Trondheim
Norwegian University of
Science and Technology

Behaviour and Modelling of Bolted Connectors in Road Safety Barriers

Bendik Male Kolberg

Eirik Tvester Willand

Civil and Environmental Engineering

Submission date: June 2014

Supervisor: Magnus Langseth, KT

Co-supervisor: David Morin, KT
Hieu Nguyen Hoang, Sintef

Norwegian University of Science and Technology
Department of Structural Engineering



MASTEROPPGAVE 2014

FAGOMRÅDE: Stålkonstruksjoner	DATO: 10.06.2014	ANTALL SIDER: 118 + (25)
----------------------------------	---------------------	-----------------------------

TITTEL:

Oppførsel og modellering av bolteforbindelser i veirekkverk

Behaviour and modelling of bolted connectors in road safety barriers

UTFØRT AV:

Bendik M. Kolberg

Eirik T. Willand



SAMMENDRAG:

Formålet med denne masteroppgaven er å studere oppførselen til boltkoblingen mellom skinne og stolpe i et vegrekkverk i stål når utsatt for last i kombinasjoner av strekk og skjær. Modeller av laboratorietester utført på vegrekkverket ble laget ved bruk av elementmetoden.

Alle laboratorietestene gikk i brudd ved utrivning av gjengene på bolten i koblingen. Maksimum lastkapasiteten til koblingen sank med henholdsvis 15.9 og 17.3 prosent når lastet i 15° og 30° fra lastkonfigurasjonen i ren strekk. En tostegs elementmodell ble laget for å simulere resultatene fra laboratoriet. Relative forskyvninger av en ujenget bolt og mutter fra en initiell modell ble påført en separat elementmodell av kun bolten og mutteren med gjenger. En full model av vegrekkverket fra laboratorietestene med gjenget bolt og mutter ble lagd og sammenlignet med tostegsmodellen.

Resultat fra elementmodellene viser at deformasjon i forkant av brudd er styrt av deformasjon i skinnen, stolpen og skivene i vegrekkverkskoblingen. Brudd er kontrollert av den gjengede bolten, og bruddlasten er sterkt påvirket av materialet. Det er mulig å modellere koblingen i vegrekkverket utsatt for kombinasjoner av skjær- og strekklast med akseptabel nøyaktighet. Utrivning av gjengene i bolten kan konsekvent bli oppnådd i elementmodellene. Maksimum lastkapasitet i koblingen oppnådd ved tostegs modellen var nære maksimum lastkapasitet oppnådd i laboratoriet for enkelte av lastkombinasjonene. Den fulle modellen oppnådde nære resultater til laboratorietestene, hvor avviket fra gjennomsnittlig maksimum lastkapasitet i rent strekk var på mellom 1.1 til 2.7 prosent.

FAGLÆRER: Professor Magnus Langseth

VEILEDER(E): Postdoktor David Morin, Sintef forsker Hoang Nguyen-Hieu

UTFØRT VED: Institutt for konstruksjonsteknikk, NTNU, Trondheim

Institutt for konstruksjonsteknikk

FAKULTET FOR INGENIØRVITENSKAP OG TEKNOLOGI
NTNU – Norges teknisk-naturvitenskapelige universitet

MASTER'S THESIS 2014

for

Bendik Male Kolberg and Eirik Tveter Willand

Behaviour and modelling of bolted connectors in road safety barriers

Oppførsel og modellering av bolteforbindelser i veirekkverk

Road side safety barriers are one of the most efficient measures to reduce the risk of run-off-road traffic accidents. A safety barrier is made of w-beam rails fixed to sigma posts by bolts and hex-nuts. In a situation where an errant vehicle hits the safety barrier, the bolts are designed to fail and thereby initiate a release of the w-beam from the sigma posts. Such a release will have a significant effect on the performance of the guardrail system. Thus, a good knowledge on how bolted connections behave during vehicle impact is necessary to optimize the design of the safety barriers.

Research activities have been carried out at SIMLab-Centre for research based innovation at NTNU during the last years on the behaviour and modelling threaded steel fasteners. Special focus has been on their behaviour when subjected to tensile, shear and combined loading conditions at elevated rates of strain. However, in the case of a vehicle impact on a safety barrier, the deformation of the bolts is combined with local deformations of the posts and the w-beam. Thus, the aim of the present master's thesis is to use a special purpose test rig to study the behaviour of a sigma post fixed to a w-beam under multi-axial (combination of tension and shear) loading conditions. The component tests will be used to validate a finite element model for parametric studies. The tests carried out and the advanced numerical simulations shall establish a basis for an engineering model of bolted connections for large scale numerical simulations of road safety barriers.

The report shall be written according to the requirements given by the Department of Structural Engineering.

Supervisors: Magnus Langseth and David Morin, NTNU
Hieu Nguyen Hoang, SINTEF Materials and Chemistry

The master's thesis must be submitted to the Department of Structural Engineering, NTNU, no later than June 10th 2014.

NTNU, 22 January 2014

Magnus Langseth
Professor

Abstract

The purpose of this thesis is to study the behaviour of the connection between the guardrail and post in a steel road safety barrier subject to tensile, shear and combined loading conditions. This is accomplished by performing laboratory tests on a special-built test rig. Finite element models of the connection are created and validated in order to form a basis for large scale numerical simulations of road safety barriers.

The laboratory tests all failed by thread stripping of the bolt in the connection. The ultimate failure load decreased by 15.9 and 17.3 percent when loading in 15° and 30° from pure tension, respectively. A two-step finite element model was created to simulate the behaviour of the threaded bolt and nut assembly in question. The relative displacement between the bolt and the nut in an initial model of the guard rail and post with an unthreaded connection was enforced on a separate model of the bolt and nut with threads. A full model including the threaded connection was created and compared to the two-step model.

The results indicate that the behaviour prior to failure is controlled by deformations in the guardrail, post and washers. Failure is controlled by the threaded bolt, and the ultimate load is highly dependent on the bolt material. It is possible to model the bolted connection, subject to combined tension and shear loading conditions, with an acceptable degree of accuracy. A consistent failure mode can be achieved with both the two-step model and the full model. The ultimate loads experienced in the two-step model were in close proximity to the experimental results in some load combinations. The full model was close to the laboratory results in most load combinations, where the deviation from the average failure load in pure tension was 1.1 - 2.7 percent.

Sammendrag

Formålet med denne masteroppgaven er å studere oppførselen til boltkoblingen mellom skinne og stolpe i et vegrekkverk i stål når utsatt for last i kombinasjoner av strekk og skjær. Modeller av laboratorietester utført på vegrekkverket ble laget ved bruk av elementmetoden.

Alle laboratorietestene gikk i brudd ved utrivning av gjengene på bolten i koblingen. Maksimum lastkapasiteten til koblingen sank med henholdsvis 15.9 og 17.3 prosent når lastet i 15° og 30° fra lastkonfigurasjonen i ren strekk. En tostegs elementmodell ble laget for å simulere resultatene fra laboratoriet. Relative forskyvninger av en ugjenget bolt og mutter fra en initiell modell ble påført en separat elementmodell av kun bolten og mutteren med gjenger. En full model av vegrekkverket fra laboratorietestene med gjenget bolt og mutter ble lagd og sammenlignet med tostegsmodellen.

Resultat fra elementmodellene viser at deformasjon i forkant av brudd er styrt av deformasjon i skinnen, stolpen og skivene i vegrekkverkskoblingen. Brudd er kontrollert av den gjengede bolten, og bruddlasten er sterkt påvirket av materialet. Det er mulig å modellere koblingen i vegrekkverket utsatt for kombinasjoner av skjær- og strekklast med akseptabel nøyaktighet. Utrivning av gjengene i bolten kan konsekvent bli oppnådd i elementmodellene. Maksimum lastkapasitet i koblingen oppnådd ved tostegs modellen var nære maksimum lastkapasitet oppnådd i laboratoriet for enkelte av lastkombinasjonene. Den fulle modellen oppnådde nære resultater til laboratorietestene, hvor avviket fra gjennomsnittlig maksimum lastkapasitet i rent strekk var på mellom 1.1 til 2.7 prosent.

Preface

The work presented in this master's thesis was performed at the Norwegian University of Science and Technology (NTNU) for the Department of Structural Engineering. The thesis is a result of 20 weeks work during the spring of 2014.

The objective of the thesis was first to investigate the behaviour of a bolted connection in a road safety barrier section subject to various loading conditions. Second, finite element models of the tests were created. The analysis performed were compared to the experimental data to validate the finite element models.

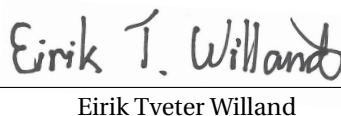
We would like to extend our appreciation to and thank our supervisors Professor Magnus Langseth and Postdoc David Morin for discussions and guidance during the work with this master's thesis. Their assistance has been crucial for the completion of this project - and their response has been quick and helpful, which has been highly appreciated.

A special thank is directed to PhD Henning Fransplass of the Norwegian Public Roads Administration for his continued support and guidance during this thesis.

We would also like to thank Senior Engineer Tore Wisth for his invaluable help performing the laboratory tests, and Egil Fagerholt for setting up and conducting the DIC analysis.

Trondheim, 10.06.2014


Bendik Male Kolberg


Eirik Tveter Willand

Contents

1	Introduction	1
1.1	Road safety	1
1.1.1	Traffic accidents	1
1.1.2	The effect of road safety barriers on road safety	3
1.2	Road Safety Barriers	5
1.2.1	Steel rail road safety barriers	6
2	Literature Review	9
2.1	"Black bolts under combined tension and shear"	9
2.2	"Failure mechanisms of mild steel bolts under different tensile loading rates"	10
2.3	"Computational analysis of a deformable safety barrier"	12
2.3.1	Bolt tests	12
2.3.2	W-beam and Σ -post tests	15
2.3.3	Numerical modelling and analyses	17
2.4	"Tensile behaviour of threaded steel fasteners at elevated levels of strain"	20
2.5	"Development of an Arcan test setup for characterization of road restraint systems"	21
2.5.1	Material tests and models	21
2.5.2	Finite element modelling and parameter study	24
3	W-Beam, Σ-Post & M10 Bolts	29
3.1	W-beam & Σ -post	29
3.2	M10 bolts	30
4	Theory	33
4.1	Analysis and Designs of Threaded Assemblies	33

4.1.1	Factors that influence the strength of screw threads	34
4.2	Digital Image Correlation	36
5	Laboratory Work	39
5.1	Design of the laboratory tests	39
5.1.1	Geometry of the road safety barrier	39
5.1.2	The cradle	40
5.1.3	Design of the loading clamp	41
5.2	Changes to the test rig	43
5.3	Setting up the DIC	44
5.4	Implementation of the tests in the laboratory	44
5.5	Results of the laboratory tests	46
5.5.1	0° configuration	46
5.5.2	15° configuration	48
5.5.3	30° configuration	49
5.6	Laboratory test observations	50
5.7	Sources of errors and variations in the test results	52
5.8	Hardness test on the bolt	53
6	Material Models	55
6.1	W-beam and Σ -post	55
6.2	Bolts	58
6.2.1	Finite element model of the bolt tensile test	58
6.2.2	Fracture criterion	61
7	Finite Element Models	63
7.1	The initial model	64
7.1.1	Mesh	65
7.1.2	Boundary conditions and constraints	69
7.1.3	Interactions	69
7.1.4	Element types	70
7.2	Computational efficiency	70
7.3	Sensitivity of the friction coefficient	72
7.4	Validity of the material model of the W-beam and Σ -post	76
7.5	Bolt size	79
7.6	Mesh size	80

7.7	The bolt thread stripping model	83
7.7.1	Mesh	83
7.7.2	Boundary conditions and constraints	85
7.7.3	Interactions	86
7.8	The full model	87
8	Results	89
8.1	Analytical failure load	89
8.2	Results of the initial model	90
8.3	Results of the finite element threads stripping model	93
8.4	Results of the full finite element model	100
9	Discussion	105
9.1	Laboratory results	105
9.2	Accuracy of the finite element models	107
9.2.1	The initial model	107
9.2.2	The thread stripping model	107
9.2.3	The full road safety barrier model	110
9.3	Validity of the laboratory test versus the real road safety barrier	112
10	Conclusion	113
10.1	Concluding remarks	113
10.2	Suggestions for further work	114
	Bibliography	116
A	Geometry	119
A.1	Geometry of the W-beam	119
A.2	Geometry of the Σ -post	120
A.3	Geometry of the washers	121
A.4	Geometry of the loading clamp	122
A.5	Geometry of the cradle	123
A.6	Geometry of the M10 bolt and nut	125
B	Laboratory Tests Assembly	127
C	Geometrical Measurements	129

D	Calculations of the Bolt Stripping Load	135
E	Design Calculations on the Loading Clamp According to EC3	137

List of Tables

1.1	The effect of road safety barrier as medians on multi-lane roads	3
1.2	The effect of roadside road safety barriers	4
1.3	Definition of the N2 containment class	7
2.1	Elastic behaviour at different degrees of freedom	19
2.2	Formula for maximum load and mode of failure of threaded assemblies .	21
3.1	Comparison of material properties	29
3.2	Force capacity of the M10 bolt	31
5.1	Capacity calculations of the pin	42
5.2	Capacity calculations of the vertical plate	42
5.3	Capacity of the M12 bolts	43
5.4	Results from laboratory tests in 0° configuration	46
5.5	Results from laboratory tests in 15° configuration	48
5.6	Results from laboratory tests in the 30° configuration	49
6.1	Material parameters for the W-beam and Σ -post	56
6.2	Material parameters of the bolt	60
7.1	Approximate element sizes for the mesh in the initial model	65
7.2	Approximate element sizes in the mesh sensitivity study	81
8.1	Bolt failure load	89
8.2	Peak forces from the finite element bolt thread stripping models	98
8.3	Termination loads for the full model	100

9.1 Average ultimate thread stripping load 105

9.2 Deviation in the ultimate failure loads by failure mode 106

9.3 Ultimate load in the laboratory tests and bolt FE model 107

9.4 Ultimate load in the 0° configuration of the full finite element model 110

A.1 Bolt geometric parameters 125

A.2 Nut geometric parameters 125

A.3 Thread geometric parameters 126

C.1 Geometric data of the W-beam 131

C.2 Geometric data of the Σ -post 132

C.3 Thickness of the washers 133

C.4 Diameter of the bolts 133

D.1 Symbols 136

D.2 Parameters used for calculating bolt stripping load 136

List of Figures

1.1	Road deaths per 100 000 population	2
1.2	Road traffic accidents in Norway	2
1.3	Different types of road safety barriers	6
1.4	Illustrations of the road safety barrier	7
1.5	Parts in the road safety barrier connection	8
2.1	Test rig for combined tension-shear loading	10
2.2	Tension-shear interaction	10
2.3	Failure mechanism of the bolt threads	11
2.4	Bolt testing force-displacement at 1mm/min	13
2.5	Maximum, average and minimum failure load based on load rate	14
2.6	Nominal geometry of a material test sample	15
2.7	W-beam and Σ -post material tests	16
2.8	Material test extraction zones	17
2.9	Model of the road safety barrier	18
2.10	Geometry of the threaded rod with purpose-made fixtures	20
2.11	Location of material test samples in the W-beam and Σ -post	22
2.12	Engineering stress-strain relationships	22
2.13	Force-displacement curves for the bolt specimen	23
2.14	Force-displacement curves of in-plane single shear tests	24
2.15	Finite element model of the road safety barrier by D'Angelo	25
2.16	Force-displacement relationships from the numerical model	26
2.17	Loading clamp as designed by D'Angelo	27
4.1	Failure load versus threads in the grip	35
4.2	Nut dilation factor and bolt stripping factor	35

4.3	Coordinates systems in a DIC camera model	36
5.1	Laboratory test setup	40
5.2	Loading clamp for the laboratory tests	41
5.3	Slots in the loading clamp	43
5.4	DIC setup used in laboratory tests	44
5.5	Connection used to apply the loading	45
5.6	Configuration of the tests at different angles	45
5.7	The two points where the DIC data was extracted	46
5.8	Force-displacement curves for tests in the 0° configuration	47
5.9	Force-displacement curves for tests in the 15° configuration	48
5.10	Force-displacement curves for tests in the 30° configuration	49
5.11	Deformed bolt and 30×30×3 mm washer in the 30° configuration	50
5.12	Deformation of W-beam in 30° configuration	50
5.13	Deformation of the washers	51
5.14	Deformed Σ -post from test two in the 0° configuration	51
5.15	Bolt cut in half in preparation for the hardness test	53
5.16	Result from the hardness test on the bolt	53
6.1	Strains up to necking for W-beam and Σ -post	56
6.2	Material model of the W-beam	57
6.3	Material model of the Σ -post	57
6.4	FE model of the bolt material test	58
6.5	Geometry of the bolt material test specimen	59
6.6	Evolution of the bolt material data model	59
6.7	Material model of the bolt	60
6.8	Cockcroft-Latham parameter vs material test data	61
6.9	Comparison between the tensile test simulation and the material test on the bolt	62
7.1	The initial finite element model	64
7.2	Mesh of the bolts	66
7.3	Mesh of the W-beam and the W-beam patch	66
7.4	Mesh of the Σ -post and the Σ -post patch	66
7.5	Mesh of the washers used between the W-beam and Σ -post	67
7.6	Mesh of the y-joint and pin	67

7.7	Mesh of the longitudinal washers of the W-beam and Σ -post	68
7.8	Mesh of the loading clamp	68
7.9	Typical amplitude of a smooth step definition	69
7.10	Kinetic versus internal energy for the deformed parts	71
7.11	Various friction coefficients for the whole model in the 0° configuration . .	72
7.12	Various friction coefficients for the whole model in the 30° configuration .	73
7.13	Various friction coefficients for washer contact in the 0° configuration . .	74
7.14	Various friction coefficients for washer contact in the 30° configuration . .	74
7.15	Comparison of the response between various friction coefficients on the pin in the 30° configuration	75
7.16	Plastic strains in the Σ -post in 0° near the first thread strip	76
7.17	Plastic strains in the W-beam in 0° near the first thread strip	77
7.18	Plastic strains in the Σ -post in 30° near the first thread strip	78
7.19	Plastic strains in the W-beam in 30° near the first thread strip	78
7.20	Bolt size sensitivity in the 0° configuration	79
7.21	Difference in relative displacement of the bolt and nut between 9 mm and 10 mm bolt size	80
7.22	Mesh size sensitivity in the 0° configuration	81
7.23	Mesh size sensitivity in the 30° configuration	82
7.24	The bolt stripping finite element model	83
7.25	Bolt parts with mesh	84
7.26	Nut parts with mesh	85
7.27	Displacement extraction nodes	86
7.28	The full model	87
8.1	Nodes where displacements were extracted in the finite element model and DIC analysis	90
8.2	Force-displacement comparison of the test results and the initial finite element model in the 0° configuration	91
8.3	Force-displacement comparison of the test results and the initial finite element model in the 15° configuration	91
8.4	Force-displacement comparison of the test results and the initial finite element model in the 30° configuration	92
8.5	Force-displacement of the thread stripping model in the 0° configuration .	94
8.6	Evolution of the bolt threads in the 0° configuration	95

8.7	Force-displacement of the thread stripping model in the 15° configuration	96
8.8	Evolution of the bolt threads in the 15° configuration	97
8.9	Force-displacement of the thread stripping model in the 30° configuration	98
8.10	Evolution of the bolt threads in the 30° configuration	99
8.11	Full model force-displacement curves in the 0° configuration	100
8.12	Full model force-displacement curves in the 15° configuration	101
8.13	Thread stripping in 15° configuration	102
8.14	Full model force-displacement curves in 30° configuration	102
8.15	Thread stripping in 30° configuration	103
9.1	Force-displacement relationship of the bolt stripping model with the modified material	109
9.2	Comparison of the threads in the full model	111
A.1	Cross-section view of the W-beam with dimensions	119
A.2	Top view of the W-beam with dimensions	119
A.3	Cross-section view of the Σ -post with dimension	120
A.4	Underside view of the Σ -post with dimension	120
A.5	Cross-section view of the longitudinal washers of the W-beam with dimensions	121
A.6	Top view of the the longitudinal washer of the W-beam with dimensions	121
A.7	Top view of the longitudinal washer of the Σ -post with dimensions	121
A.8	Top view of the loading clamp with dimensions	122
A.9	Side view of the loading clamp with dimensions	122
A.10	Front view of the cradle with dimensions	123
A.11	Side view of the cradle with dimension	124
A.12	Nominal Geometry of the DIN 601 M10 bolt	125
A.13	Geometry of the M10 nut	125
A.14	Geometry of the threads	126
B.1	Model of the test assembly	127
B.2	Exploded model of the test assembly	128
C.1	Thickness measurement points of the W-beam	129
C.2	Thickness measurement points of the Σ -post	130

E.1 Eccentricity	139
E.2 EC3-1-8, Table 3.9	140
E.3 Estimated effective weld area	141
E.4 Bolt forces at 30° rotation	142

1 Introduction

This thesis is part of an ongoing project at *SIMLab* at *NTNU* in partnership with the *Norwegian Public Roads Administration* to determine the behaviour of road safety barriers subjected to combinations of loading, and to create valid finite element models of the road safety barrier. In this thesis the bolted connection in a standard steel road safety barrier will be investigated. Laboratory tests will be performed on the sections of the assembled road safety barrier to determine the behaviour of the bolted connection when subjected to a combination of quasi-static tensile and shear loading. Numerical models of the road safety barrier section and the bolted connection will be proposed and a validation study conducted.

1.1 Road safety

1.1.1 Traffic accidents

Road traffic accidents are among the leading causes of death and injury all around the world. The *World Health Organization* estimates that 1.24 million people are killed on the road every year, and 20 to 50 million people sustain non-fatal injuries[1]. This makes road traffic injuries the eight leading cause of death in the world. Figure 1.1 shows the number of road deaths per 100 000 population based on *WHO* regions. The number of deaths on the road has decreased in many countries across the world, proving that efforts to prevent road fatalities are effective. There are however still many places in the world where the number of deaths is increasing, mainly middle-income regions where vehicles are becoming more abundant.

Norway has approximately three fatalities on the road per 100 000 population, among the lowest in the world[2]. Road traffic accidents in Norway in the period 2003 to 2012 are summarized in figure 1.2 . The number of fatalities and personal injuries is still

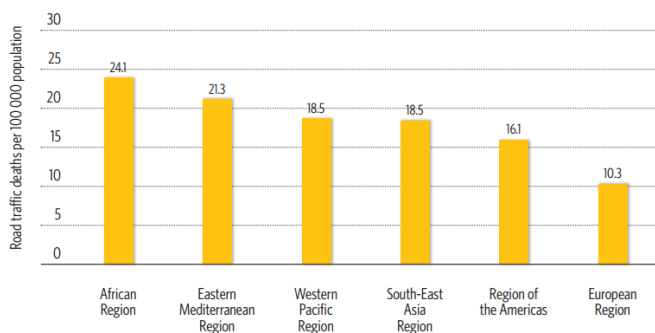


Figure 1.1: Road deaths per 100 000 population[1]

unacceptably high, and there is an ongoing effort to reduce it further. This effort is summarized in the *zero-vision* which states that no road traffic accidents resulting in death or life-long injury should occur. The zero-vision was adopted by the Norwegian Public Roads Administration in 1997, and passed by the Norwegian parliament as part of the *National Transport Plan* in February 2001[3].

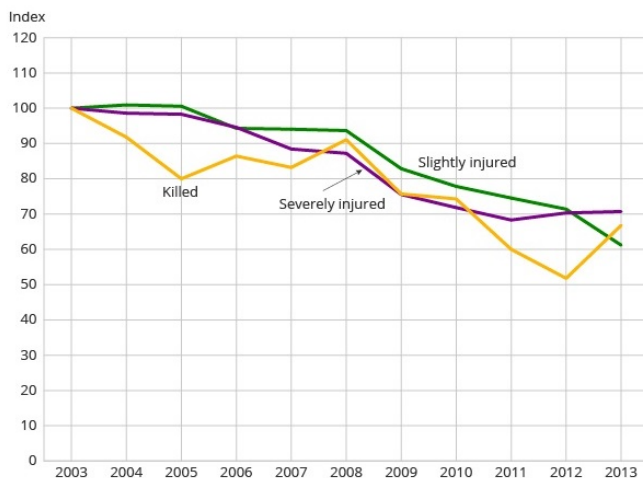


Figure 1.2: Road traffic accidents in Norway[2]

1.1.2 The effect of road safety barriers on road safety

Road safety barriers are much used measures to increase the safety of travel on roads. They are used alongside roads and as medians on roads to restrict vehicles from traveling outside of their carriageway in a dangerous manner. They are as such primarily designed to reduce the severity of accidents, not to prevent them. Medians restricts vehicles from entering ongoing traffic while roadside road safety barriers restrict vehicles from colliding with roadside obstacles or traveling into dangerous terrain. The effectiveness of measures to increase road safety, such as the use of road safety barriers, has been studied extensively. A meta study conducted by the *Institute of Transport Economics* [4] at the *Norwegian Center for Transport Research* provides data on the effectiveness of road safety barriers. Some of the results from this study are shown in table 1.1 and 1.2. The meta study combines data from many different studies and the statistical significance of several results reported is questioned. It does however show the general effects of using road safety barriers.

Table 1.1: The effect of road safety barriers as medians on multi-lane roads[4]

Severity	Best estimates [%]	Uncertainty [%]
Any road safety barrier		
Fatal	-15	-33;+7
Injury	-38	-68;+23
Steel road safety barrier		
Fatal	-12	-32;+13
Injury	-5	-8;+19
Wire road safety barrier		
Fatal	-	-
Injury	-18	-39;+8
Concrete road safety barrier		
Fatal	-38	-69;+24
Injury	-12	-22;0

Table 1.1 shows the effect of using road safety barriers in the median of multi-lane roads. It can be seen that both fatal accidents and accidents resulting in injury are reduced. Different types of road safety barriers have different effectiveness. The use of concrete road safety barriers has the greatest reduction in fatal accidents, while wire road safety barriers have the greatest reduction in accidents resulting in personal injury.

Concrete road safety barriers are much stiffer than those made from steel or wire, and are more effective at preventing vehicles from crossing over the median into ongoing traffic. Most fatal accidents in this scenario are head-on collisions, which explains the effectiveness of the concrete road safety barriers. However, the higher stiffness also results in more serious injuries when colliding with the road safety barrier itself. This explains why the less stiff wire road safety barrier is more effective at preventing accidents resulting in personal injury. The use of road safety barriers as medians in multi-lane roads has the expected effect of decreasing accidents where vehicles cross the median, while accidents in the median itself are increased.

Table 1.2: The effect of roadside road safety barriers

Severity	Best estimates [%]	Uncertainty [%]
Steel road safety barrier		
Fatal	-43	-90;+221
Injury	-48	-76;+14
Wire RSB relative to steel RSB		
Fatal	-44	-98;+1188
Injury	-68	-91;+17
Steel RSB relative to concrete RSB		
Fatal	+75	+70;+81
Injury	-74	+78;-69

Table 1.2 show the effect of using road safety barriers alongside roads. Only roadside steel barriers are compared to the scenario with no road safety barrier alongside the road. Some comparisons are however made between the effectiveness of other types of road safety barriers. Steel road safety barriers reduce the number of both fatal and injury related accidents by more than 40 percent. The meta study also shows that the risk of fatalities or injuries due to road run-off is reduced by 24 and 54 percent respectively. The risk of collisions with roadside obstacles is reduced by 58 and 43 percent respectively for accidents resulting in fatalities or personal injuries.

Road safety barriers appear to be an effective measure in increasing the safety of traveling on roads. The overall risk of fatalities or injuries in vehicular accidents is reduced by the use of road safety barriers, even though the effect varies depending on several factors. Different types of road safety barriers, the type of accident and the type of vehicle involved are among many factors that determine the effectiveness of the road safety barrier.

1.2 Road Safety Barriers

The definitions of road safety barriers in this thesis are based on those of The Norwegian Public Roads Administration. They provide manuals with specifications on road safety barriers for use on Norwegian public roads[5]. The primary objective of a road safety barrier is defined as to contain errant vehicles in a controlled way and redirect the vehicle in a small angle back towards the carriageway or along the barrier until it stops.

Road safety barriers on Norwegian roads are commonly fashioned from concrete, steel rails or wires. Concrete road safety barriers are usually concrete slabs either pre-produced or in-situ produced. Road safety barriers made with steel rails are the most common. They are fashioned with steel rails with a W-shaped cross-section mounted on posts of steel, wood or plastic. Road safety barriers made with wires are also in use. When using wire the road safety barrier is assembled from several wires fastened between posts. The posts can be made with either steel, plastic or wood, just as for steel rail road safety barriers. Examples of different types of road safety barriers are shown in figure 1.3.

Different types of road safety barriers are used based on the appropriate conditions along the road. They are divided into performance classes based on several parameters:

- Containment class (T1, T2, T3, N1, N2, H2, H4, L2, L4) - Accounts for speed limit, traffic volume and roadside terrain. The most used classes are N1 and N2 which are designed for passenger cars.
- Working width (W) and dynamic deflection (D) - These express the barrier's stiffness. The working width (W) is the maximum horizontal distance between the safety barrier's traffic face before impact and its rearmost point after impact. The dynamic deflection (D) is the horizontal distance between the safety barrier's traffic face before and after impact. (W) and (D) are important parameters when faced with roadside hazards such as cliffs, where the space besides the road for the road safety barrier to deform is limited.
- Impact severity class (A, B, C) - classifies the risk of personal injury on impact and are dependent on the stiffness of the barrier. (A) and (B) entail relatively little risk of serious personal injury.

Additional parameters such as economical, environmental and aesthetic considerations are accounted for secondary.



(a) Concrete road safety barrier



(b) Steel rail road safety barrier



(c) Wire road safety barrier

Figure 1.3: Different types of road safety barriers

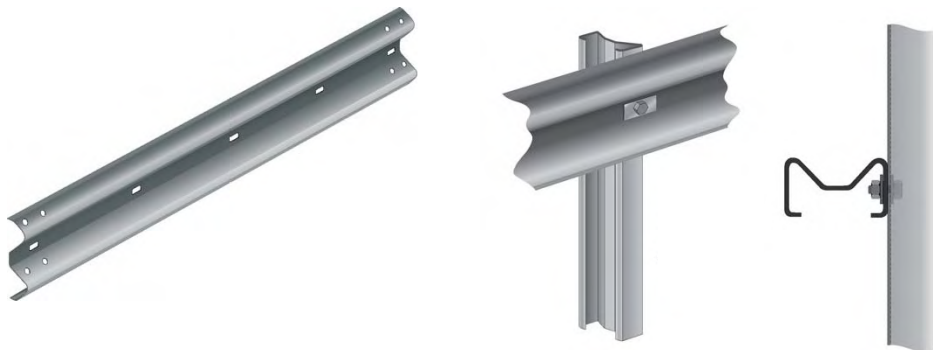
1.2.1 Steel rail road safety barriers

The road safety barrier studied in this thesis is assembled from steel rails mounted on steel posts. This is a standardized road safety barrier used by the Norwegian Public Roads Administration[6]. The road safety barrier is classified as N2, which is a common class designed for passenger cars. The N2 class is defined in table 1.3.

Table 1.3: Definition of the N2 containment class[5]

N2	<ul style="list-style-type: none"> • Speed limit ≤ 60 km/h and AADT¹ ≤ 12000 • Speed limit ≥ 70km/h and AADT ≤ 1500 • By retaining walls and precipices(gradients steeper than 1:1:5) that are higher than 1.5-4m • For bridges and culverts with lengths ≤ 4m and an AADT ≤ 1500 • On motorways
	1) Annual average daily traffic

The steel rail is made with a W shaped cross-section and will in this thesis be referred to as a *W-beam*. The W-beam is illustrated in figure 1.4a, while more specific cross-sectional geometry can be seen in Appendix A.1. The W-beam is mounted on steel posts with a Σ -shaped cross-section, which will be referred to as a Σ -post. The Σ -post is illustrated with a mounted W-beam in figure 1.4b, while cross-sectional geometry can be seen in Appendix A.2. The steel quality used in both the W-beam and the Σ -post is S235. They are both coated in a heat-treated sink coating, thickness 85μ for the W-beam and 140μ for the Σ -post.



(a) W-beam

(b) W-beam mounted on Σ -post

Figure 1.4: Illustrations of the road safety barrier[5]

The connection between the W-beam and the Σ -post is very important to the behaviour of the road safety barrier. The connection must be designed so that the steel rail remains in the proper height above the carriageway so as to redirect the vehicle back onto the carriageway without resulting in large retardations or injuries when impacted. In the case of a road safety barrier with a W-beam mounted on Σ -posts, the Σ -post will be bent down towards the ground when the road safety barrier is impacted. The

connection is designed to break and release the W-beam in such a manner that the W-beam is not dragged too low by the Σ -posts, allowing vehicles to pass above the steel rail, but not so early that the vehicle will be able to pass underneath. This consideration makes understanding the behaviour of the connection very important. The W-beam is connected to the Σ -post by a bolted connection. The connection comprises of

- 1) One threaded bolt M10×45, quality 4.6.
- 2) One washer 115×40×5, quality S235, with hole for M10 bolt.
- 3) One washer 30×30×3, quality S235, with hole for M10 bolt.
- 4) One nut M10.

The connection is illustrated in figure 1.5.

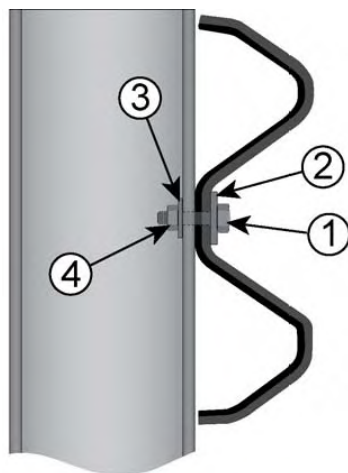


Figure 1.5: Parts in the road safety barrier connection[5]

2 Literature Review

Several studies related to the road safety barrier have previously been conducted at SIMLab at NTNU in collaboration with the Norwegian Public Roads Administration. A PhD thesis by H. Fransplass related to the subject was completed, as well as a master's thesis by H. O. Bakken-Berg and H. Iversen, and another by L. D'Angelo. Data and results from these previous studies form a foundation for this thesis, and the studies are reviewed in this chapter. In addition a literature survey was performed to see what other studies relating to road safety barriers, and their bolted connections, have previously been conducted.

2.1 "Black bolts under combined tension and shear" [7]

In 1979 H. Shakir-Khalil and C. Ho published an article on "the behaviour, response, and ultimate carrying capacity of black bolts subjected to varying tension-shear ratios". Here they performed tests on M20 grade 4.6 black bolts in combinations of tension and shear in increments of 15° from 0° to 90°. Tests were run with double nuts in cases where the force was applied at angles of 15° or less. This was done to avoid thread stripping, which indicates that this was a problem experienced in tension dominated tests. Tests were run on two groups of black bolts and a third group was used in a separate test on bolted plate connections. The test rig used can be seen in figure 2.1. Material tests on the bolt groups found a 5 percent deviation in maximum stress between the groups, while a deviation up to 50 percent was found in the yield stress. The tests in pure tension resulted in failure of the bolt in the threaded area, which was anticipated given the smaller stress area in comparison to the shank. When loading in combined tension and shear, the shear loading plane was located at the shank of the bolt. In almost all tests the bolts failed in the shear plane of loading. One of the main results found in the tests was that the maximum capacity of the bolts is found in a combination of tension and shear where

the tension force is dominant. However, if the shear plane of loading is in the threads the maximum capacity is found in pure tension. The results of interaction between different levels of tension and shear on the bolts can be seen in figure 2.2.

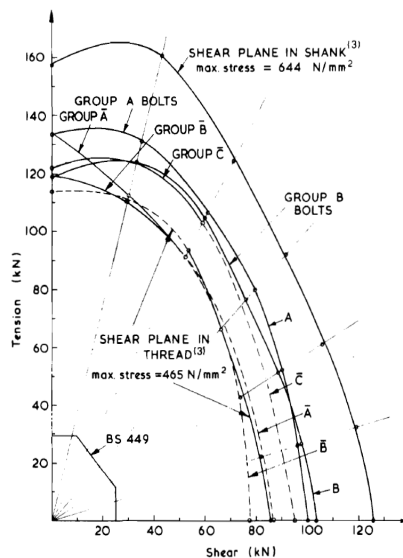
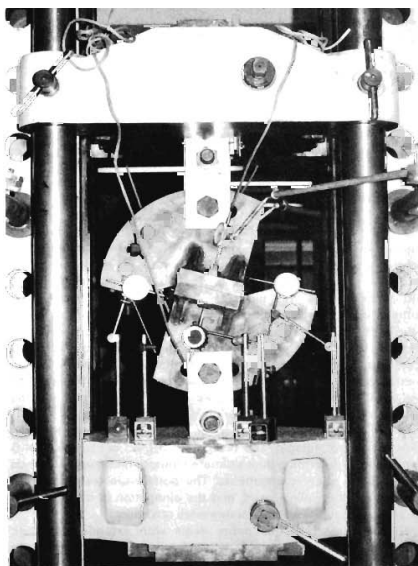


Figure 2.1: Test rig for combined tension-shear loading[7] Figure 2.2: Tension-shear interaction[7]

The two main test groups are group A and B. Shakir-Khalil and Ho found a ratio between tension and shear capacity to be in the range of 0.75 to 0.87, where the higher ratio was found in the group of bolts with the lower yield strength.

2.2 "Failure mechanisms of mild steel bolts under different tensile loading rates" [8]

In 1994 A.P. Mouritz published a paper examining "the plastic deformation and failure behaviour of mild steel bolts subjected to tensile loads exerted at strain rates ranging from about 10^{-5} to 10^2 s^{-1} ". Mouritz reached four main conclusions based on his research:

- The threads of the bolts have a lower tensile failure strength than the shank of the bolts. It is therefore important to account for the strength of the threads when using bolts in design.

- The relative tensile failure strength of the threads compared to the shank of the bolts decreases with increasing strain rate.
- The bolt shanks experienced approximately 30 percent elongation before failing regardless of strain rate, indicating that the plastic deformation behaviour of the bolt shank is not influenced by the strain rate.
- The threads fail by a two stage process: The tip of the threads are first plastically deformed and then sheared off at higher loads. Secondly, the remaining thread is plastically deformed into the pitch of the thread. The failure mechanism of the threads do not appear to be influenced by the strain rate. This two-stage process can be seen in figure 2.3.

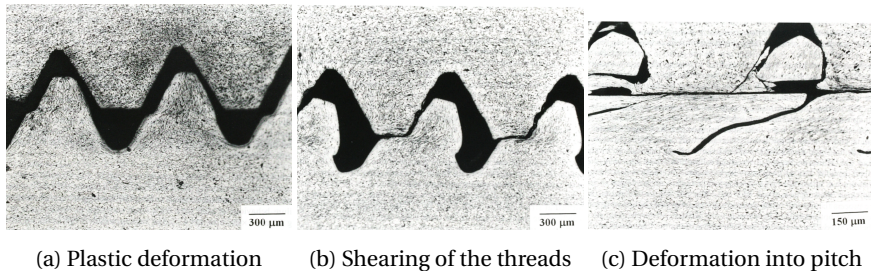


Figure 2.3: Failure mechanism of the bolt threads[8]

Mouritz used three different methods to apply the range of strain rates used in the tests. A strain rate of $2.5 \times 10^{-5} s^{-1}$ was applied using an unspecified tensile testing machine. Strain rates of $\sim 1 - 10 s^{-1}$ were applied using a drop tower impact test, and strain rates $\sim 10^2 s^{-1}$ were applied using an underwater explosive shock testing technique. The bolts examined were mild steel bolts of grade 4.6 with a diameter of 6 mm and length 90 mm. Mouritz ran tensile tests on both the shank and the threads of the bolts. During testing of the unmodified bolts Mouritz found that the bolt would fail in the threads. In order to test the ultimate tensile strength of the shank Mouritz reduced the diameter of the shank from 6 mm to 3 mm, 4 mm and 5 mm in various bolts.

The three different methods of applying the tensile loading makes comparison of the results from each method more difficult. It is however possible to compare relative tensile failure strength of the bolt threads and the shank from each method. Mouritz found the tensile failure strength of the threads to be between 29 percent and 52 percent of the shank's with a strain rate of $2.5 \times 10^{-5} s^{-1}$. With a strain rate of $\sim 1 - 10 s^{-1}$ this

relation was ~ 38 percent. In the underwater explosive testing with strain rate $\sim 10^2 \text{ s}^{-1}$ the tensile failure strength of the threads were 8-15 percent of the shank's.

2.3 "Computational analysis of a deformable safety barrier" [9]

In 2007 H.O. Bakken-Berg and H. Iversen completed a master's thesis at NTNU "with the aim of creating a numerical model of a guardrail to better understand the distribution of forces during impact". Their thesis is highly relevant to the work performed in this thesis, and will be discussed in detail.

The road safety barrier investigated in the thesis of Bakken-Berg and Iversen is the same N2 steel guardrail with steel posts investigated in this thesis, and discussed in section 1.2. In their thesis they investigated the properties of the road safety barrier bolt, W-beam and Σ -post. The bolt was tested in tension, shear and the thread capacity. Material tests of the W-beam and Σ -post were performed, as well as an investigation into the effects of the forming process and coating on the material behaviour. A numerical model of the road safety barrier was proposed where a simplified vehicular impact is simulated. The effect of different velocities and angles of impact loading in the model was investigated.

2.3.1 Bolt tests

The bolts tested by Bakken-Berg and Iversen are the M10 grade 4.6 steel bolts specified for the N2 guard rail by the Norwegian Public Roads Administration. These were tested in pure tension, pure shear, and thread capacity in tension. Displacement control was used in the testing, and different rates of loading were applied in an effort to study the effect of different strain rates. Tests in pure tension and pure shear were loaded in three different velocities, 1 mm/min, 10 mm/min and 100 mm/min. Only loading at 1 mm/min and 100 mm/min was employed during testing of the thread capacity. The results from the tests at 1 mm/min are shown in force-displacement curves in figure 2.4.

Bakken-Berg and Iversen found that the force-displacement relationship in pure tension had a fairly expected behaviour. In pure shear the force-displacement curves show how one shear plane fails at maximum failure load, and a lower peak where the second shear plane fails. In the case of bolt stripping Bakken-Berg and Iversen found

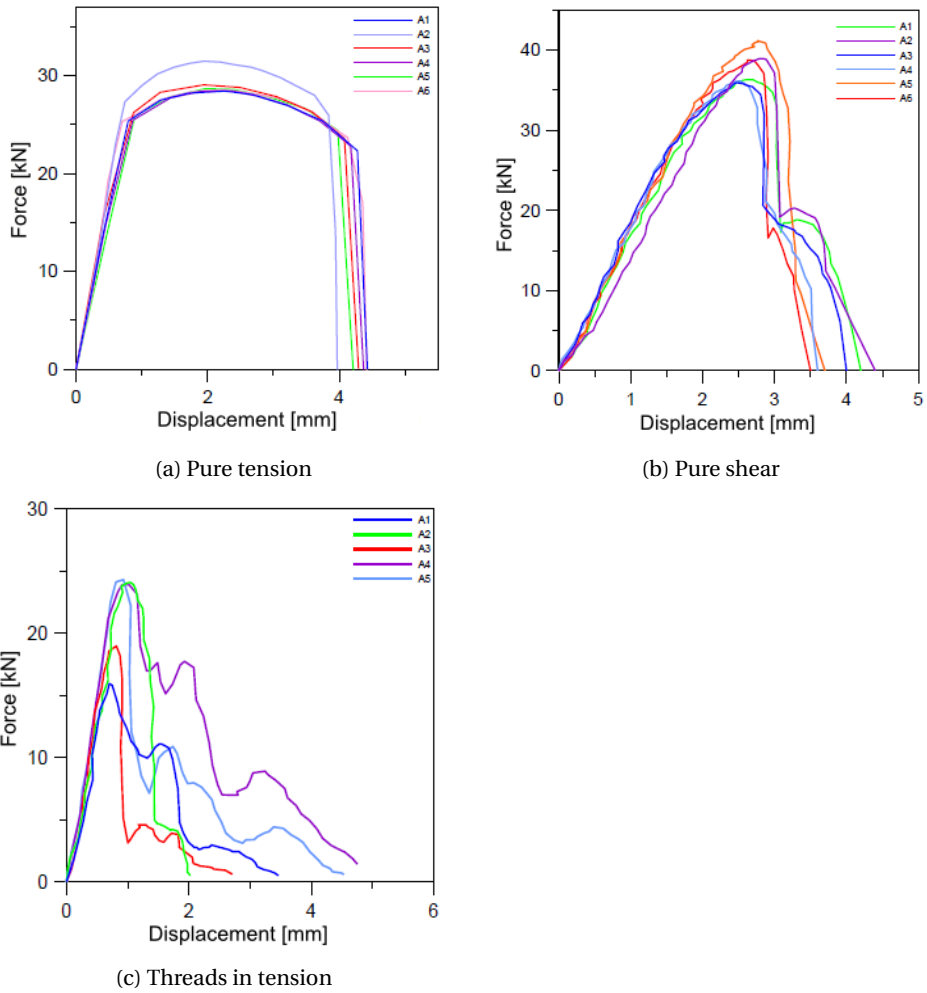


Figure 2.4: Bolt testing force-displacement at 1 mm/min[9]

that the maximum failure load was achieved at the stripping of the first thread, with subsequent lower peaks as more threads are stripped.

The maximum, average and minimum failure load of the bolt at different rates of loading is shown in figure 2.5.

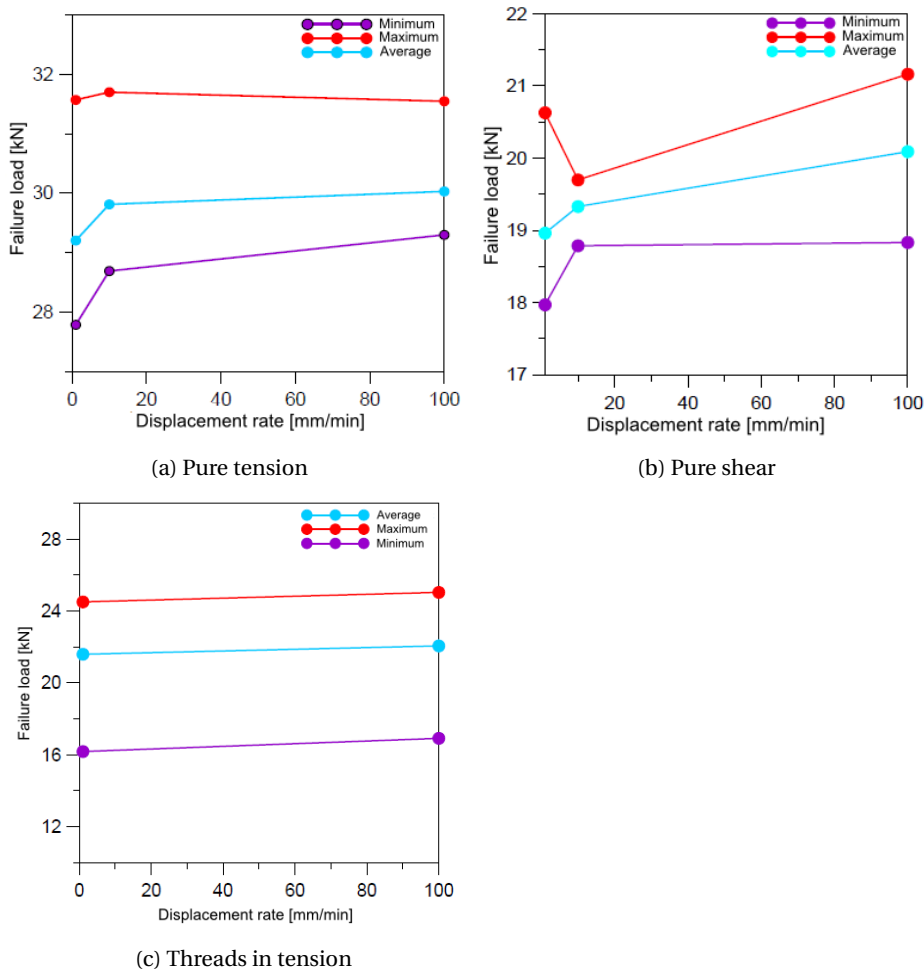


Figure 2.5: Maximum, average and minimum failure load based on load rate[9]

Bakken-Berg and Iversen found that the bolt fastened by the nut would fail by thread stripping when loaded in tension. The threads were estimated to have approximately 75 percent of the capacity of the bolt cross-section. Bakken-Berg and Iversen also concluded that the maximum failure load in tension increased with increasing strain rate, but could not make the same conclusion with enough confidence about the bolt in shear or thread stripping. When testing in pure tension Bakken-Berg and Iversen found that the bolt

would fail in the threads if the threaded engagement was insufficient. This shows that the failure mode of the bolt is dependent on the threaded engagement of the bolt.

2.3.2 W-beam and Σ -post tests

Bakken-Berg and Iversen performed a thorough investigation into the material properties of the W-beam and Σ -post. All tests were performed as uniaxial tension tests on extracted material samples. Nominal geometry of the material samples can be seen in figure 2.6. The W-beam and Σ -post are specified to have the same steel grade S235, which translates into a yield stress of 235 MPa and a ultimate stress between 360 and 610 MPa. Bakken-Berg and Iversen chose to only perform material tests on the W-beam, concluding that the same material would behave similarly for the Σ -post.

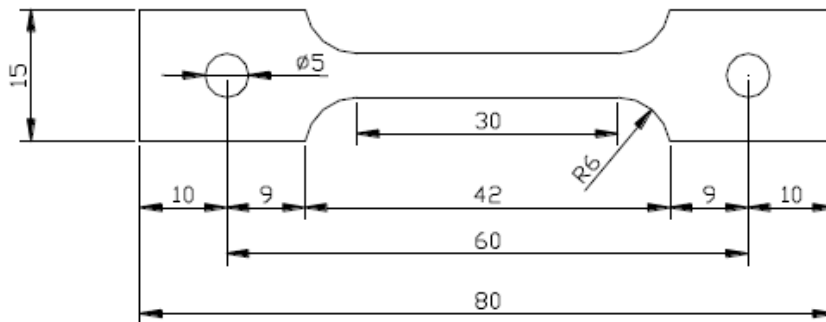


Figure 2.6: Nominal geometry of a material test sample[9]

Four properties of the steel were tested: isotropy, the effect of the heat-treated sink coating, the effect of the cold-roll forming of the W-beam cross-section, and variation between different batches of the W-beam. The resulting stress-strain curves are shown in figure 2.7.

Isotropy tests found that the steel was effectively isotropic. The test samples were extracted from an undeformed steel plate with a sink coating: two samples at 0°, 45° and 90°. No clear differences were observed in the behaviour of the samples.

Tests on the effect of heat-treated sink coating on the steel showed that the coating resulted in a higher yield plateau of the steel by 20-30 MPa, but that the yield stress, ultimate stress and hardening curves remained approximately the same. It was not

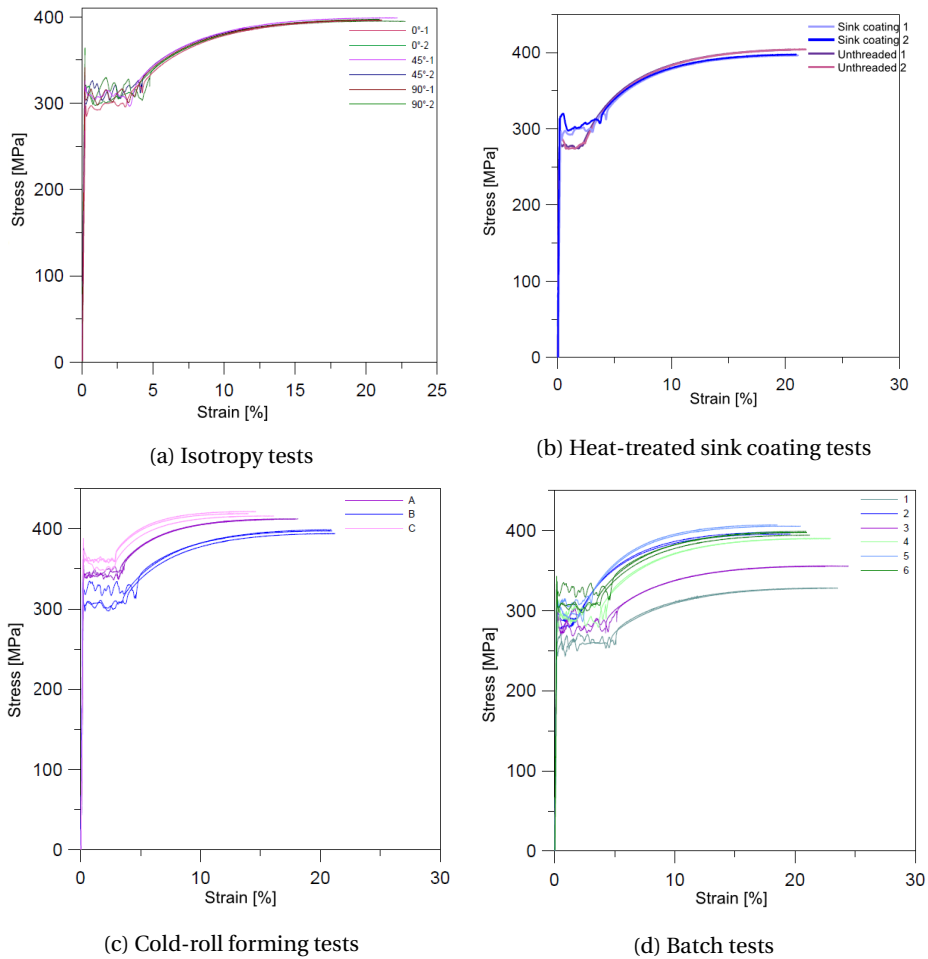


Figure 2.7: W-beam and Σ -post material tests[9]

concluded whether this was due to the properties of the sink or if the heat-treatment of the steel was the cause. Two material tests were extracted from untreated steel plates and compared to the equivalent samples from the isotropy tests.

The cold-roll forming process used to shape the W-beam and Σ -post was found to affect the material properties of the steel. Sections of the steel which had undergone plastic deformation due to the forming process experienced higher yield stress, and less strain before necking. Test samples were extracted from three different zones of the W-beam cross-section, and equivalent zones were assumed for the Σ -post. These zone

are shown in figure 2.8.

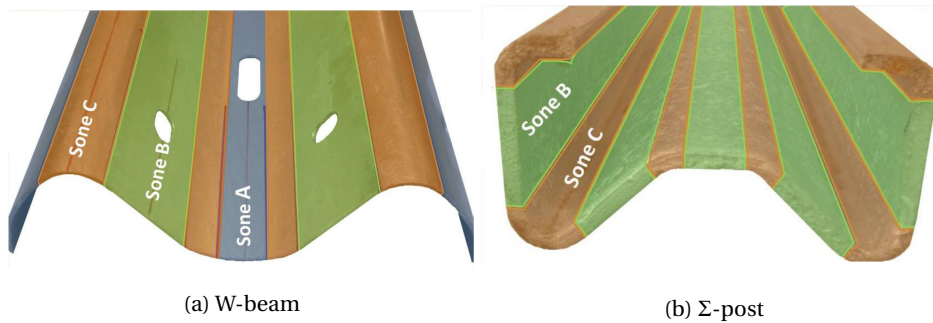


Figure 2.8: Material test extraction zones[9]

As can be seen in figure 2.7c, zone C, which is the part of the W-beam cross-section with the largest curvature, has the highest yield stress. This effect appears to be proportional to the deformation of the steel cross-section. Zone C has approximately 20 percent higher yield stress than zone B, while zone A has approximately 13 percent higher yield stress than zone B.

When testing the difference in material properties based on production batches, Bakken-Berg and Iversen found large differences in properties. Yield stress varied between 250 and 330 MPa, while the ultimate tensile strength varied between 300 and 400 MPa. Bakken-Berg and Iversen determined the Young's modulus to be approximately 210 GPa regardless of batch, which is the expected value. They further assumed the Poisson's ratio to be 0.3 and the mass density to be 7860 kg/m³.

2.3.3 Numerical modelling and analyses

Bakken-Berg and Iversen conducted numerical analyses of the road safety barrier subjected to an idealized vehicular impact. In their analyses they used the *FEA* program *Abaqus CAE*. The model proposed by Bakken-Berg and Iversen can be seen in figure 2.9. The model consists of a larger section of the road safety barrier, with several Σ -posts. The main focus of the analyses performed by Bakken-Berg and Iversen is concerned with the effect of different angles of loading and velocities of the vehicular impact on the road safety barrier. This is a more macroscopic level of the road safety barrier than what is studied in this thesis.

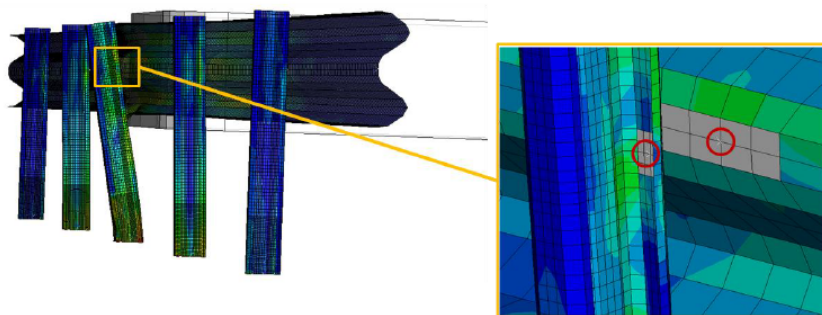
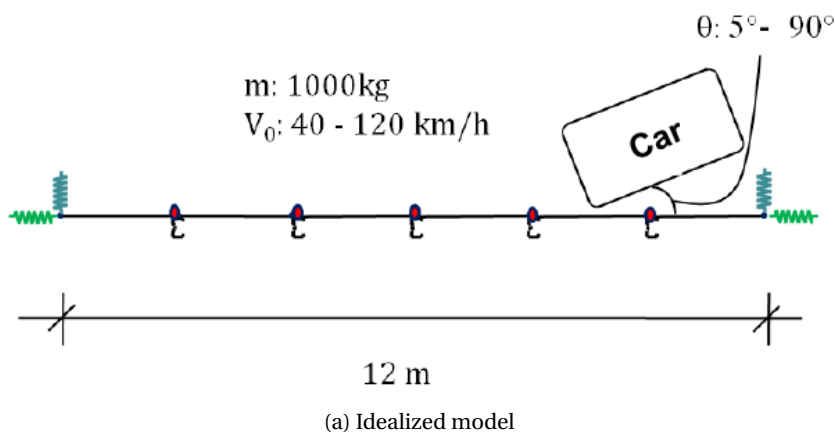


Figure 2.9: Model of the road safety barrier[9]

Material models of the W-beam and Σ -post were based on the results from the material tests previously discussed. Due to the variation in the material from the cold-forming process, a parameter study was conducted where the materials of the W-beam and Σ -post were varied and also different zones of the material were included. Bakken-Berg and Iversen found that the material with the lowest yield stress experienced the greatest displacement and lowest peak force. Comparing results from analyses where the W-beam and Σ -post were divided into zones with different material properties to analyses with no zone divisions, it was found that the zone division resulted in greater stiffness and yield stress of the road safety barrier.

To model the bolted connection in Abaqus Bakken-Berg and Iversen used a *bushing element*. The bushing element is a 1D idealization of a connection between two surfaces

which can be assigned failure criteria in addition to both elastic and plastic behaviour. Using a "bushing" element reduces computational cost but reduces the accuracy of the solution. Bakken-Berg and Iversen used the collected data from the bolt tests to produce a failure criteria and material model for the "bushing" element. The elastic behaviour was modelled using the data in table 2.1.

Table 2.1: Elastic behaviour at different degrees of freedom

Degree of freedom	Elastic force [kN/mm]
U1	40.945
U2	18.390
U3	18.390
UR1	rigid
UR2	rigid
UR3	rigid

In addition, the following failure criteria was used:

$$\left(\frac{U_1}{29205}\right)^2 + \left(\frac{\sqrt{U_2^2 + U_3^2}}{18961}\right)^2 = 1 \quad (2.1)$$

This is based on an interaction formula between tension and shear in the material proposed by Bakken-Berg and Iversen.

Bakken-Berg and Iversen used nonlinear springs at the ends of the W-beam to simulate the response from the extended guardrail. The elastic properties of the spring is based on a simple spring stiffness calculated by $K=EA/L$, where E is the Young's modulus, A is the guardrail cross-section area and L is the length of the guardrail which is not included in the model. The nonlinear properties were based on a study of the road safety barrier's response in numerical analyses, however they were not discussed in detail.

From their numerical analyses of the road safety barrier Bakken-Berg and Iversen concluded that the bolted connection is crucial for the intended behaviour of the road safety barrier. They found that their model of the bolted connection using a "bushing" element failed at an opportune stage of the vehicular collision with the road safety barrier. They noted that the "bushing" element used in the model failed primarily due to vertical shear forces. The shear forces are the result of the deformation and bending of the Σ -post towards the ground, pulling the W-beam with it through the bolted connection.

2.4 "Tensile behaviour of threaded steel fasteners at elevated levels of strain"[10]

The road safety barrier is designed to handle high velocity vehicular impacts, which results in high strain rates in the barrier. The bolted connection in the road safety barrier is a vital part of the assembly which is then also subjected to high strain rates. In the absence of studies on the subject, Fransplass performed an experimental program on threaded assemblies subjected to loading at high strain rates. The main focus of the program was to study the maximum load and the mode of failure of the rods by varying the loading rate, the grip length and the thread engagement length. Fransplass performed tensile tests on M5 threaded rods with material grade 4.6. Loads with low and medium strain rates between $10^{-4} - 10^{-1} s^{-1}$ were applied with a servo-hydraulic testing machine. Loading with high strain rates between $10^1 - 1.9 \times 10^3 s^{-1}$ were applied using a *Split-hopkins tension bar(SHTB)*. Fransplass performed his tests using threaded rods(external threads) with purpose-made threaded fixtures(internal threads), illustrated in figure 2.10.

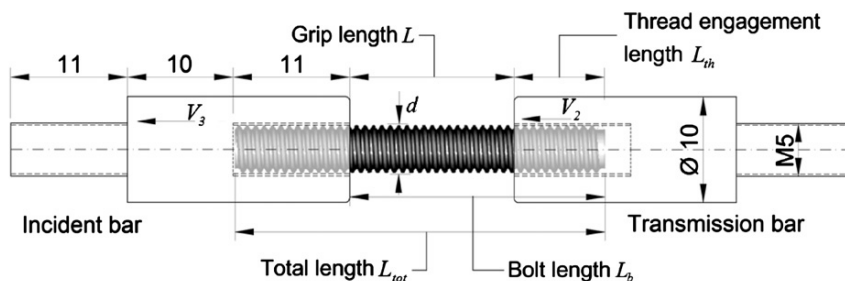


Figure 2.10: Geometry of the threaded rod with purpose-made fixtures[10]

This allowed stress concentrations associated with threaded assemblies to be avoided. A higher steel grade in the threaded fixtures than in the threaded bolt also ensured that the failure mode of internal thread stripping did not occur in the testing. Fransplass performed material tests at elevated strain rates and Vickers hardness measurements of the rods. Results from the material tests found that the stress-strain relationship is dependent on the strain rate. Tests with higher strain rates resulted in higher nominal-, ultimate-, and fracture stress as well as greater ductility. This result was also evident from the rod tensile tests, although the nominal tensile stress was higher in the material tests.

Fransplass also found that different failure modes resulted in very different stress-strain relationships. The thread engagement length and the grip length were also found to influence the stress-strain behaviour of the threaded rods. Fransplass proposed a fitted equation for the rate-dependent ultimate tensile strength of the material:

$$\sigma_s^* = \sigma_{s0} \left(1 + \frac{\dot{\epsilon}}{\dot{\epsilon}_0} \right)^C \quad \text{or} \quad \sigma_s^* = \sigma_{s0} \left(1 + \frac{V_2 - V_3}{V_0} \right)^C \quad (2.2)$$

where σ_{s0} and C are material parameters calibrated from tensile tests. $V_2 - V_3$ is the test velocity. This was used to augment a model by Alexander[11] to predict the maximum load and mode of failure of threaded assemblies at static loading conditions:

Table 2.2: Formula for maximum load and mode of failure of threaded assemblies

	Alexander	Fransplass
F_{bb}	$\sigma_s A_s$	$\sigma_s^* A_s$
F_{bs}	$f \sigma_s A S_s C_1 C_2$	$f \sigma_s^* A S_s C_1 C_2$
F_{ns}	$f \sigma_s A S_n C_1 C_3$	-

where F_{bb} is the bolt breaking load, F_{bs} is the bolt stripping load and F_{ns} is the internal stripping load. No augmented formula for internal thread stripping was proposed due to only the first two failure modes being present in Fransplass' tests.

2.5 "Development of an Arcan test setup for characterization of road restraint system" [12]

In 2012 L. D'Angelo completed a master's thesis at NTNU as a continuation of the SIMLab effort on road safety barriers. The thesis concerns itself with creating preliminary numerical models and analyses of the N2 steel road safety barrier, material testing of the components included in said barrier, and generating material models. The main results of the thesis are suggestions for a clamping system connected to the W-beam, allowing for laboratory testing of the road safety barrier in combinations of tension and shear.

2.5.1 Material tests and models

D'Angelo performed material tests on the components of the road safety barrier in order to determine their mechanical behaviour. Both uniaxial tension tests and in-plane single shear tests were performed. Specimens were taken from three different locations of the

W-beam, while only one location was tested for the Σ -post. The reasoning for testing several locations was to determine the influence of the cold-roll forming of the cross-sections on the mechanical behaviour. The Σ -post is however curved to such an extent that viable specimen could only be extracted from one location. The sampling locations are shown in figure 2.11.

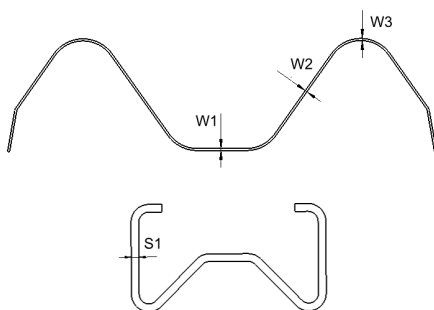
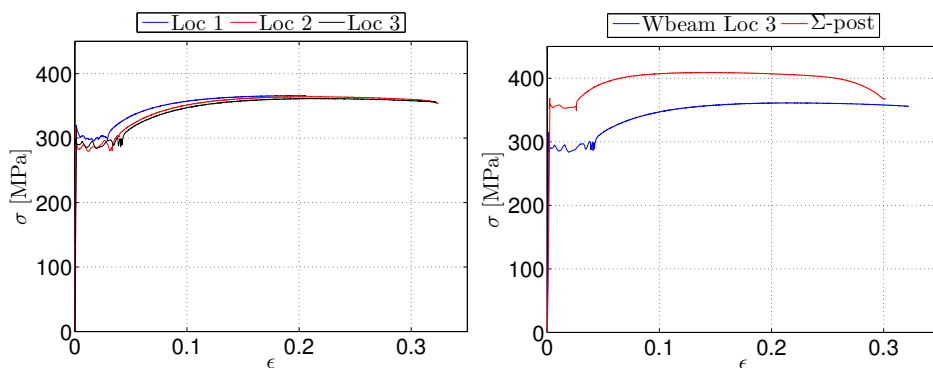


Figure 2.11: Location of material test samples in the W-beam and Σ -post [12]

Uniaxial tension tests on the specimen were performed quasi-statically using a strain rate of $25 \times 10^{-3} \text{ s}^{-1}$. Five specimen from each location in the W-beam and Σ -post were tested. D'Angelo found mostly consistent force-displacement behaviour when comparing specimen from the same location. Plots of the engineering stress-strain relationships were produced for sake of comparison. These are shown in figure 2.12.



(a) Representative engineering stress-strain in the three W-beam locations

(b) Representative engineering stress-strain in the W-beam and Σ -post

Figure 2.12: Engineering stress-strain relationships[12]

As can be seen in figure 2.12a, D'Angelo found that there was some difference be-

tween the behaviour of the different locations of the W-beam. Location W1 had a somewhat higher yield stress than the other two, which D'Angelo argues could be an effect of the cold-roll forming process. The W-beam locations W2 and W3 consist of straight sections, while location W1 is more curved. D'Angelo explains that with the use of cold-roll forming of steel the yield stress increases while ductility decreases. This argument is also applied when comparing the stress-strain relationship of the W-beam and the Σ -post, see figure 2.12b. The Σ -post is even more curved than the W-beam. By this argument, the Σ -post would through cold-roll forming have a higher yield stress even when made from the same steel alloy as the W-beam.

D'Angelo also performed uniaxial tension tests on M5 bolts where the specimen were taken from the shank of the bolt. The force-displacement curves are shown in figure 2.13. The results showed that even though the bolts experienced similar elastic behaviour and yield, there was some difference in the hardening curves and point of failure. There were some geometrical uncertainties stemming from the shearing of the bolt shank cross-section in producing the test specimen, which could account for some of the differences in behaviour.

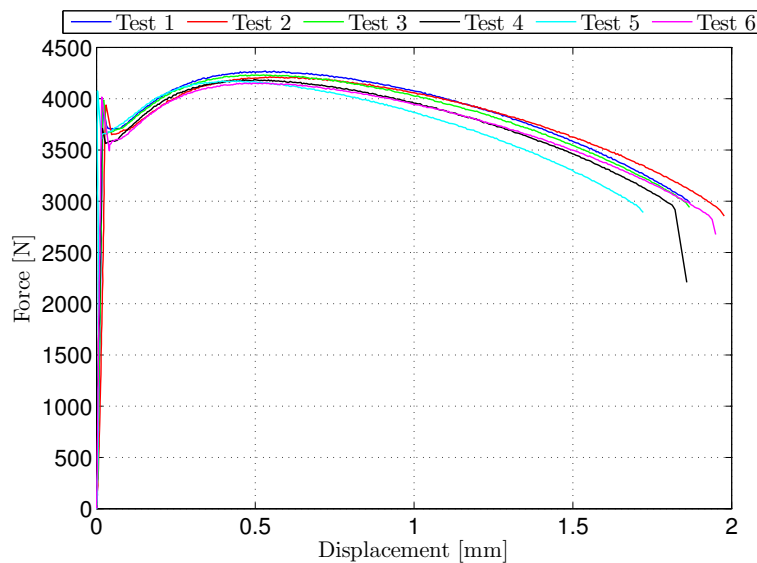


Figure 2.13: Force-displacement curves for bolt specimen[12]

D'Angelo performed in-plane single shear tests on three specimen from each location in the W-beam and four specimen from the one Σ -post location. The strain rate in the

tests was $3.0 \times 10^{-3} s^{-1}$. As in the uniaxial tension test there is consistency between samples from the same location. When comparing the three locations in the W-beam D'Angelo found that also in the in-plane single shear stress test the specimen from location W1 had a higher yield stress and lower ductility. When comparing the results from the W-beam versus the Σ -post the Σ -post displayed a higher yield stress and overall force capacity. Plots of the force-displacement relationships of the W-beam and Σ -post can be seen in figure 2.14.

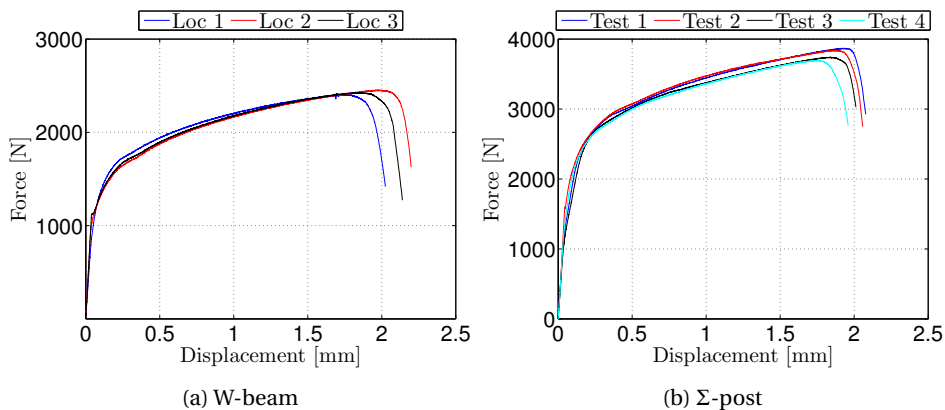


Figure 2.14: Force-displacement curves of in-plane single shear tests[12]

2.5.2 Finite element modelling and parameter study

D'Angelo suggested a finite element model of the road safety barrier with the bolted connection. This model was used for preliminary analyses of the behaviour of the road safety barrier when loaded in a combination of tensile and shear forces. D'Angelo also studied the effect of different geometrical variations in the model, such as length of the W-beam and misalignment of the bolt. The finite element model was based on a reference model provided by the Norwegian Public Roads Administration and modified by D'Angelo. D'Angelo used a Voce hardening rule to generate material models for the finite element model parts, based on the material tests previously discussed. The model consisted of shell segments of the W-beam and Σ -post. The bolt and washers were modelled using solid elements. The bolt was modelled with a simplified geometry without threads, but with a cylindrical shank, head and nut. Solid element patches were inserted into the W-beam and Σ -post around the holes for the bolted connection, in an

effort to better simulate contact and deformation in this location. The finite element model suggested by D'Angelo can be seen in figure 2.15.

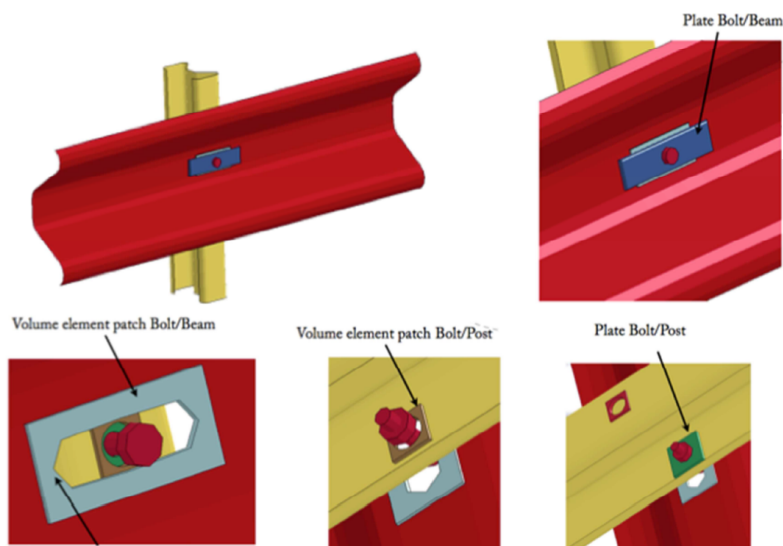


Figure 2.15: Finite element model of the road safety barrier by D'Angelo[12]

D'Angelo found in his analyses that the tension-shear ratio in loading greatly affects the capacity of the connection. The highest ultimate load was found when loading in pure tension and decreasing incrementally with increasing shear loading. This can be seen in figure 2.16a. D'Angelo analysed the influence of varying the length of the W-beam in his model. As can be seen in figure 2.16b, longer sections of the W-beam resulted in higher ultimate force and ductility of the road safety barrier. In reality the W-beam in a road safety barrier will be continuous far beyond a single bolted connection to a Σ -post, and free ends such as used in the model by D'Angelo are unrealistic. But in the case of studying the bolted connection itself it is noteworthy that the simulated length of the W-beam affects the capacity of the connection in analyses. D'Angelo also analysed the effect of misalignment of the bolt in the slotted hole of the W-beam. The force-displacement relationships of horizontal and vertical misalignment can be seen in figure 2.16c and 2.16d. D'Angelo found that horizontal misalignment of the bolt had a significant effect on the behaviour of the model. The ultimate force was greatest when the bolt was displaced to the end of the slotted hole, where the contact area between

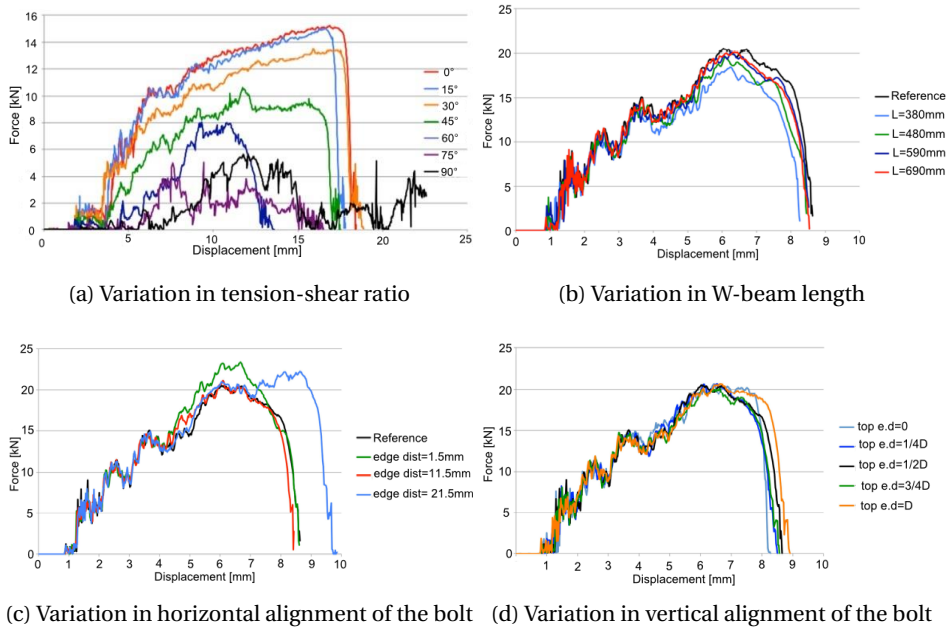


Figure 2.16: Force-displacement relationships from the numerical model [12]

the bolt head and washer is greatest. Vertical misalignment of the bolt did not show any significant variation in the behaviour.

D'Angelo subsequently used the FE model to propose a clamping system for the road safety barrier used to load the road safety barrier in combinations of tension and shear during laboratory testing. The clamp is designed to be bolted to the top of the W-beam and fastened with two rows of five bolts. D'Angelo performed a study to verify adequate stiffness of the loading clamp so that it does not significantly deform during laboratory testing of the road safety barrier. This is to eliminate influence of the clamp on test results. The clamp proposed by D'Angelo can be seen in figure 2.17.

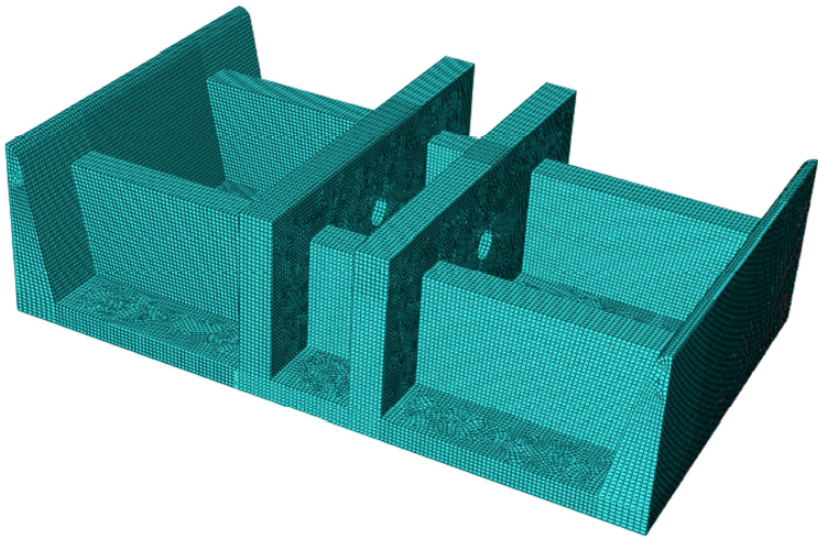


Figure 2.17: Loading clamp as designed by D'Angelo[12]

3 W-Beam, Σ -Post & M10 Bolts

Following the literature review the relevant knowledge obtained concerning the parts of the road safety barrier is discussed.

3.1 W-beam & Σ -post

The W-beam and Σ -post are made from steel grade S235 which is cold-roll formed into the appropriate cross-sections. *NS-EN 10025-2*[13] specifies the mechanical properties of steel grade S235. Material tests performed by Bakken-Berg and Iversen[9], and D'Angelo[12], all show the material properties of the W-beam and Σ -post differing from the values specified for steel grade S235 in *NS-EN 10025-2*. This is summarized in table 3.1.

Table 3.1: Comparison of material properties

	Yield strength [MPa]		Ultimate tensile strength [MPa]	
S235	≥ 235		360 - 510	
	W-beam	Σ -post	W-beam	Σ -post
Bakken-Berg & Iversen	250 - 330	-	300 - 400	-
D'Angelo	320 - 340	350-420	340 - 360	400 - 420

The yield stress of 235 MPa specified by *NS-EN 10025-2* is a minimum value. It is worth noting that the material tests performed by Bakken-Berg and Iversen, and D'Angelo, all experienced markedly higher yield stress than what is specified for steel grade S235. There is also much variation in the yield stress of each of the material tests. A result of this is that the material properties of steel products such as the W-beam and Σ -post might vary significantly from the assumed yield stress of 235 MPa, and amongst

themselves. The ultimate tensile strength from the material tests are mostly in the range specified by the standard. The low ultimate tensile strength from the tests performed by Bakken-Berg and Iversen stem from tests on different production batches of the W-beam that for various reasons had been discarded. There is however much variation in the ultimate tensile strength of the different material tests. The uncertainty of the ultimate tensile strength of the steel is reflected in the width of the specified ultimate tensile strength for steel grade S235.

The material tests on the W-beam and Σ -post seem to indicate that the cold-roll forming of the cross-sections significantly affect the material properties. The sections of the cross-sections with the largest curvatures, and therefore larger plastic strains, experience higher yield stress and ultimate tensile strength. They are also less ductile. All these changes in the properties are expected consequences of the cold-roll forming process.

It has been seen that there is much variation in the material properties of the W-beam and Σ -post: differences between the two cross-sections, differences between produced batches of each cross-section and within sections of the cross-sections themselves. The behaviour of the road safety barrier is dependent on the material in its parts, and the variation in properties found during testing indicates that the performance of the road safety barrier might vary.

The uncertainty and variation in the material properties is challenging with regards to finite element modelling of the road safety barrier with the bolted connection. The purpose of the finite element model is to describe the physical behaviour of the road safety barrier as accurately as possible using the finite element method. This requires the creation of material models to describe the behaviour of the steel in the different parts of the road safety barrier. Both the validity and general application of the finite element model is reduced if the material properties modelled are not representative of the materials in the road safety barrier parts.

3.2 M10 bolts

The threaded bolt in the bolted connection of the road safety barrier is a *DIN 601* bolt size M10 with steel grade 4.6. This translates into a bolt with 10mm diameter, yield stress of 240 MPa and ultimate tensile stress of 400 MPa. *Eurocode 3-1-8*[14] gives specifications for the capacity of individual fasteners. The capacity of the M10 bolt

according to the Eurocode is summarized in table 3.2 along with the results from tests on the bolt performed by Bakken-Berg and Iversen[9]. The capacities from the Eurocode are calculated without the safety factor of 1.25.

Table 3.2: Force capacity of the M10 bolt

	$F_{tensile}$ [kN]	F_{shear} [kN]	$F_{threads}$ [kN]
EC3-1-8	20.9	27.8	-
Bakken-Berg & Iversen	28- 32	35-40	16-25

Comparing the capacity from the eurocode with the results from laboratory testing by Bakken-Berg and Iversen it can be seen that the eurocode gives significantly lower capacity. The eurocode is conservative in its capacity even without the inclusion of the safety factor. A conservative calculation of the capacity is often satisfactory since it provides safety from failure. However, the bolted connection in the road safety barrier is required to fail at an opportune level of loading as not to allow vehicles to pass over or under the guardrail. If the capacity of the bolt is significantly higher than what is calculated from the eurocode, the road safety barrier might end up with a capacity exceeding the intended limit.

The bolted connection in the road safety barrier will experience loads in a combination of tension and shear. Shakir-Khalil and Ho found that the capacity of the bolt is greatest when loaded in a combination of tension and shear, where the tension load is dominant. This is however dependent on the shear plane of loading. If the shear plane of loading is in the shank the observation above is correct, but Shakir-Khalil and Ho determined that the ultimate capacity was found in pure tension if the shear plane of loading is in the threaded section. In the road safety barrier a correctly assembled bolted connection has its shear plane of loading in the shank section of the bolt.

Also noteworthy is the capacity of the bolt threads compared to the bolt tensile capacity. The threads experience lower capacity than the cross-section in tension. The thread testing by Bakken-Berg and Iversen was performed using a standard M10 nut when loading the bolt in tension. Bakken-Berg and Iversen found in their tests that the bolt would fail in the threads when loaded in tension if the threaded engagement was insufficient. This shows that the threaded engagement is significant in determining the failure mode of the bolt loaded in tension. It also indicates that the bolt with a standard M10 nut will exhibit thread stripping as its failure mode during tension loading. This is

supported by the experiments of Shakir-Khalil and Ho[7], Mouritz[8] and Fransplass[10]. Shakir-Khalil and Ho experienced thread stripping in their tests when loading in 15° or less, *i.e* tension dominated loading. They used double nuts in these instances in order to eliminate thread stripping as a failure mode. Mouritz found that the threads had lower ultimate tensile strength than the shank of the bolt, and had to modify the shank cross-section in his tests in order to induce failure in the shank material. Mouritz also found that the relative strength of the threads compared to the bolt shank is reduced with an increase in strain rate. Fransplass found that the failure mode of bolts is dependent on the threaded engagement, grip length and strain rate. Fransplass also found that higher strain rates increase the ultimate tensile strength of the bolt. The purpose of the road safety barrier with the bolted connection is to absorb vehicular impacts, which entails fast loading and high strain rates. This increase in the bolt strength during high strain rates must be accounted for when designing the bolted connection, if the bolt is to fail at the desired stage of the collision.

4 Theory

In this chapter the theory on the calculation of failure loads of threaded assemblies will be presented, as well as a brief introduction on the workings of a DIC analysis.

4.1 Analysis and Designs of Threaded Assemblies

The work of Alexander[11] describes how the maximum load level of a threaded assembly can be calculated. There are three different failures modes for a fastener assembly subject to static tensile overload:

- **Bolt breaking** - Occurs when the internally threaded material, the nut in this case, is relatively strong and the length of thread engagement is relatively long.
- **Bolt thread stripping** - Occurs when the internally threaded material is relatively strong and the length of thread engagement is short.
- **Internal thread stripping** - Occurs when the internally threaded material is relatively weak and the length of thread engagement is short.

To determine the bolt stripping load, F_{bs} , and bolt breaking load, F_{bb} , the following formulas can be used:

$$F_{BB} = \sigma_s \cdot A_s \quad (4.1)$$

$$F_{BS} = \sigma_s \cdot AS_s \cdot C_1 \cdot C_2 \cdot 0.6 \quad (4.2)$$

The formula for F_{bs} is based on numerous experimental results with a wide range of mechanical property combinations and is derived by Alexander. As seen from equation 4.2 the bolt stripping load is dependent upon several factors discussed in the following

section. All equations needed to determine the various factors in equation 4.2 are presented in Appendix D.

4.1.1 Factors that influence the strength of screw threads

The geometrical design has a lot of influence on the strength of screw threads. The tensile stress area of the bolt, A_s , has a proportional relationship with the bolt breaking load, as seen in equation 4.1. The shear area of the external threads, AS_s , is the area of intersection between the external threads and a cylinder with a diameter equal to the minor diameter of the mating nut and with height equal to the length of thread engagement. The length of thread engagement, LE , is less than the height of the bolt, due to the presence of the countersink. It was found empirically that the portion of the nut for which the countersink is present only contributes 40 percent of the strength compared to an equal height without the countersink.

The material properties of the bolt and nut are important with regards to the strength of screw threads. The ultimate strength of the externally threaded material, i.e. the bolt, σ_s ; is directly proportional to the bolt breaking load as seen from equation 4.1. Moreover, the relationship between the ultimate strength of the internally threaded material, i.e. the nut, σ_n , and σ_s is important when determining C_2 . This relationship in addition to the relationship between the shear area of the internal threads, AS_n , and AS_s make up R_s , the relative strength of the nut to bolt threads. Figure 4.2b shows the relationship between the bolt stripping factor C_2 and R_s .

The ratio between the shear strength and ultimate tensile strength is also a factor in equation 4.2. Based on a wide range of ultimate tensile strength tests a value of 0.6 is used. There is however some uncertainty in this factor as it is impossible to investigate this factor in isolation due to the simultaneous bending of the threads.

Other factors that influence the strength of screw threads is nut dilation, the coefficient of friction, the number of threads in the grip as well as the applied torque. During loading the 60° threads cause dilation of the nut resulting in an increased minor diameter and in a reduced effectiveness of both the internal and external threads. This is accounted for by the C_1 parameter which is illustrated in figure 4.2a. A low coefficient of friction reduces the resistance to thread stripping, as it allows the nut to dilate more readily. In addition to increasing the bolt breaking load, a reduction in the number of threads in the grip may cause necking to occur at the engaged threads within the nut which will cause a reduction in stripping load. Figure 4.1 shows a typical relationship

between the failure load and the number of threads in the grip.

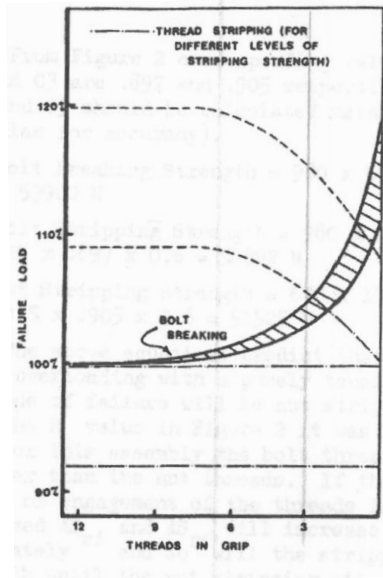


Figure 4.1: Failure load versus threads in the grip[11]

If the load is applied through tightening of the nut or bolt both F_{bb} and F_{bs} is markedly reduced. The reduction in F_{bb} is caused by the additional shear force introduced by the applied torque transmitted through the threads to the shank of the bolt, while the reduction in F_{bs} is due to the severe nut dilation caused by the applied torque.

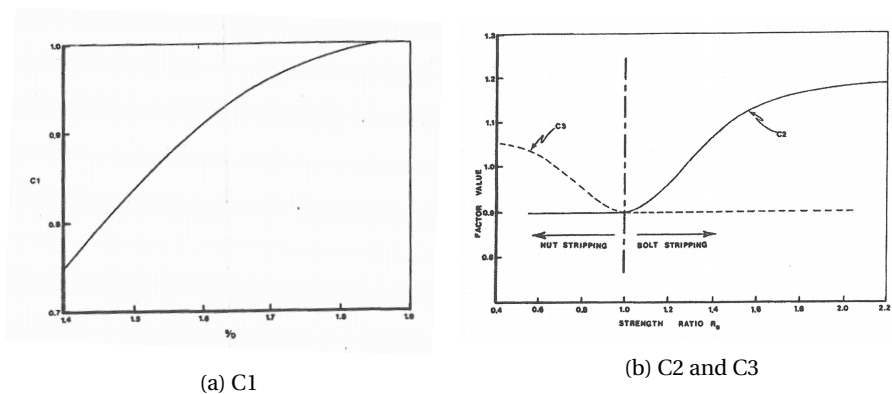


Figure 4.2: Nut dilation factor and bolt stripping factor[11]

4.2 Digital Image Correlation

Digital image correlation will be used in the laboratory tests to measure displacements. Digital image correlation, referred to as DIC, is an optical technique that employs image registration techniques to track and measure changes in images. DIC tracks features in space and assign them to a predetermined coordinate system. Deformation of the specimen between a reference state and a deformed state is described by a set of parameters in the DIC algorithm. These parameters are calculated in an optimization algorithm where the differences in grayscale values between the reference and the current image is minimized. Further details concerning this optimization process can be found in the thesis by E. Fagerholt[15].

A mathematical transformation is used to relate the image coordinate system to the coordinate system of the specimen and is often referred to as the "camera model". An illustration is shown in figure 4.3. This is described in detail by Fagerholt.

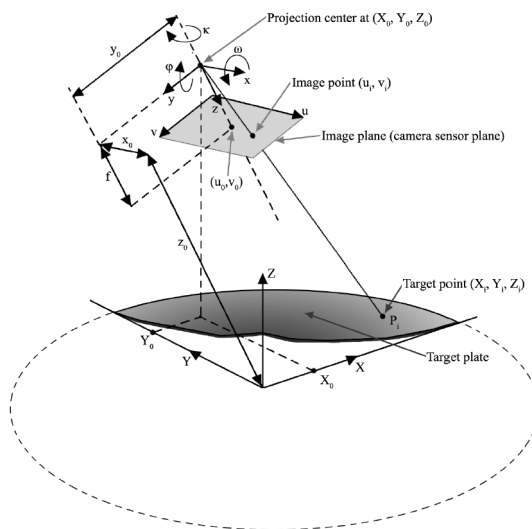


Figure 4.3: Coordinates systems in a DIC camera model[15]

For engineering purposes DIC can be used to measure displacements, rotations and strain gradients in complex geometries by post-processing images taken during a test. In addition, the experimental data provided by DIC can be used to verify finite element simulations as the data is directly comparable.

The main advantages of using DIC compared to extensometers or strain gauges is that the geometry can be quite complex, as no contact with the test sample is required. As the analysis is done by post-processing it is easy to measure relative displacements between various locations of the test sample. To ensure high accuracy the cameras are calibrated before the test, so that the DIC software can calculate the cameras position relative to each other as well as the test sample. The main advantage of using 3D-DIC as opposed to 2D-DIC is that the out-of-plane deformation is taken into account in the measurements.

Disadvantages of using DIC compared to strain gauges or extensometers is that a clear line of sight is required which excludes the possibility for measuring response of internal components. When applying 3D-DIC a significant amount of preparation in setup and calibration of the cameras is required. Also, when comparing 2D-DIC to 3D-DIC, the image post-processing of 3D-DIC is considerably more extensive.

5 Laboratory Work

Laboratory tests were performed on the road safety barrier to study the behaviour of the road safety barrier during loading. The main focus is the bolted connection between the W-beam and the Σ -post. The behaviour of the standard bolt used in the road safety barrier have been studied previously and it is desired to study the behaviour of the full connection. The road safety barrier was tested in pure tension and in combinations of tension and shear.

5.1 Design of the laboratory tests

The road safety barrier tested in the laboratory consists of cut sections of the W-beam and Σ -post connected by the bolted connection with washers. The road safety barrier is fastened via the Σ -post to a cradle which allows for rotation of the road safety barrier. This is to enable loading in a combination of tension and shear. The loading is applied through a loading clamp which is fastened to the W-beam in order to ensure evenly distributed loading. Longitudinal washers are used in the connection between the W-beam and the loading clamp, and the Σ -post and the cradle. The cradle with the road safety barrier is placed into a *Dartec 500 universal testing machine* which is used to apply the load. The setup can be seen in figure 5.1.A more schematic view of the laboratory test setup can be seen in Appendix B.

5.1.1 Geometry of the road safety barrier

The configuration of the road safety barrier tested in the laboratory consists of 400 mm long sections of the W-beam and Σ -post. Exact geometry of the W-beam and Σ -post can be seen in Appendix A.1 and A.2. The length is based on the lengths used by D'Angelo in his numerical model of the road safety barrier[12]. This length also provides for easier

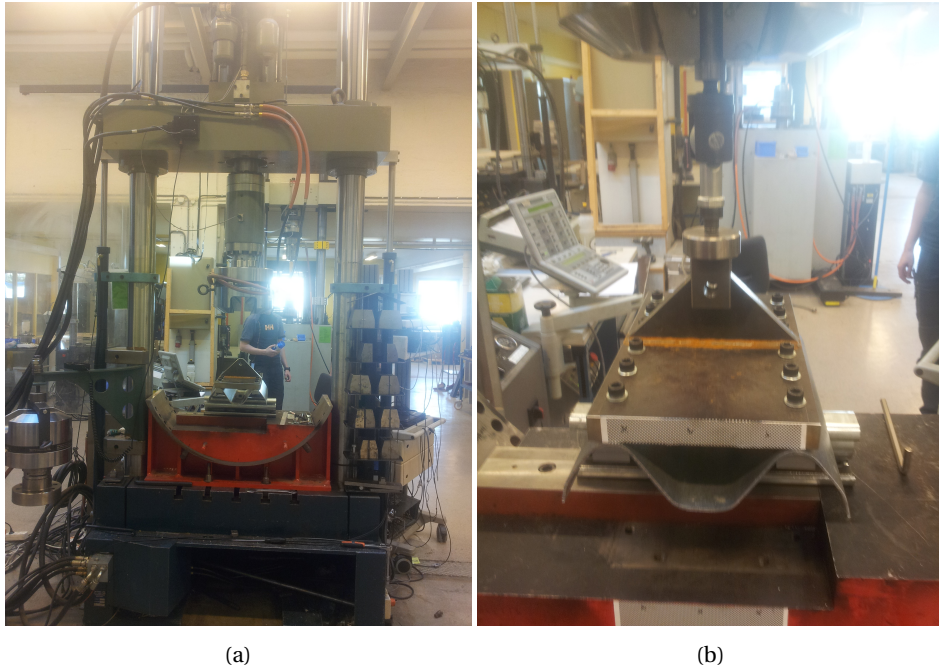


Figure 5.1: Laboratory test setup

testing in the laboratory. The cold-roll forming process of the W-beam and Σ -post do not produce perfect geometries according to specifications. Some geometrical imperfections are to be expected, notably in the cross-sectional thickness. During laboratory testing the thickness of the W-beam and Σ -post cross-sections used were measured. The data is documented in Appendix C.

5.1.2 The cradle

The cradle used in the laboratory tests was purpose made for the study of "Oblique loading of aluminium crash components" in the PhD thesis of Reyes[16] at SIMLab. In this thesis the cradle is used to rotate the road safety barrier to enable loading in a combination of tension and shear. The cradle consists of a wagon connected to a fixed base. The wagon can rotate in a circular groove in increments of 5° from 0° to 30° . The geometry of the cradle can be seen in Appendix A.5.

5.1.3 Design of the loading clamp

The loading clamp is specially designed for the laboratory tests. The purpose of the loading clamp is to evenly distribute the applied load onto the W-beam. This is to avoid local deformation of the W-beam and ensure that the load is properly transferred to the bolted connection. A design for the loading clamp was proposed by D'Angelo in his thesis[12]. This was found to be unnecessarily complex to make and overly cumbersome. A more simple design was adopted instead. The loading clamp can be seen in figure 5.2. The exact geometry with measurements can be seen in Appendix A.4. The load is applied to a pin which is inserted through the hole in the vertical plate. A series of M12 bolts connect the loading clamp to the W-beam. The loading clamp must be adequately rigid so that it does not deform and influence measurements made during testing. To make sure of this design calculations in accordance with Eurocode 3 have been carried out[14, 17]. The calculations for necessary capacity of the loading clamp are based on a maximum load on the bolt of 50 kN. This value was determined as an adequate upper value based on the numerical analyses by D'Angelo of the road safety barrier. Detailed calculations on the capacity of the loading clamp can be seen in Appendix E. The results from the calculations are summarized next.

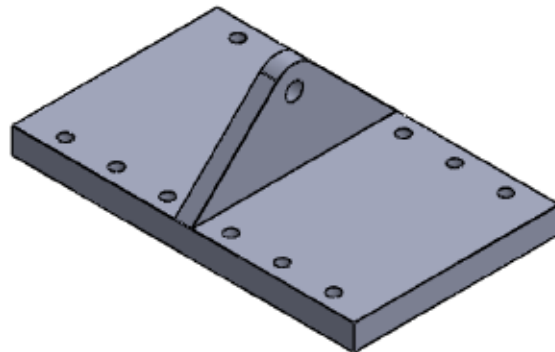


Figure 5.2: Loading clamp for the laboratory tests

The pin must have an adequate shear and moments capacity to transfer the load. An adequate diameter of the pin to carry the shear forces is calculated, and this diameter is then used in controlling the moment capacity and interaction capacity of the pin. The results of the calculations are summarized in table 5.1.

Table 5.1: Capacity calculations of the pin

Shear capacity	D_{min}	18.2 mm
Moment capacity	M_{Ed}	0.188 kNm
	M_{Rd}	0.539 kNm
Interaction	$\left(\frac{M_{Ed}}{M_{Rd}}\right)^2 + \left(\frac{F_{v,Ed}}{F_{v,Rd}}\right)^2 \leq 1$	0.96

It can be seen that the pin requires a minimum diameter of 18.2 mm. The diameter of the bolt is set to 20 mm in a conservative effort. This diameter is sufficient for both moment capacity of the bolt and the interaction capacity.

The vertical plate of the loading clamp must have adequate thickness to resist the shear forces transferred from the pin. The pin connection between the clamp and the Dartec 500 machine limits the height of the plate above the pin hole to 20 mm. This affects the necessary thickness of the vertical plate to have enough bearing resistance. The vertical plate is also susceptible to bending moments about the weak axis, due to the unsymmetrical cross-section of the Σ -post. The moment capacity about the weak axis based on the calculated necessary thickness is therefore calculated. The capacity of the weld between the vertical and the horizontal plate is controlled. The results from the calculations are summarized in table 5.2.

Table 5.2: Capacity calculations of the vertical plate

Necessary thickness	t_{min}	16.4 mm
Moment capacity	M_{Ed}	1.3 kNm
	M_{Rd}	3.352 kNm
Weld capacity	q_w	139 N/mm
	$f_{w,d}$	332.6 N/mm

The bearing resistance of the vertical plate requires a minimum thickness of 16.4 mm. This is increased to 20 mm in a conservative effort. It can be seen that both the moment resistance and the weld resistance of the vertical plate is adequate.

The M12 bolts used to connect the loading clamp to the W-beam are controlled for adequate capacity. The bolts must transfer the load when in pure tension but also in

a combination of tension and shear. In the calculations only the four bolts closest to the vertical plate are assumed to carry the load. The results from the calculations are summarized in table 5.3. The results shown are per. bolt.

Table 5.3: Capacity of the M12 bolts

Pure tension	$F_{t,Ed}$ $F_{t,Rd}$	18.3 kN 24.2 kN
Tension and shear interaction	$\frac{F_{v,Ed}}{F_{v,Rd}} + \frac{F_{t,Ed}}{1.4 F_{t,Rd}} \leq 1$	0.89

5.2 Changes to the test rig

When the laboratory specimen were to be assembled for the first time it was discovered that the holes of the loading clamp did not match the holes in the W-beam. It was discovered that the holes on the top of the two arcs of the W-beam were closer than expected. The reason for this was discrepancies in the dimensions between the drawing of the W-beam and the produced section. Since the loading clamp was designed according to production drawings of the W-beam the bolt holes of the clamp had to be modified. This was done by turning them into slots. The final version of the clamp is shown in figure 5.3.

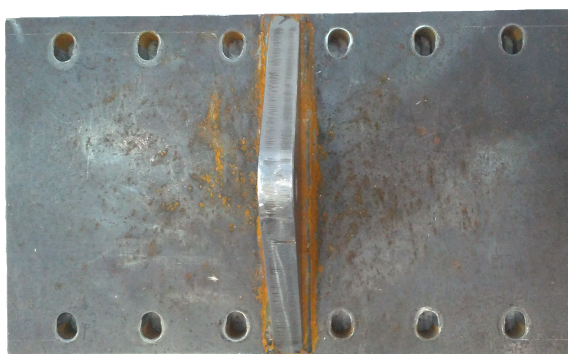
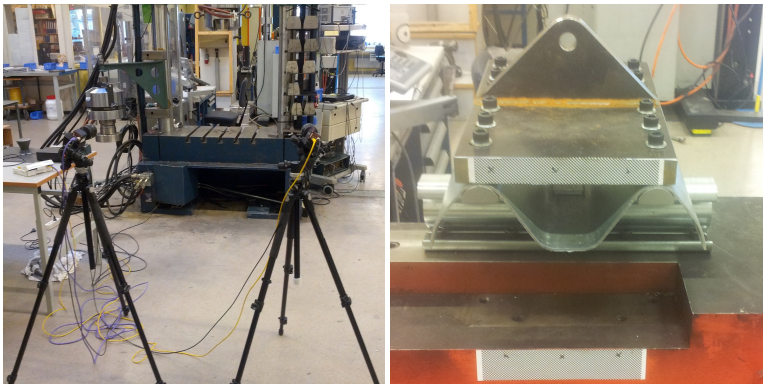


Figure 5.3: Slots in the loading clamp

5.3 Setting up the DIC

In order to get accurate measurements of the displacements in the road safety barrier section during laboratory testing it was decided to use DIC. Both force and displacement data were automatically extracted from the Dartec 500 during testing, but it was desired to eliminate possible displacements in the Dartec itself which could be introduced in the displacement data. DIC was used to measure the relative displacement between the cradle and the loading clamp. To be able to detect any out-of-plane movement it was decided to use a 3D-DIC setup. The setup consisted of two cameras connected to a laptop to be able to record the data. The velocity of the test rig was set to 1 mm/s, while the DIC software was set to record one image every third second in order to limit the amount of data. As this provided more than 600 images during the test the resolution of the test results would be at an acceptable level. Grayscale sheets were glued to parallel surfaces of the cradle and the loading clamp to give the DIC-software reference points to measure the relative displacement from. The camera setup that was used along with the grayscale sheets glued to the surfaces of interest are shown in figure 5.4a and 5.4b.



(a) Camera setup for DIC

(b) Grayscale sheet locations

Figure 5.4: DIC setup used in laboratory tests

5.4 Implementation of the tests in the laboratory

A total of 14 tests were run on the road safety barrier in the laboratory. Six at 0° and four at 15° and 30°. Displacement control at 1 mm/s was used for the loading of each test.

Force and displacement data were extracted from the Dartec 500 machine for each test. Displacement of the loading clamp relative to the cradle was also extracted using DIC. Each test was run to failure of the bolted connection.

The test specimen were assembled as described in section 5.1 and seen in figure 5.1. The connection between the Dartec 500 and the loading clamp consisted of a pin connection, followed by a rod and a joint connection. This can be seen in figure 5.5. Care was taken for each test that the pin connection and the joint connection were aligned one on top of the other, so that no extra loading angles were added to the tests.

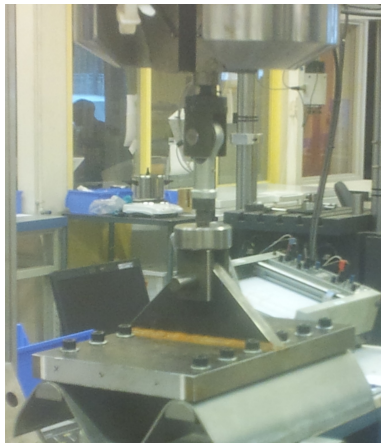


Figure 5.5: Connection used to apply the loading

The configuration of the tests at different angles of loading can be seen in figure 5.6. In the 15° and 30° configuration the position of the cradle in the Dartec 500 had to be rotated. This was in order to properly align the pin connection with the joint connection as previously described.

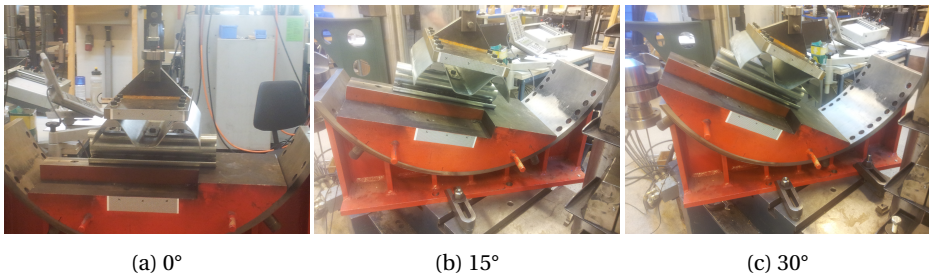


Figure 5.6: Configuration of the tests at different angles

5.5 Results of the laboratory tests

In this section the results from the laboratory test will be presented. Relative displacements of the road safety barrier were extracted using DIC from two points on the loading clamp right above the longitudinal washers of the W-beam. The displacement data used in the force-displacement curves are from the rightmost of the two point. The two points used for data extraction are illustrated in figure 5.7.

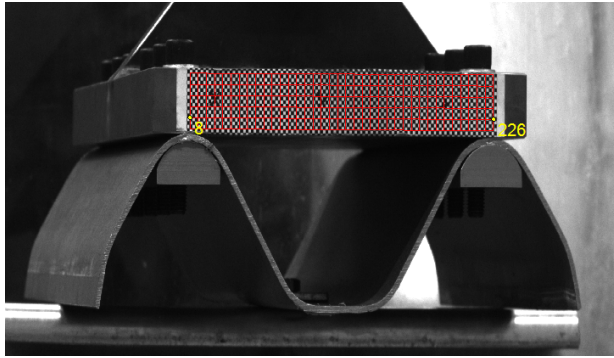


Figure 5.7: The two points where the DIC data was extracted

5.5.1 0° configuration

A total of six tests were run in the 0° configuration. Out of these, five are included in the results. The fourth test run in the 0° configuration experienced an error where the connection to the Dartec 500 was not properly clamped. This resulted in erroneous application of the displacement inconsistent with the other tests, and these results are therefore omitted. The results of the remaining five tests in the 0° configuration are presented in table 5.4 and can be seen in figure 5.8. Test 1 was terminated before the bolt had been pulled all the way through the nut.

Table 5.4: Results from laboratory tests in 0° configuration

	F_1 [kN]	F_u [kN]	n_u
Test 1	19.64	22.73	4
Test 2	18.00	21.74	2
Test 3	19.79	19.79	1
Test 5	19.93	21.44	3
Test 6	21.39	21.39	1

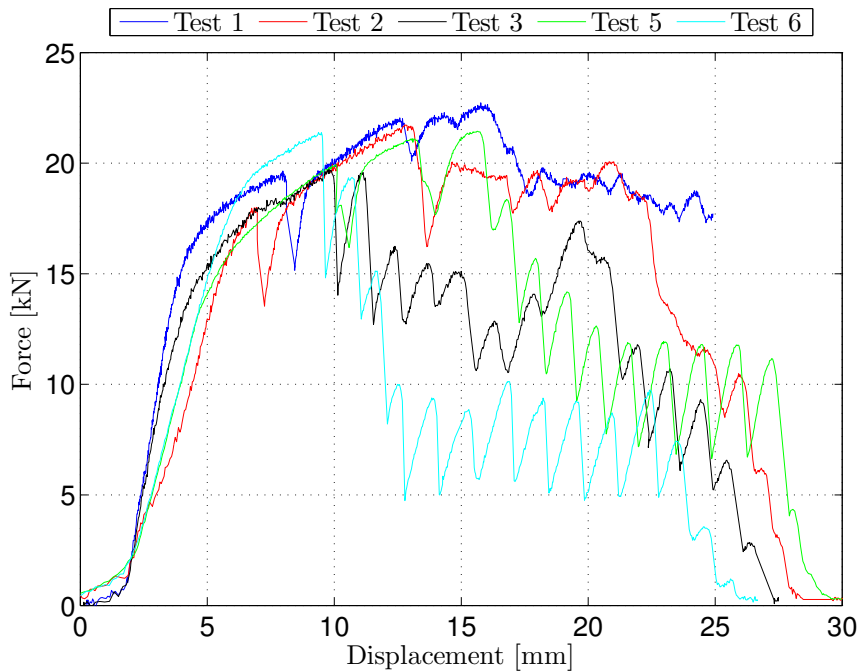


Figure 5.8: Force-displacement curves for tests in the 0° configuration

The results in figure 5.8 show clear signs of thread stripping. Peaks with sudden drops in the force indicate the failure of a thread. The number of peaks further indicate that it is the threads in the bolt that fails, as the nut only has 3-4 threads. The ultimate load, F_u , varied between 19.8 and 22.7 kN, while the force level when the first thread stripped, F_1 , was in the region 18.0-21.4 kN. This relatively large variation in F_u was also seen in the tests performed by Bakken-Berg and Iversen, discussed in section 3.2. The number of threads stripped when the ultimate load occurred, n_u , was inconsistent between the tests and varied from one to four.

5.5.2 15° configuration

In table 5.5 and figure 5.9 the results from the four tests in the 15° configuration are presented.

Table 5.5: Results from laboratory tests in 15° configuration

	F_1 [kN]	F_u [kN]	n_u
Test 1	14.14	18.23	3
Test 2	15.41	17.18	2
Test 3	17.48	17.57	2
Test 4	15.41	18.95	2

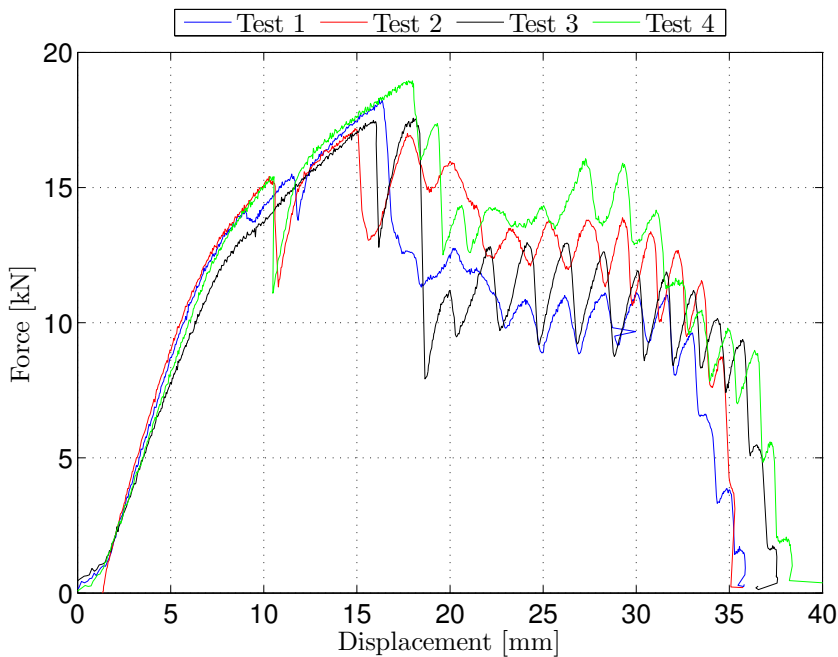


Figure 5.9: Force-displacement curves for tests in the 15° configuration

In the 15° configuration the variation seen in F_u and F_1 was approximately the same as in the 0° configuration, only at a lower load level. A tendency in n_u was seen, where all but one test reached the ultimate load as the second thread stripped. There is in addition some uncertainty with regards to n_u in test 1, where the drop in the force level when what seems to be the failure of the first thread occurred is not as significant as what was seen in the other tests.

5.5.3 30° configuration

Four tests were run in the 30° configuration. The results are presented in table 5.6 and figure 5.10.

Table 5.6: Results from laboratory tests in the 30° configuration

	F_1 [kN]	F_u [kN]	n_u
Test 1	17.93	17.93	1
Test 2	14.68	14.68	1
Test 3	14.99	18.58	3
Test 4	19.74	19.74	1

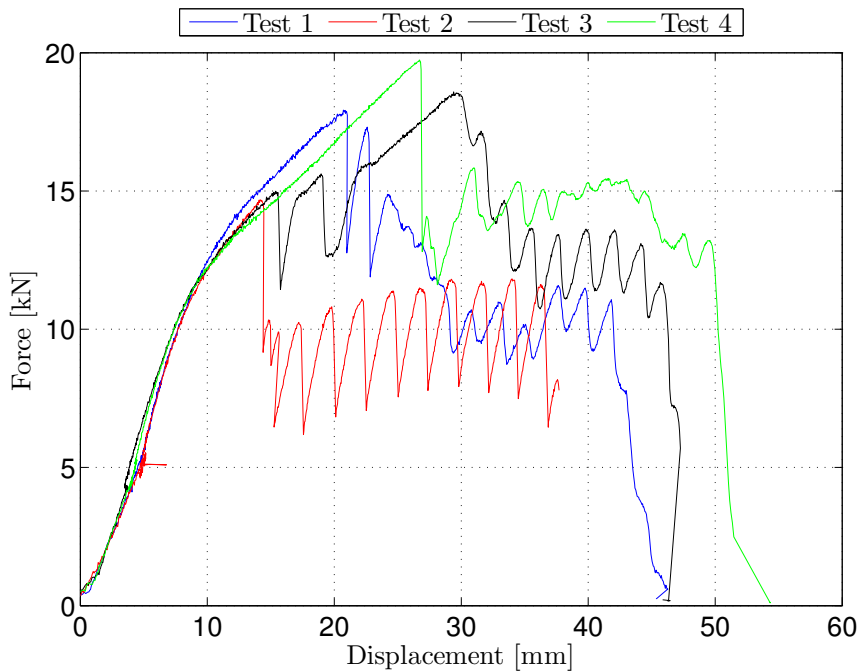


Figure 5.10: Force-displacement curves for tests in the 30° configuration

In the 30° configuration a rather large variation in both F_u and F_1 was seen. F_u and F_1 ranged from 14.7 to 19.7 kN. In all but test 3 n_u is equal to 1, while in test 3 n_u is equal to 3. Due to the rather large discrepancies in both F_u and n_u no certain tendencies could be seen based on the four tests performed in the 30° configuration.

5.6 Laboratory test observations

The failure mode in all the laboratory tests was thread stripping. The threads in the bolt deformed and failed as the force applied by the Dartec 500 increased. In figure 5.11 a typical bolt and nut after failure is shown.



Figure 5.11: Deformed bolt and 30×30×3 mm washer in the 30° configuration

As seen in figure 5.11 some of the material from the bolt remained in the nut after fracture. It is clear that the bolt material is weaker than that of the nut, but there were sign of deformation of the nut as well. The bolt in figure 5.11 has been bent in the area where the nut initially was mounted. This was true for all configurations. In the 0° configuration this was mainly due to the rotation of the road safety barrier caused by the deformation of the Σ -post. In the 15° and 30° configurations the rotation about the longitudinal axis of the W-beam caused by the rotation of the test rig resulted in even more bending of the bolt.

Plastic deformation of the W-beam was observed in all the tests. The magnitude of the deformation did vary however, as can be seen in figure 5.12.

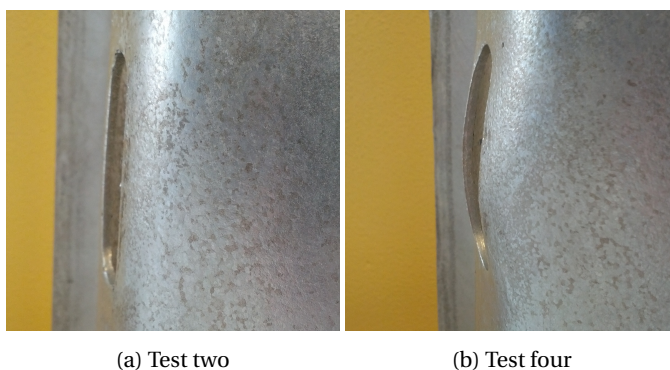
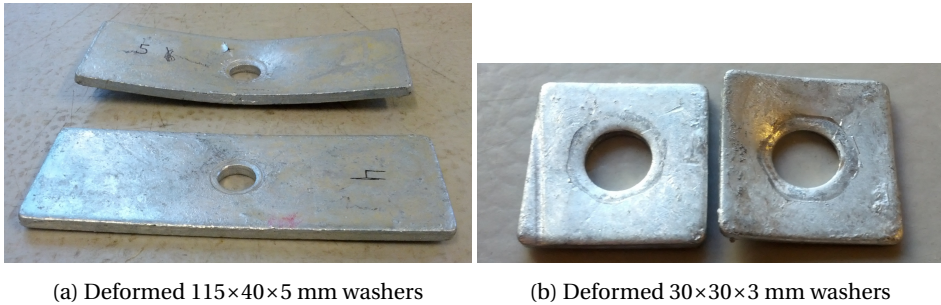


Figure 5.12: Deformation of W-beam in 30° configuration

The clear difference in plastic deformation between test two and four in the 30° configuration can be seen as a direct effect of the difference in ultimate load between the two tests. The same variation in plastic deformation was seen in both of the washers used in the bolt connection, as can be seen in figure 5.13.



(a) Deformed 115×40×5 mm washers

(b) Deformed 30×30×3 mm washers

Figure 5.13: Deformation of the washers

The deformation seen in the W-beam, the Σ -post and both washers are naturally closely related to each other and the peak load of the test. The tests with the largest peak loads also had the largest plastic deformations. The Σ -post did not have as much plastic deformation as the W-beam, partly due to the material being slightly stiffer and the fact that the section itself was thicker. In figure 5.14 one of the Σ -posts with the most plastic deformation is displayed.



Figure 5.14: Deformed Σ -post from test two in the 0° configuration

5.7 Sources of errors and variations in the test results

The many connections in the test rig is an important factor when considering the reasons for the variations seen in the test results. The bolt connecting the W-beam with the Σ -post and the bolts connecting the clamp with the W-beam are inserted through slots, making significant relative movement of the parts possible. In both of the aforementioned connections the slots and the holes were aligned by visual estimates. This may in turn lead to discrepancies in the response as the effect of misalignment of the bolt affect the response of the system, as discussed in section 2.5.2.

Geometrical imperfections in the parts could also cause variations in the results. For instance some of the washers were bent prior to testing. Variations in the thickness of the test samples were recorded in table C.3. The thickness of both the W-beam and the Σ -post was measured for each test sample. The data is presented in table C.1 and C.2. The average thickness of the Σ -post varies by 4-5 percent while the W-beam varies by 7-8 percent. Taking into account that the thickness of the 30×30×3 mm washer varies by approximately 20 percent and the 110×40×5 mm washer by up to 15 percent the stiffness of the test rig may be affected; especially if all of the parts are close to either their maximum or minimum thickness.

The amount of torque used to tighten the bolt and nut between the Σ -post and the W-beam may also have influenced the results. The torque level used was not measured, but the bolt was tightend as much as possible by hand with a short armed wrench. The tests in the 0° configuration were performed first and amount the of torque used to tighten the bolt may vary more in this configuration than in the two others, as the torque was not applied in a consistent manner in the first couple of tests. As documented by Bakken-Berg and Iversen[9], and D'Angelo[12], there were variations in the material properties among different samples of the bolt, W-beam and the Σ -post. Both the yield stress and the ultimate tensile strength can vary, as discussed in section 2.3.2, which could cause significant variation in the behaviour of the test samples.

5.8 Hardness test on the bolt

A Vickers hardness test was conducted in an effort to determine if the material properties of the bolt varied through the cross-section. A bolt was cut in half along the longitudinal axes of the bolt as illustrated in figure 5.15. Indicated on the figure is the area of the bolt where the hardness test was performed.



Figure 5.15: Bolt cut in half in preparation for the hardness test

The test was performed with 10 kgf. The result of the hardness test is presented in figure 5.16. The Vickers pyramid number varied from 178 to 195 throughout the

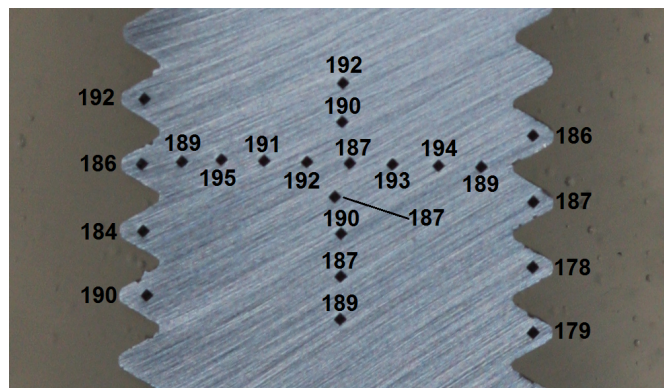


Figure 5.16: Result from the hardness test on the bolt

section. Since the test was performed on only one bolt it not possible to draw any certain conclusion from the test. However, the six lowest Vickers pyramid numbers occurred in the threads. This indicates that the threads might be slightly softer than the core of the bolt. To verify this however, a more thorough investigation should be conducted.

6 Material Models

The uniaxial tension tests and the corresponding data used to establish the material models of the W-beam, the Σ -post and the bolt were performed by L. D'Angelo during his master's thesis at NTNU in 2012[12].

6.1 W-beam and Σ -post

Five tests were carried out on the material of both the W-beam and the Σ -post. For both the W-beam and the Σ -post one out of the five tests was chosen as basis for the material model. For the W-beam the material test data from location W1 in figure 2.11 was used as this was the only part of the section where any plastic deformations was seen in the laboratory tests. The stress-strain relationship data of the material was calculated from the force-displacement data from the material test using *Matlab*. The stress and strain data calculated is only viable up to necking in the material test. To determine when necking occurred the following criteria was used:

$$\sigma(\epsilon) = \frac{d\sigma}{d\epsilon} \quad (6.1)$$

In figure 6.1 the material test data and the necking criteria in equation 6.1 is plotted.

To eliminate the effect of geometrical changes in the specimen the stress-strain curves were converted to true stress-true strain curves by the following equations:

$$\epsilon = \ln(1 + \epsilon_e) \quad \sigma = \sigma_e(1 + \epsilon_e), \quad (6.2)$$

where ϵ_e and σ_e are the engineering strains and stresses respectively. The Young's modulus, E , was calculated based on the middle third of the elastic area of the stress-strain curve using linear regression. The yield stress was determined as the average stress of the

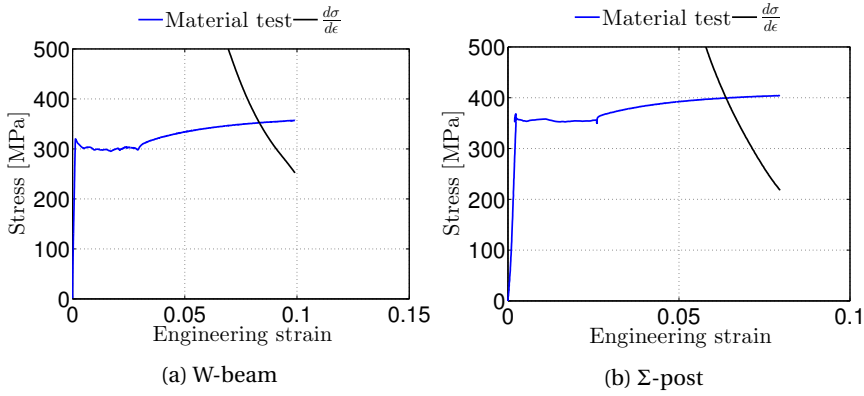


Figure 6.1: Strains up to necking for W-beam and Σ -post

yield plateau. To model the W-beam and the Σ -post a modified *power law* formulation including the plateau strain was used [18]:

$$f(n) = \begin{cases} \sigma_Y & \text{if } \epsilon_{eq} \leq \epsilon_{plat} \\ K(\epsilon_{eq} + \epsilon_0)^n & \text{otherwise} \end{cases} \quad (6.3)$$

where K and n are material coefficients, ϵ_{eq} is the equivalent plastic strain at plateau exit and σ_Y denotes the initial yield stress. The plateau strain and the power law expression intersects at $(\epsilon_{plat}, \sigma_Y)$ when:

$$\epsilon_0 = \left(\frac{\sigma_Y}{K}\right)^{\frac{1}{n}} - \epsilon_{plat} \quad (6.4)$$

In Matlab a nonlinear least-square fitting function was used to find the coefficients for the material models. The resulting material models are plotted against their respective material test for the W-beam and the Σ -post in figure 6.2 and 6.3. A summary of the material parameters found for the W-beam and the Σ -post are shown in the table 6.1.

Table 6.1: Material parameters for the W-beam and Σ -post

Material	E	σ_y	σ_{eq}	K	n
W-beam	203 000	306	0.025	540.4	0.1278
Σ -post	204 000	361	0.020	581.4	0.1040

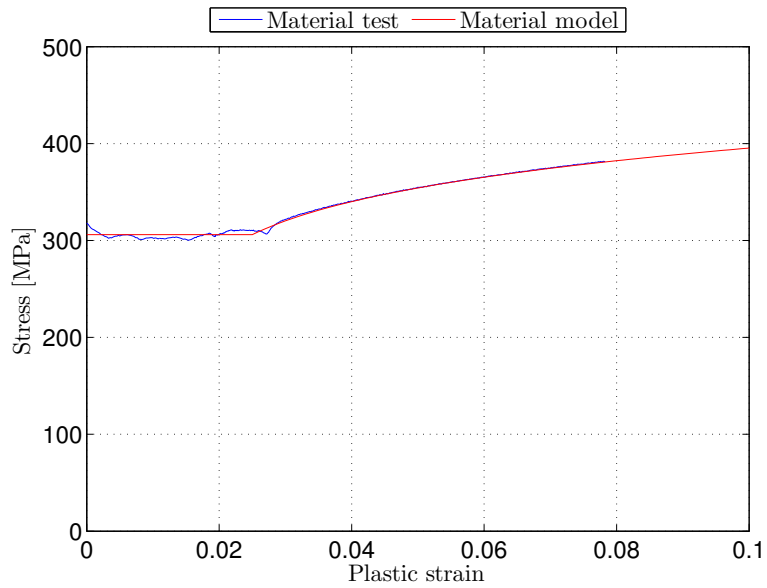
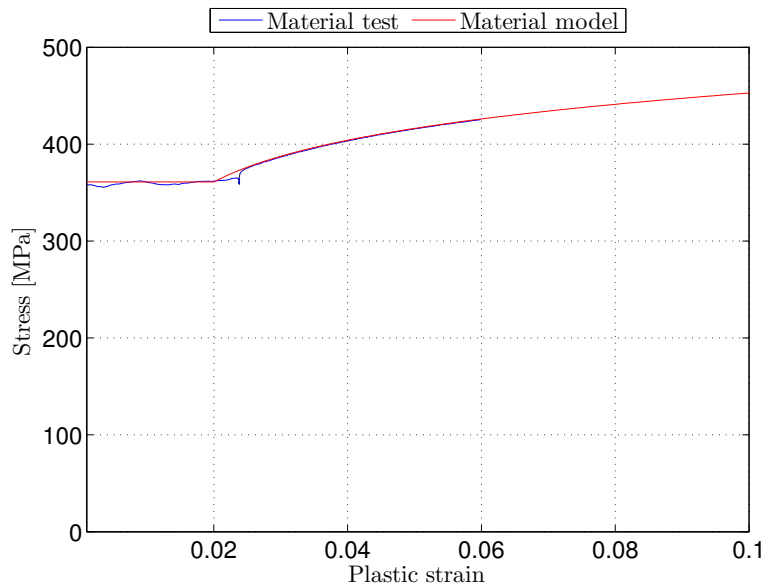


Figure 6.2: Material model of the W-beam

Figure 6.3: Material model of the Σ -post

6.2 Bolts

The same procedure as for the W-beam and Σ -post was used to process the test data for the bolt, but as the extended power law did not fit very well to the bolt test data it was decided to use a *Voce* formulation instead:

$$R(p) = Q_R \left(1 - e^{\left(\frac{\theta_R}{Q_R} \right) \cdot p} \right) \quad (6.5)$$

where Q_R and θ_R are material coefficients and p is the equivalent plastic strain. To fit the model to the material test only one Voce term was needed. However, to adjust the behaviour of the material after necking a second Voce term was fitted through iterative simulations of the bolt tensile test using *Abaqus*.

6.2.1 Finite element model of the bolt tensile test

The finite element model of the bolt material test was modelled using *Abaqus/Explicit*. The model was created in order to create a working material model of the bolt which is viable beyond necking. An iterative process was performed where the material model fitted to data up to necking was inserted into the finite element model, and then adjusted based on the response in the analyses. When the material model was deemed satisfactory accurate it was used in the finite element model to create a damage criteria. The finite element model of the bolt material test can be seen in figure 6.4.

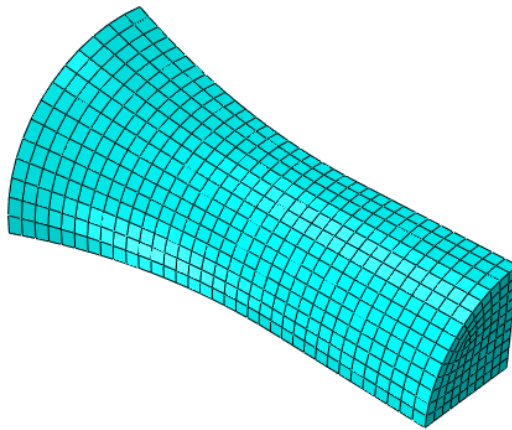


Figure 6.4: FE model of the bolt material test

The model was created exploiting the symmetry of the material test specimen in order to reduce computational costs. Symmetry was enforced using symmetry constraints in Abaqus. The geometry of the material test specimen was taken from the thesis of D'Angelo[12] and can be seen in figure 6.5. As can be observed only the unthreaded center area of the bolt specimen was modelled.

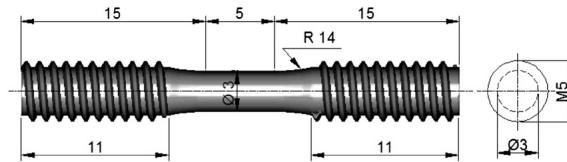


Figure 6.5: Geometry of the bolt material test specimen[12]

Loading was applied using displacement control, where a displacement of 10 mm was applied over a time period of 0.1 second to the end of the specimen. The model was created using solid elements of the type *C3D8R*, which is the default solid element in Abaqus/Explicit. It is desirable that the material model be as accurate as possible, and a fine mesh of size 0.2 mm was used. The evolution of the material test model during loading can be seen in figure 6.6.

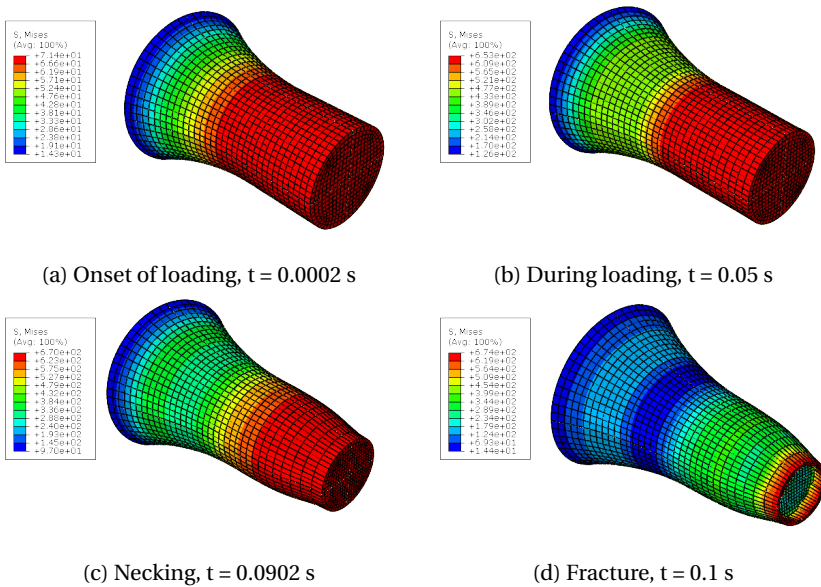


Figure 6.6: Evolution of the bolt material data model

The material parameters are presented in table 6.2. The fit of the material model with both the initial and final parameters versus the material test is illustrated in figure 6.7.

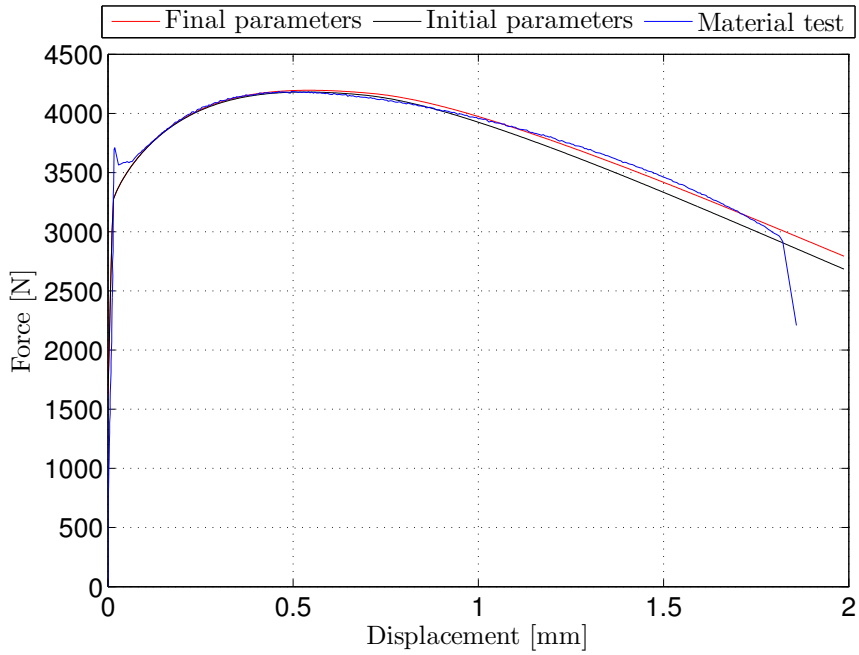


Figure 6.7: Material model of the bolt

Table 6.2: Material parameters of the bolt

Material	E	σ_y	Q_1	θ_1	Q_2	θ_2
Bolt	192 000	453	191.3	5900	100	40

6.2.2 Fracture criterion

To create a failure criterion for the bolt material model an uncoupled version of the *Extended Cockcroft-Latham criterion* was employed[19]:

$$\dot{D} = \left(\frac{\phi \hat{\sigma}_I + (1 + \phi)(\hat{\sigma}_I - \hat{\sigma}_{III})}{S_0} \right)^{s_0} \dot{p} \quad (6.6)$$

where $\hat{\sigma}_I \geq \hat{\sigma}_{II} \geq \hat{\sigma}_{III}$ are the ordered eigenvalues of the Cauchy stress tensor, $S_0 > 0$, $s_0 > 0$ and $0 \leq \phi \leq 1$ are constants defining the damage evolution and D is the damage variable. By setting $s_0=1$ and $\phi=1$ the Cockcroft-Latham criterion is obtained:

$$\dot{D} = \left(\frac{\hat{\sigma}_I}{S_0} \right) \dot{p} \quad (6.7)$$

When fracture occurs, D is equal to its critical value D_C , and thus:

$$D = \int_0^L \dot{D} dt \rightarrow \int_0^{p_f} \hat{\sigma}_I dp = D_C S_0 = W_C \quad (6.8)$$

where W_C is the Cockcroft-Latham parameter. To determine S_0 the material test of the bolt was simulated with $S_0=1$ and W_C sufficiently large so that fracture would not occur. A value of 10^{12} for D_C was used resulting in W_C of the same magnitude. The value of W_C was then extracted from the model at the same displacement as the failure occurred in the material test that the material model was based on. This is illustrated in figure 6.8. The value of D_C was then set to 1 and S_0 to 616 MPa.

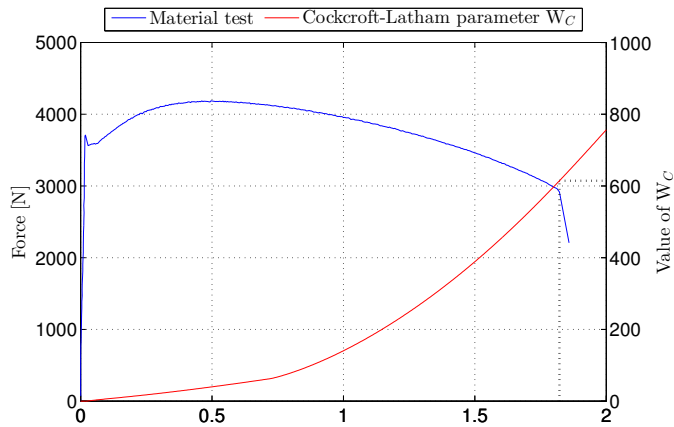


Figure 6.8: Cockcroft-Latham parameter vs material test data

The finite element model of the tensile test of the bolt was run using the established failure criterion. The resulting force-displacement comparison with the material test data is presented in figure 6.9.

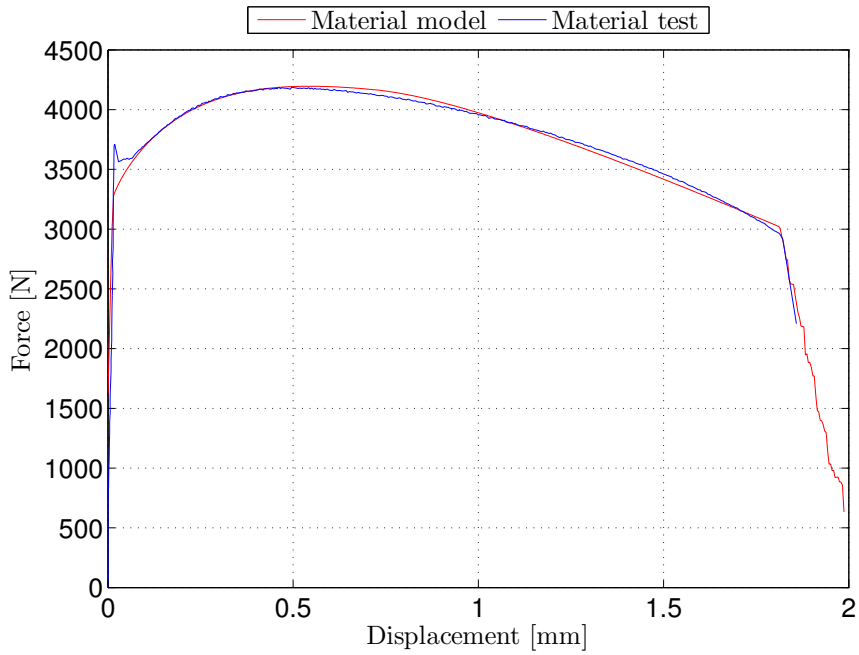


Figure 6.9: Comparison between the tensile test simulation and the material test on the bolt

7 Finite Element Models

Finite element models of the road safety barrier were created using the finite element code ABAQUS/Explicit. Abaqus/Explicit is a general-purpose finite-element analyzer that employs an explicit integration scheme. The geometry of the W-beam and the Σ -post was based on drawings received from H. Fransplass at the Norwegian Public Roads Administration, while the dimensions of the bolt, nut and washers were measured directly from the parts used in the laboratory tests. All geometries used are presented in Appendix A.

An initial model of the road safety barrier was created to be a basis for further refined models that can represent the behaviour of the connection in as accurate a way as possible. The main purpose of the initial model was to be a robust starting point using default settings and basic elements, interactions, boundary conditions and a relatively coarse mesh. The failure mode in all the laboratory tests was bolt thread stripping. This failure mode requires a fine mesh in the threads of the bolt which is much finer than the mesh used in the initial model. It was therefore decided to create a separate model of the bolt and nut with threads to model the thread stripping in order to save computational time. This also allowed for better control of the thread stripping simulations, and direct comparison of analyses results to laboratory tests performed by Bakken-Berg and Iversen[9].

When thread stripping was successfully modelled in the bolt thread stripping model, a full model of the road safety barrier with the bolted connection was created. The bolt and nut from the bolt stripping model were inserted into the initial model to create what will be referred to as the *full model*. Running this model proved very computationally expensive, and only a few analysis were run using this setup. The design of the finite element models will be presented in the current chapter, while the results of the finite element models will be presented in chapter 8.

7.1 The initial model

In figure 7.1 an outline of the initial model is presented.

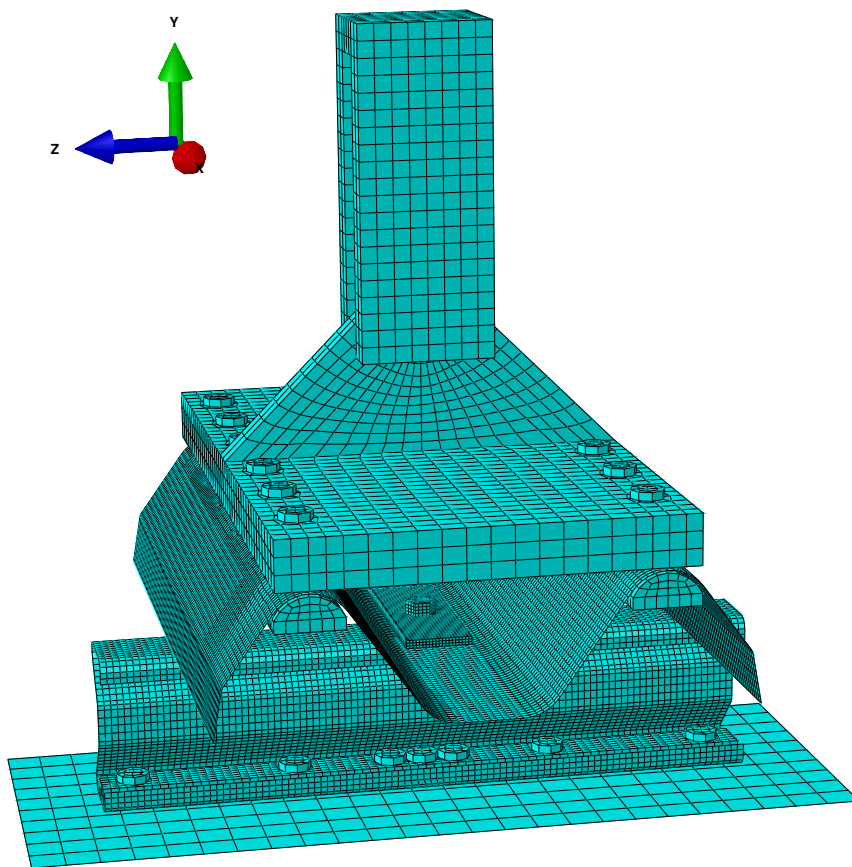


Figure 7.1: The initial finite element model

The initial model was created to replicate the laboratory test performed on the road safety barrier. As can be seen in figure 7.1, the cradle was excluded from the model, and a modified model of the connection to the Dartec 500 was created. The rigid surface of the cradle was simplified using a rigid plane. The connection between the loading clamp and Dartec 500 was modelled with the same degrees of freedom as used in the laboratory test, in order to replicate the actual loading conditions. This modified connection will

be referred to as the *y-joint*. To further simplify the initial model the bolt and nut were modelled as a single part. This would effectively eliminate thread stripping as a failure mode, but since no failure criteria was implemented in the initial model this was of no consequence.

7.1.1 Mesh

The Σ -post and the W-beam were both modelled using shell elements. The zones where contact with the washers is initiated were however modelled using solid element patches with a finer mesh. This was done in an effort to accurately model the plastic deformation which was witnessed in the W-beam, Σ -post and washers in vicinity of the bolted connection during laboratory testing. The remaining parts were modelled as solid elements.

In table 7.1 the mesh used in all parts is presented. The following figures illustrates the mesh used.

Table 7.1: Approximate element sizes for the mesh in the initial model

Part	Mesh size [mm]	Elements through thickness
W-beam	8	-
W-beam patch	4	2
Σ -post	8	-
Σ -post patch	4	2
Washer 115×40×5	4	2
Washer 30×30×3	4	2
Bolt and nut	2-4	-
Bolt M12	4-6	-
Bolt M12 long	4-6	-
Y-joint	4 10	-
Pin	4-6	-
Longitudinal washer of Σ -post	5	2
Longitudinal washer of W-beam	4	-
Loading clamp	10	-

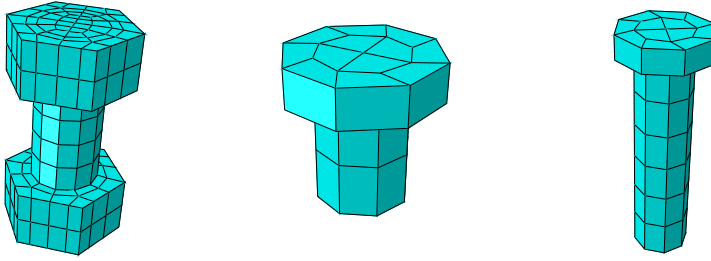


Figure 7.2: Mesh of the bolts

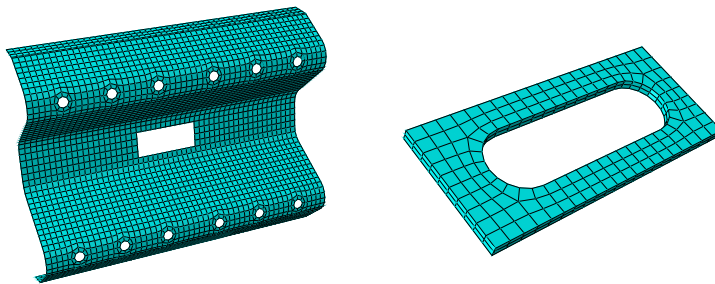
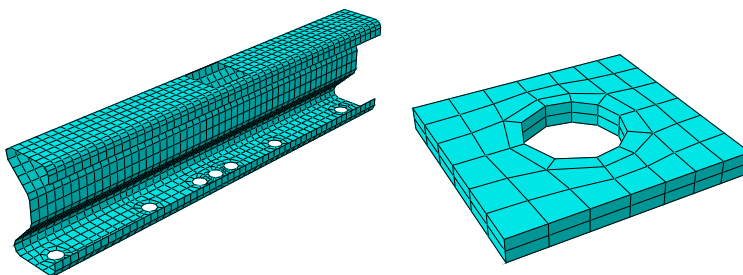


Figure 7.3: Mesh of the W-beam and the W-beam patch

Figure 7.4: Mesh of the Σ -post and the Σ -post patch

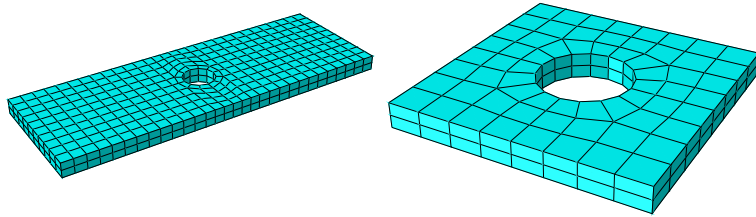


Figure 7.5: Mesh of the washers used between the W-beam and Σ -post

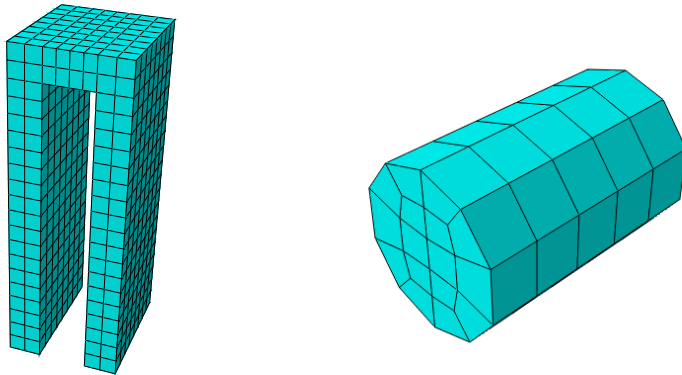


Figure 7.6: Mesh of the y-joint and pin

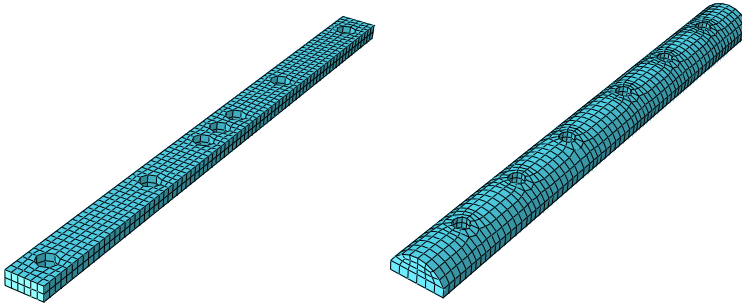


Figure 7.7: Mesh of the longitudinal washers of the W-beam and Σ -post

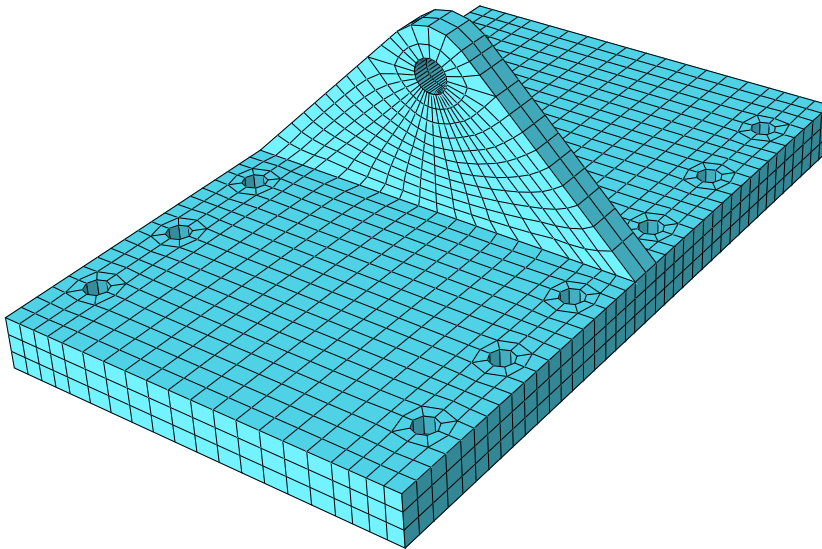


Figure 7.8: Mesh of the loading clamp

7.1.2 Boundary conditions and constraints

A rigid plane was made to model the cradle of the test rig. The rigid plane was fixed so that no movements or rotations were allowed. The end of the bolts connecting the Σ -post to the cradle were fixed to the rigid plane using tie-constraints. The bolts connecting the loading clamp to the W-beam were tied to the longitudinal washers of the W-beam. To simulate the displacement enforced by the test machine a velocity boundary condition was applied to the end of the y-joint. The y-joint was constrained against movement in the xz-plane while the velocity boundary condition was applied in the y-direction, refer to figure 7.1. All rotational degrees of freedom of the loading point of the y-joint were left free. The pin was fixed to the y-joint with a tie-constraint.

The smooth step option in Abaqus was used in applying the velocity boundary condition in order to limit the amount of kinetic energy created, and ensure the simulation remained quasi-static. A typical smooth step amplitude definition is shown in figure 7.9.

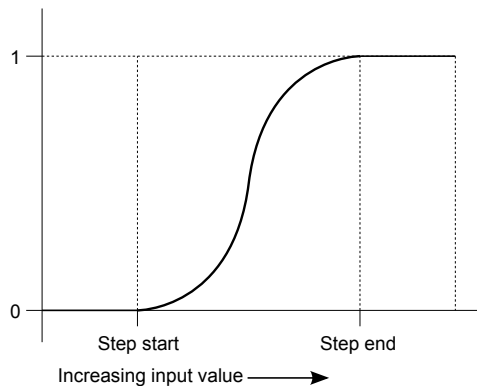


Figure 7.9: Typical amplitude of a smooth step definition

The smooth step amplitude gradually increases the velocity until it reaches its target value. As finite element models can be very sensitive to sudden changes which may cause unwanted behaviour in the simulation. Using the smooth step option reduces the possibility that dynamic noise will affect the results.

7.1.3 Interactions

The interaction parameters used for contact in the initial model were a tangential behaviour with a penalty friction formulation, and a normal behaviour with "hard" contact which should be suitable for the steel on steel contact in the model. The initial friction

coefficient was chosen to be 0.6 based on the dry, static friction coefficient of zinc on zinc friction contact[20]. A sensitivity study on the friction coefficient revealed a close relation between both stiffness and stability of the response and the friction coefficient. This will be discussed in detail in section 7.3. Master and slave surfaces were chosen based on mesh refinement on the respective surfaces, where the master surfaces were chosen to be the ones with the coarser mesh[21].

7.1.4 Element types

The element types used in the initial model were the Abaqus default elements. In solid element parts a *C3D8R* element was used. *C3D8R* is an 8-node linear brick element with reduced integration. The default shell element used is a *S4R*, which is a 4-node double curved thin shell element with reduced integration and finite membrane strains. Both of these elements should be robust and suitable for the type of response expected from the analysis[22].

7.2 Computational efficiency

The maximum stable time step size, often referred to as the critical time step, in an explicit analysis depends on the material stiffness, element size and material density:

$$\Delta t = \min\left(\frac{L_e}{c_d}\right) \quad c_d = \sqrt{\frac{E}{\rho}}, \quad (7.1)$$

where L_e is the characteristic element dimension, c_d is the dilatational wave speed of the material, E is the Young's Modulus and ρ is the material density. The critical time step is often very small, and it would therefore be inefficient to run the simulation using the same time period as the one used in the laboratory tests. To improve the efficiency of the simulation, *i.e.* reduce the computational time, time scaling, mass scaling or a combination can be used. Mass scaling increases the mass of selected elements and thereby increases the critical time step according to equation 7.1. This can be an efficient way to decrease computational time if some elements are small relative to others. If the elements in the model are of approximately the same size, time scaling is often preferred. Time scaling reduces the time period in the numerical model without increasing the time step. This should be done with caution however, as reducing the time period too much may cause the response to become affected by inertia forces. To prevent this the

time period is gradually reduced while monitoring the ratio between the kinetic energy, representing the inertia forces, and the internal energy, representing the response of the system. It is recommended that the kinetic energy is below 5-10 percent of the internal energy during most of the simulation[22]. To get a meaningful comparison between the kinetic energy and the internal energy the kinetic energy created by the rigid body motion of the clamp, the longitudinal washers of the W-beam, the pin and the top bolts were subtracted from the total kinetic energy. Comparing the ratio for different time periods using the aforementioned criteria resulted in a time period of 0.05 s using a loading rate of 1000 mm/s. A typical plot of the kinetic energy and the internal energy in the system is illustrated in figure 7.10. The kinetic energy is very close to zero, and definitely below 5 percent of the internal energy for the major part of the simulation.

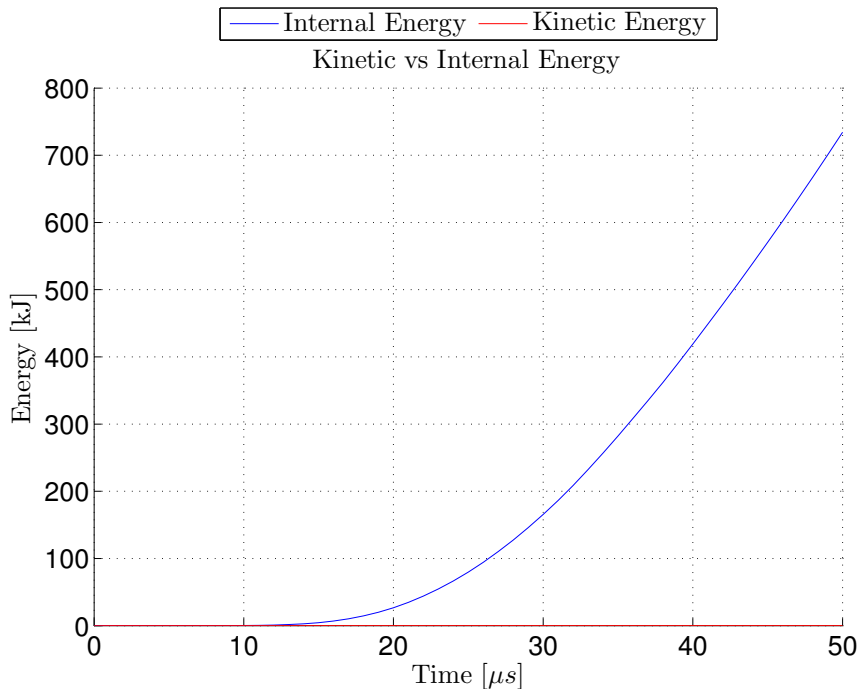


Figure 7.10: Kinetic versus internal energy for the deformed parts

7.3 Sensitivity of the friction coefficient

Since the initial model includes several interactions, the value of the friction coefficient was an important parameter; especially in the 15° and 30° configurations where the potential for sliding between the parts is considerable. A friction coefficient sensitivity study was carried out on the effect of changing the friction coefficient had on the force-displacements response of the model. The recommended friction coefficient for zinc on zinc contact is 0.6 and was used in all interactions by default[20]. Two sets of tests were performed at the 0° and 30° configurations: one where the friction coefficient in the whole model was varied and one where only the friction coefficient in the interactions in the contact with the 30×30×3 mm washer and the 115×40×5 mm washer was changed. The effects of changing the contact between the pin and the clamp from frictionless, as it was chosen by default, to a penalty type normal behaviour with friction was also studied.

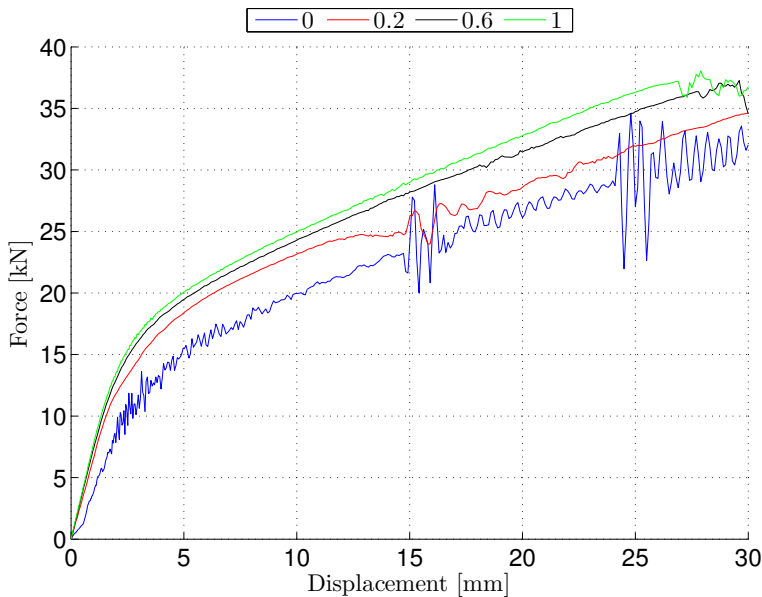


Figure 7.11: Various friction coefficients for the whole model in the 0° configuration

The results from varying the friction coefficient of the whole model in the 0° configuration are presented in figure 7.11. A lot of noise occurred by utilizing a friction coefficient of 0 due to the large number of places the surfaces in contact slipped relative to each other. As the friction coefficient increases the noise gradually disappears and the

stiffness of the response increases. In the 0° configuration the first thread of the bolt is expected to fail at about 20 kN, so the response of the model beyond this point is not of interest. A friction coefficient of 0.2 or higher can thus be used without unwanted noise corrupting the response.

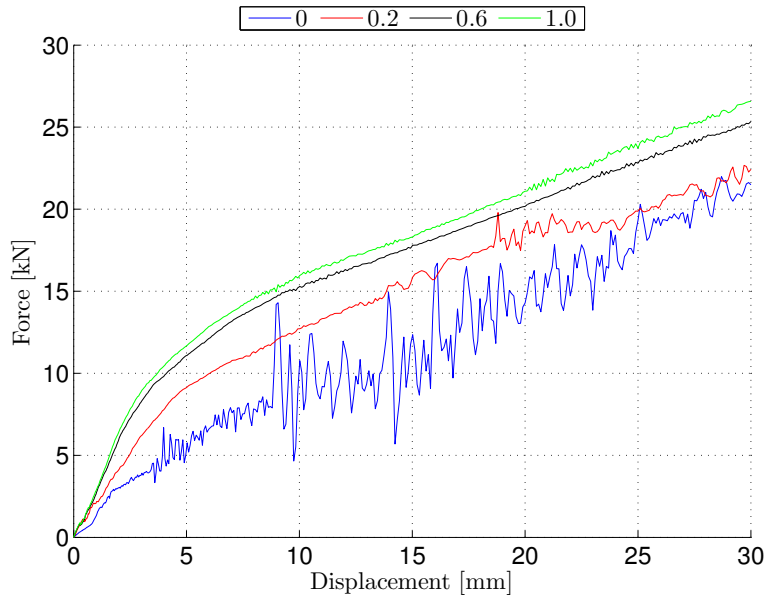


Figure 7.12: Various friction coefficients for the whole model in the 30° configuration

In figure 7.12 the force-displacement curves of various friction coefficients in the 30° configuration are shown. Friction coefficients between 0.6 and 1.0 are fairly similar in performance, while a increased noise is observed as the friction coefficient approaches zero. In the 30° configuration the first thread is expected to fail at about 20 kN, which indicates that the friction coefficient should be kept above 0.2 to avoid noise in the response.

The results of varying the friction coefficient in the interactions with the two washers used to connect the bolt are shown in figure 7.13 for the 0° configuration. The rest of the model has a friction coefficient of 0.6. A friction coefficient larger than 0.2 is sufficient to provide the necessary stability in the response. The stiffness of the system decrease slightly as the friction coefficient is reduced.

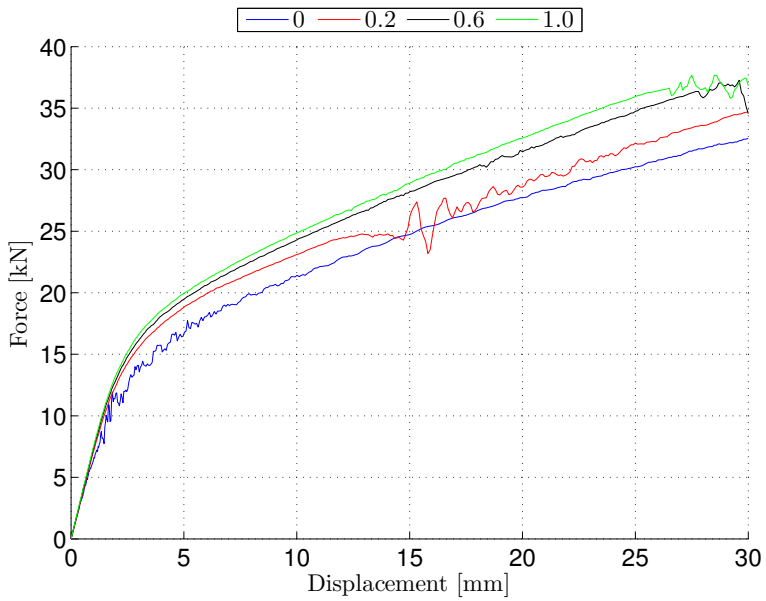


Figure 7.13: Various friction coefficients for washer contact in the 0° configuration

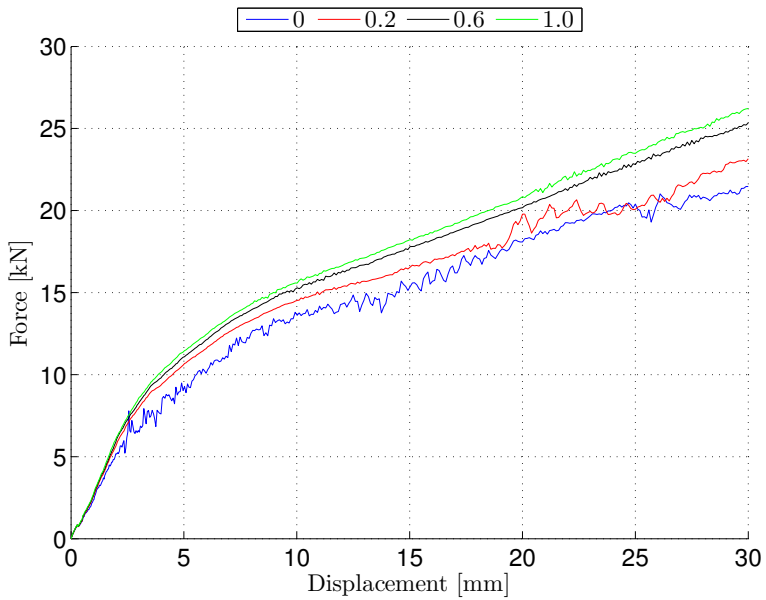


Figure 7.14: Various friction coefficients for washer contact in the 30° configuration

Figure 7.14 shows the system response when varying the friction coefficient in all contact with the $115 \times 40 \times 5$ mm washer and the $30 \times 30 \times 3$ mm washer in the 30° configuration. The rest of the system has a friction coefficient of 0.6. The overall behaviour of the system is fairly similar, however there seems to be an increasing amount of noise as the friction coefficient decreases. This is likely to be due to sudden slips between contact surfaces which causes momentary drops in the reaction force.

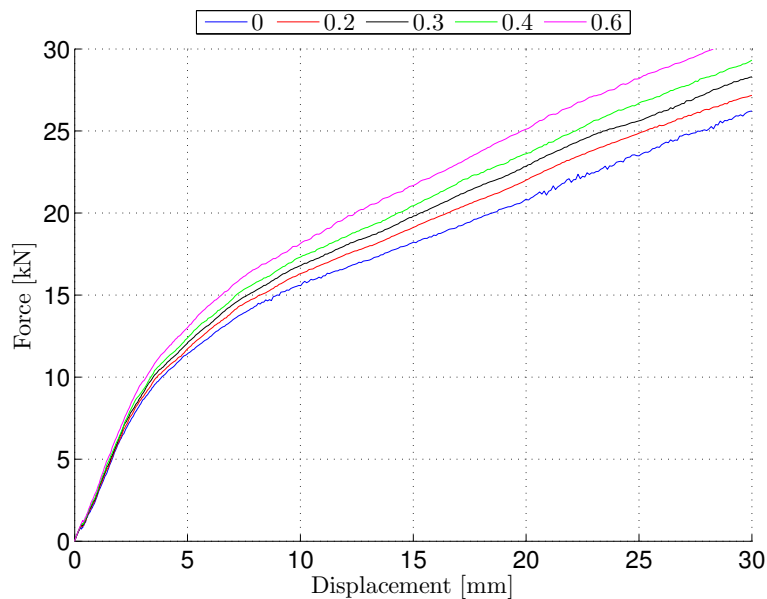


Figure 7.15: Comparison of the response between various friction coefficients on the pin in the 30° configuration

Figure 7.15 shows the response of the system when changing the friction coefficient in just the connection between the pin and the clamp. Increasing the friction coefficient appears to increase the stiffness of the system in a linear fashion. The displacement in the top of the y-joint is about 12-13 mm at 20 kN with a friction coefficient of 0.6, while a friction coefficient of 0 results in approximately 18 mm displacement at 20 kN. Choosing the appropriate friction coefficient in the interaction between the pin and the clamp certainly affects the response of the overall system.

7.4 Validity of the material model of the W-beam and Σ -post

The material models of the W-beam and Σ -post are only valid up to the point of necking as the material tests only represent the material behaviour accurately up to this point. The plastic strain when necking occurred in the W-beam was approximately 0.078 while in the Σ -post the plastic strain was approximately 0.060, corresponding to the intersection between the two curves in figure 6.1.

In figure 7.16 the strains relative to the necking strain of the post in the 0° configuration is plotted.

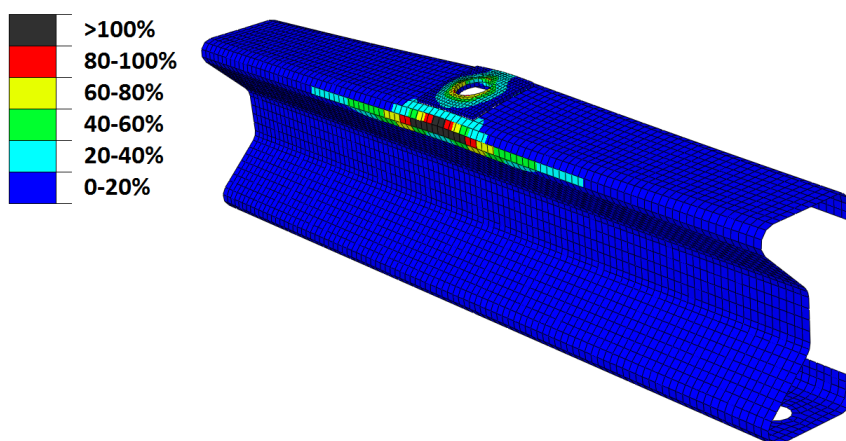


Figure 7.16: Plastic strains in the Σ -post in 0° near the first thread strip

The maximum strain in the Σ -post was 42 percent higher in the finite element model than the strain when necking occurred in the material test. It is likely that the deviation between the material model and the actual behaviour of the Σ -post increases as the strain increases. As the material model is accurate up to the necking strain, the error at a strain 42 percent higher than necking is not likely to be so large as to cause a significant change in the behaviour of the finite element model. It is also seen in figure 7.16 that only a few elements exceeds the necking strain and the effect on the entire model is likely to be small.

Figure 7.17 shows the plastic strain in the W-beam when the first thread of the bolt is expected to strip relative to the plastic strain at necking.

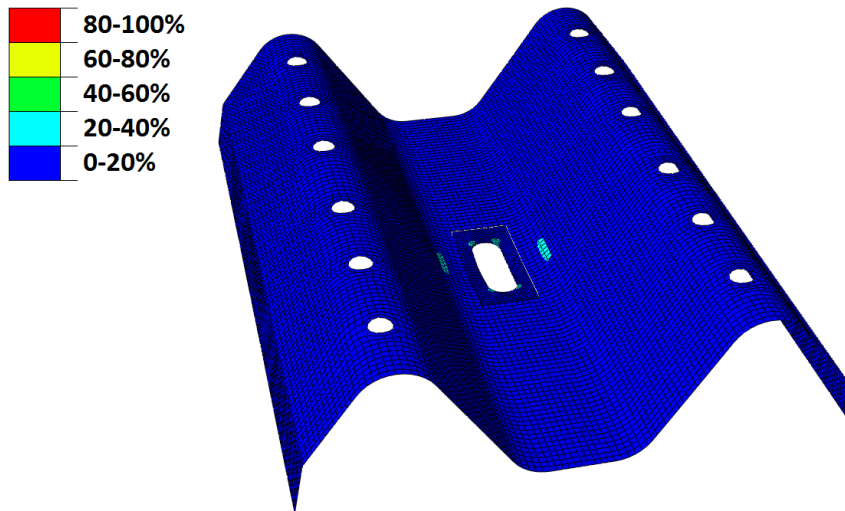


Figure 7.17: Plastic strains in the W-beam in 0° near the first thread strip

The plastic strains in the W-beam were small compared to the plastic strain at necking. The maximum plastic strain in the W-beam was only 36 percent of the strain at necking, showing that the material model used in the finite element model for the W-beam is valid.

The plastic strains of the Σ -post relative to the necking strain in the 30° configuration are shown in figure 7.18. In the 30° configuration the plastic strains were even higher than in the 0° configuration. The maximum plastic strain in the Σ -post exceeded the necking strain by 63 percent. At this level of plastic strain the material model is likely to deviate some from the actual behaviour of the material, but as this level of plastic strain only occurred in a few elements the total effect on the response of the model is likely to be small.

In figure 7.19 the plastic strains in the W-beam in the 30° configuration relative to the necking strain of the W-beam are shown. The maximum plastic strain in the W-beam was only 47 percent of the necking strain of the W-beam. It then safe to assume that the material model for the W-beam has sufficient accuracy.

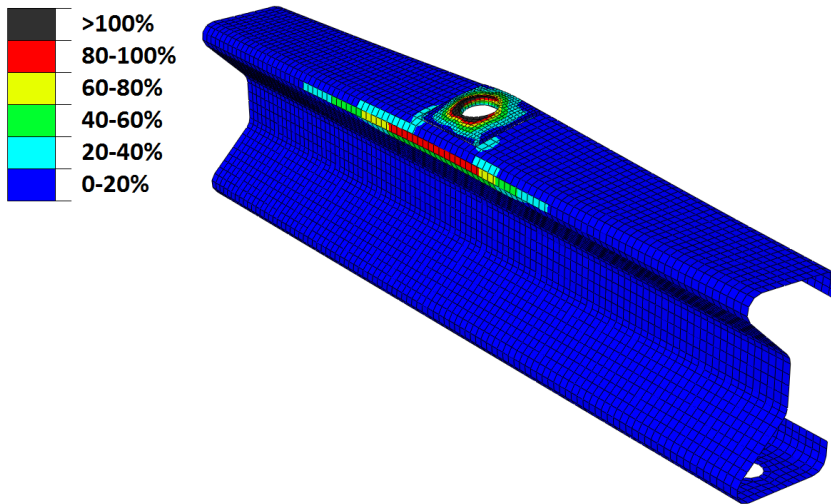


Figure 7.18: Plastic strains in the Σ -post in 30° near the first thread strip

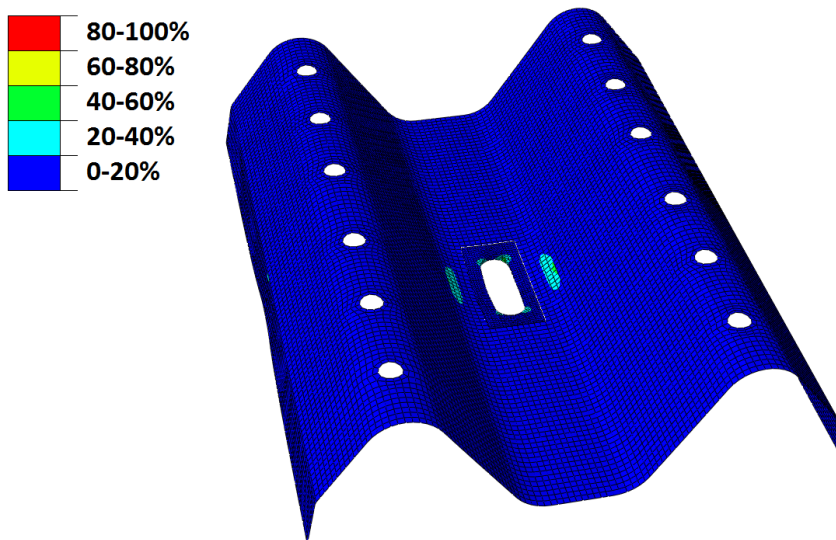


Figure 7.19: Plastic strains in the W-beam in 30° near the first thread strip

7.5 Bolt size

In the numerical model the bolt is a cylinder with a hex head on top. Since the actual bolt is threaded the diameter varies from 10 mm in the outer diameter to approximately 9 mm in the inner diameter. A small sensitivity study was carried out with diameters of 10 mm, 9.5 mm and 9 mm with the resulting force-displacement plots shown in figure 7.20.

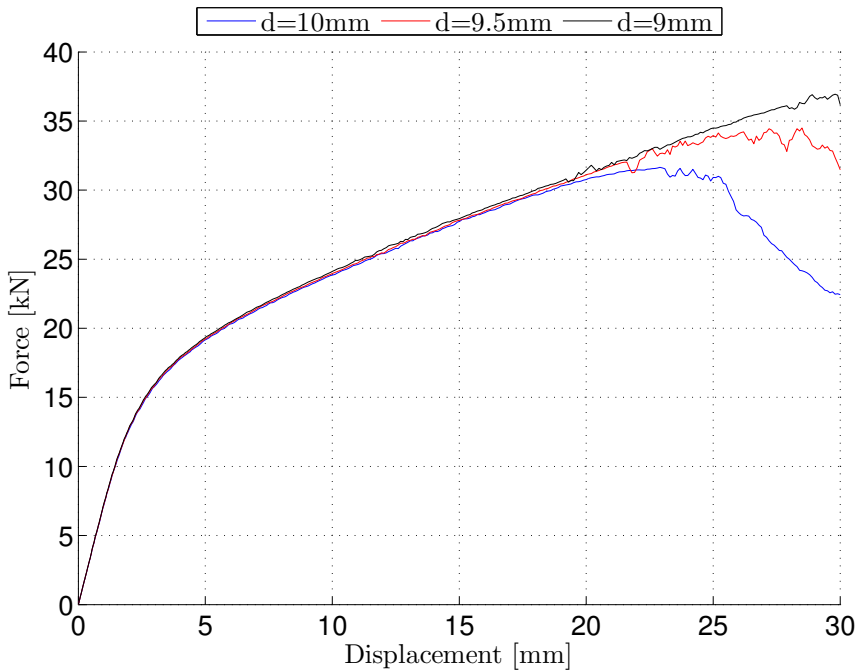


Figure 7.20: Bolt size sensitivity in the 0° configuration

It is clear that varying the bolt diameter has little influence on the response of the system up to the point when the bolt starts necking. As the response of the system after failure is without interest, the diameter of the bolt has no real effect on the response of the system as all the test are almost identical up to 20 kN.

In figure 7.21 the difference in the relative displacement between the bolt and the nut for bolt diameter 9 mm and 10 mm is shown.

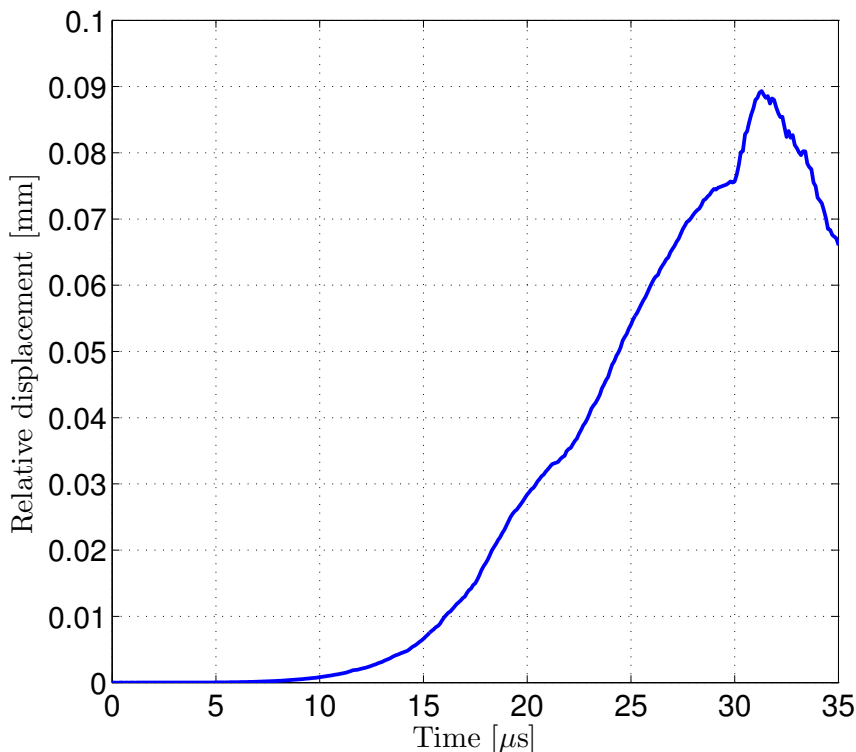


Figure 7.21: Difference in relative displacement of the bolt and nut between 9 mm and 10 mm bolt size

In the laboratory test the first thread stripped when the load was about 20 kN, which in the finite element model corresponded to a time of 33 μs in the model. The maximum deviation in relative displacement was about 0.09 mm; Compared to the 1.4 mm of total relative displacement this is significant. As expected the bolt with a diameter of 9 mm produced the largest relative displacement.

7.6 Mesh size

Due to considerations of computational time the studies on friction and bolt size were carried out on a relatively coarse mesh. The effect of refining the mesh was examined in a small mesh sensitivity study. The mesh was refined in the parts of the model subject

to plastic deformation, which included the bolt and nut, the W-beam, the Σ -post, the washers and the solid element patches. Three sets of meshes were created: a coarse mesh, a medium mesh and a fine mesh. The approximate element sizes used in the three sets are presented in table 7.2, where the elements have the same magnitude in all dimensions.

Table 7.2: Approximate element sizes in the mesh sensitivity study

Part	Coarse [mm]	Medium [mm]	Fine [mm]
W-beam	8	4	2
Σ -post	8	4	2
Bolt and nut	4	2	1
Washer 30×30×3 mm	4	2	1
Washer 115×40×5 mm	4	2	1
Solid element patch, Σ -post	4	2	1
Solid element patch, W-beam	4	2	1

The study was carried out for both the 0° and 30° configuration. The results are shown in figure 7.22 and 7.23 respectively.

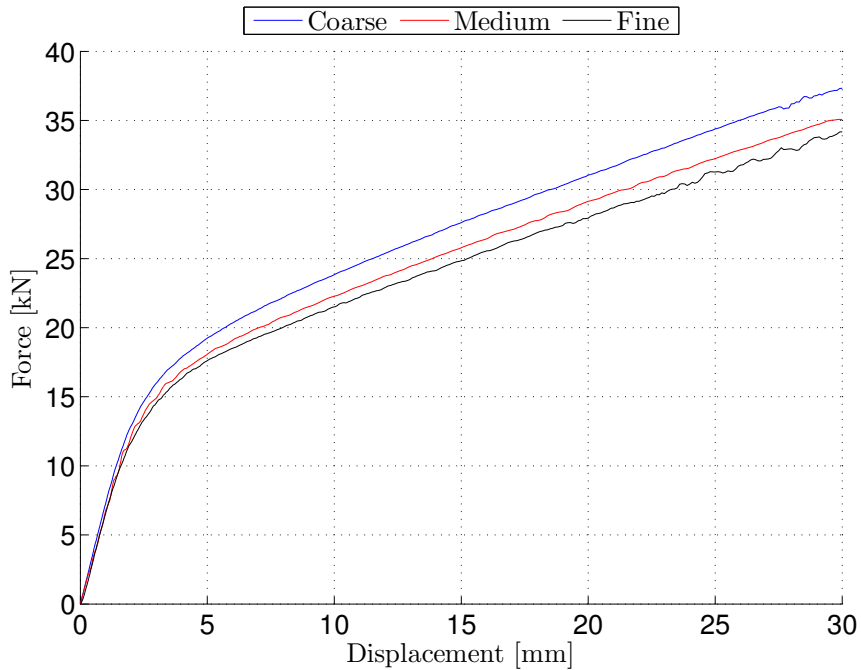


Figure 7.22: Mesh size sensitivity in the 0° configuration

As expected the coarser mesh was stiffer than the finer mesh. The difference in displacement at 20 kN was approximately 2 mm in the 0° configuration and 4 mm in the 30° configuration, which is more than 20 percent of the total displacement. This significant difference suggests that the coarse mesh is inaccurate, but the difference in computational time was also significant. The coarse mesh took about 1.5 hours to run, the medium mesh about 4.5 hours, while the fine mesh used about 27 hours. It was decided to use the medium mesh in the further studies.

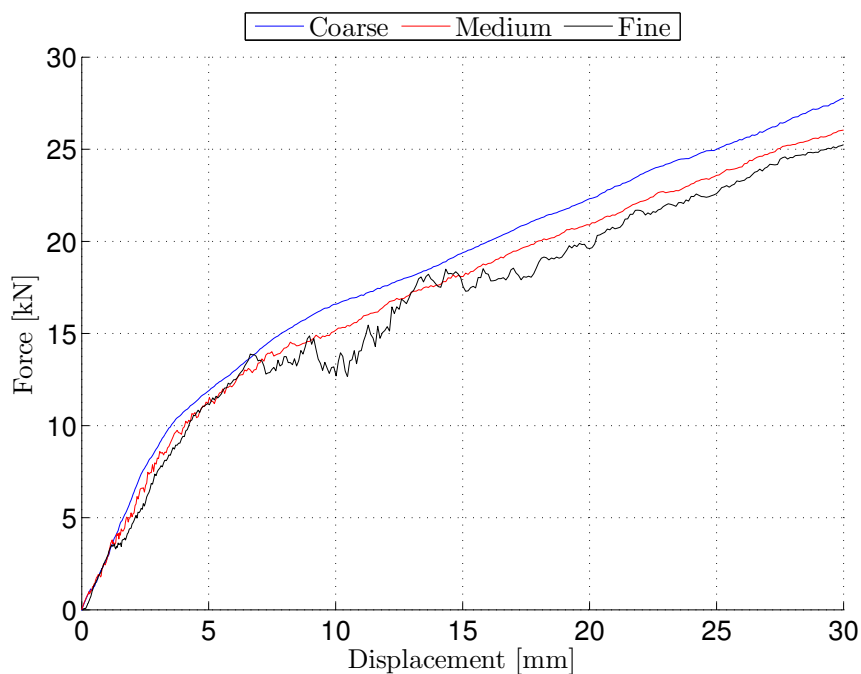


Figure 7.23: Mesh size sensitivity in the 30° configuration

In the 30° configuration a lot of noise occurred as the mesh of the model was refined, however, the reason for this noise was not found.

7.7 The bolt thread stripping model

An outline of the bolt stripping model is presented in figure 7.24.

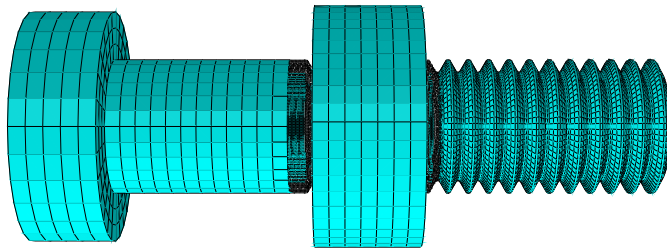
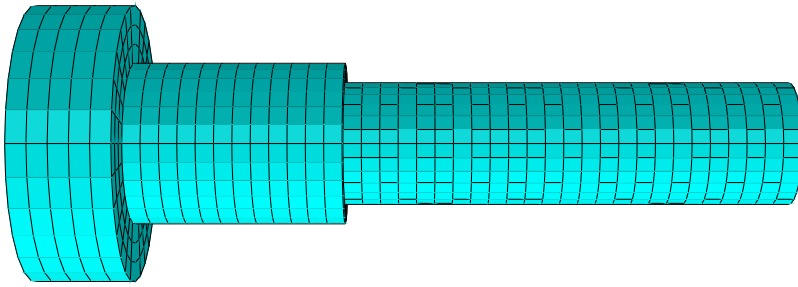


Figure 7.24: The bolt stripping finite element model

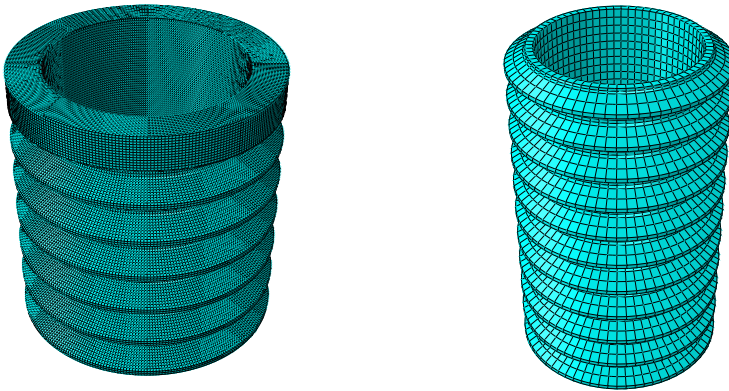
The bolt and nut were modelled using the geometry presented in Appendix A.6. The hexagonal shape of the bolt head and nut exterior were however omitted. A simplification was introduced by modelling the threads as circular. The threads of the bolt are in reality helical with a pitch of 1.5 mm, but this is severely more difficult to reproduce and mesh using Abacus/Explicit. The material model established in section 6.2 was used in both the nut and bolt.

7.7.1 Mesh

All the parts of the bolt thread stripping model were meshed with element type C3D8R described in section 7.1.4. The threads of the bolt require a very fine mesh in order to accurately model thread stripping. In order to increase computational efficiency mass scaling was used. In addition, different sections of the bolt and nut were meshed with different sizes. This was achieved by modelling the bolt and nut as several smaller parts which were then assembled. The bolt consists of three parts: The threads immediately in contact with the nut, the remaining threads and the bolt center. The different parts can be seen in figure figure 7.25.



(a) Bolt center, mesh size 1.1 mm



(b) Upper bolt thread section, mesh size 0.1 mm (c) Lower bolt thread section, mesh size 0.4 mm

Figure 7.25: Bolt parts with mesh

The threads immediately in contact were given a mesh size 0.1 mm. This allows for two elements across the tip of each thread. The remaining threads have a mesh size 0.4 mm. The bolt center has a mesh size 1.1 mm. The nut is divided into two parts: the threads and the outer remaining cylinder. These two parts can be seen in figure 7.26.

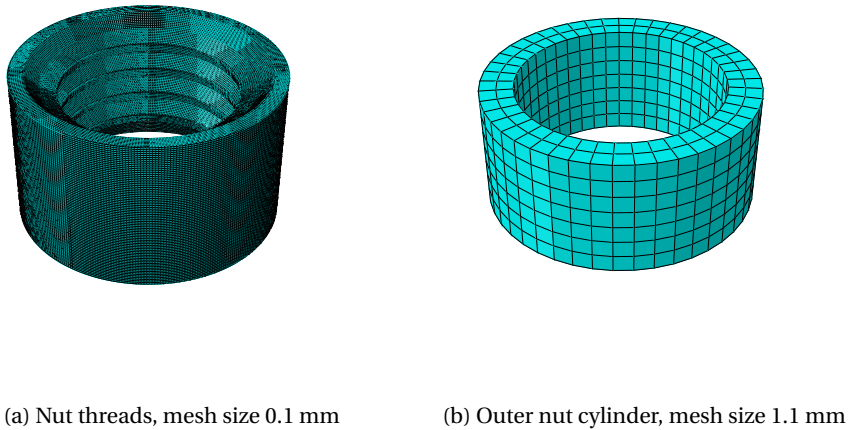


Figure 7.26: Nut parts with mesh

The nut threads are given a mesh size 0.1 mm. The outer nut cylinder is given a mesh size 1.1 mm.

7.7.2 Boundary conditions and constraints

During the laboratory tests the load was transferred from the W-beam to the bolt by the underside of the bolt head. It was further transferred via the threads to the nut, and to the Σ -post via the top of the nut. To model this behaviour in the bolt thread stripping model the nut was fixed while loading was applied to the bolt head by means of displacement control. The nut was modelled using two different techniques: one where the nut was a rigid analytical surface, and one as a deformable solid. In the case of the rigid analytical surface, the entire nut was fixed against displacement in all directions. The solid nut was fixed at the top of the nut, modelling the contact between the nut and the Σ -post. The displacements applied to the bolt were taken from displacements of the bolt in the initial model. Displacements were extracted from four nodes each at the underside of the bolt head and the top of the nut. These nodes are shown in figure 7.27.

These values were averaged and the relative displacement between the bolt head and nut calculated. In order to apply the displacement to the bolt head the head was constrained as a rigid body, and the displacement applied to a reference point in the middle of the underside of the bolt head. Displacements from the initial model in the

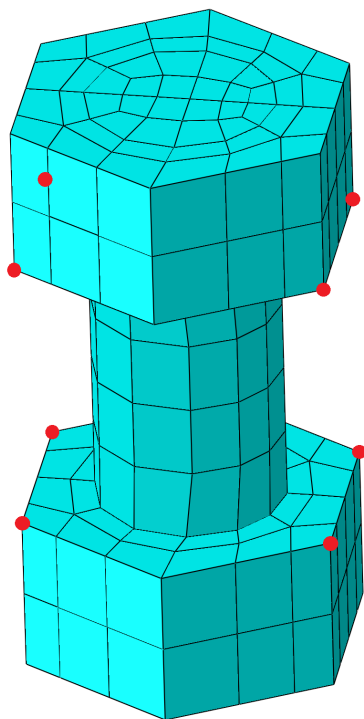


Figure 7.27: Displacement extraction nodes

0°, 15° and 30° configuration were extracted and applied separately. The three separate parts of the bolt were assembled using a tie constraint. This ties the adjacent surfaces together and allows forces to be transferred between different meshes. The same tie constraint was used for the nut.

7.7.3 Interactions

The interaction parameters used in modelling the contact in the bolt thread stripping model were the same as those used in the initial model. A tangential behaviour with a penalty friction formulation was used with a friction coefficient of 0.6. The normal behaviour was chosen as "hard" contact in Abaqus/Explicit. A general contact algorithm was used for the contact, where surface pairs between the bolt threads and the nut threads were selected. The nut surface was chosen as the master surface.

7.8 The full model

The full model is an edited version of the initial model, where the bolt and the nut from the bolt thread stripping model replace the bolt and nut used in the initial model. An outline of the full model is presented in figure 7.28.

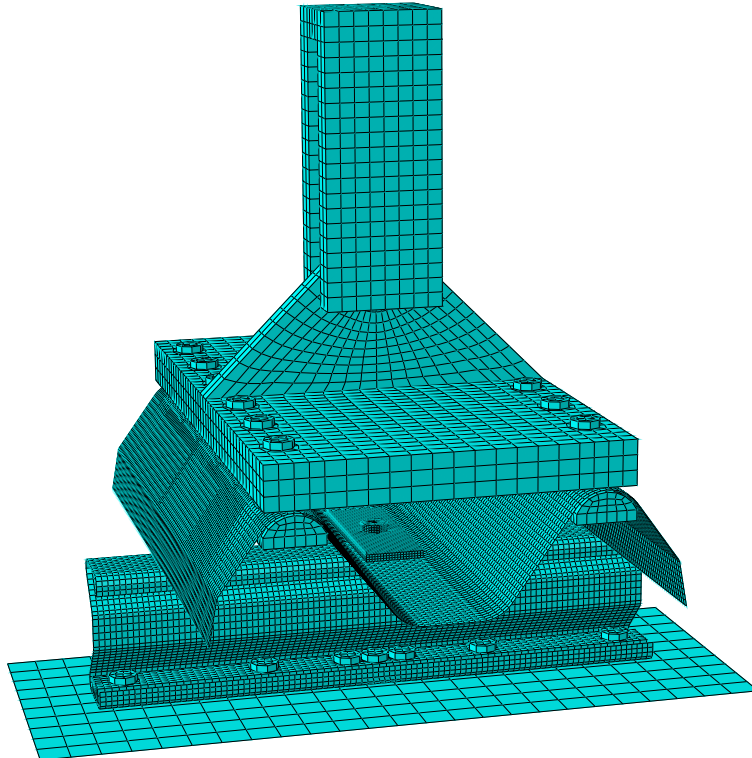


Figure 7.28: The full model

The mesh used in the full model is the medium mesh used in the mesh sensitivity study. The mesh sizes used are presented in table 7.2. The same mesh is used for the bolt and nut as used in the bolt thread stripping model. Boundary conditions and interactions are the same as those used in the initial model.

Two versions of the full model were created, one with the nut as a rigid body and one where the nut was a deformable body. As the material of the nut was uncertain, the version with the nut as a deformable body was modelled using the bolt material in the nut.

8 Results

8.1 Analytical failure load

As described in section 4.1 the bolt stripping load and bolt breaking load in threaded assemblies can be determined using the formulas and parameters presented in Appendix D. The material of the nut is unknown, but is assumed to be rigid as the laboratory tests suggested that the threads of the nut were not stripped. In effect, when determining C_2 , R_s is assumed to be 2.2, resulting in $C_2=1.19$ by equation D.1d corresponding to the right end of the curve in figure 4.2b. The resulting bolt stripping load, F_{bb} , and bolt breaking load, F_{bs} , are presented in table 8.1.

Table 8.1: Bolt failure load

σ_Y [MPa]	F_{bb} [kN]	F_{bs} [kN]
430	23.2	22.2
650	37.7	36.0

Calculations were performed with the ultimate tensile strength, σ_Y , of the bolt as both 650 MPa and 430 MPa. This corresponds to an ultimate strength equal to the true stress at necking in the tensile tests performed by D'Angelo and the ultimate strength reported for the M10 bolt by Bakken-Berg and Iversen. The results indicate that the bolt will fail by thread stripping, consistent with the laboratory tests. Using the material data from the tests performed by D'Angelo the failure load is significantly higher than what was seen in the laboratory tests. The material data from the tests performed by Bakken-Berg and Iversen resulted in failure loads in the same region as seen in the laboratory tests.

8.2 Results of the initial model

Using the DIC displacements and forces recorded by the Dartec 500 the response of the finite element model was compared to the response of the test data. The nodes where the displacements were collected for both the finite element model and the DIC analysis are shown in figure 8.1.

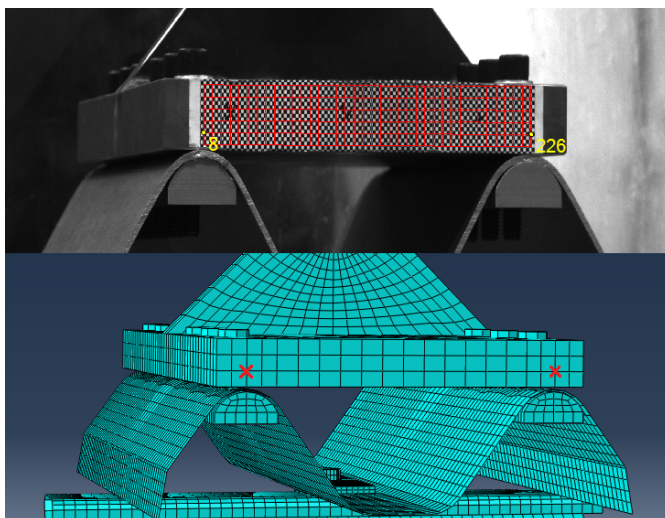


Figure 8.1: Nodes where displacements were extracted in the finite element model and DIC analysis

The points chosen were the two points right above the longitudinal washers connecting the W-beam to the clamp. In doing so the rotation of the clamp in the 15° and 30° configuration could be compared between the finite element model simulations and the laboratory tests. In the force-displacement comparisons the displacements from the right point were used, as the left point had negative displacements in the 15° and 30° configuration due to the rotation of the loading clamp.

The medium meshed model with friction coefficient 0.3 for the pin connection and 0.6 for the rest of the model was used in the final simulations. The curves were moved to coincide at a displacement of 3mm at 2 kN of force for the 0° and 15° configurations and 4mm at 3 kN force for the 30° configuration. This was done in order to eliminate the displacement discrepancies in the initial loading of the test rig. In figure 8.2, 8.3 and 8.4 force-displacement comparisons between the laboratory tests and the initial finite element model in the 0°, 15° and 30° configurations are presented.

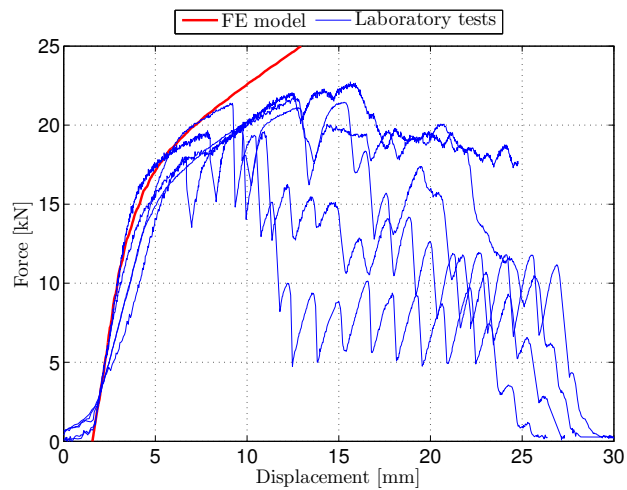


Figure 8.2: Force-displacement comparison of the test results and the initial finite element model in the 0° configuration

In the 0° configuration the finite element model showed an overall behaviour close to that of the laboratory tests. The match between the finite element model and the laboratory tests is satisfactory up to the point where thread stripping occurred in the laboratory tests.

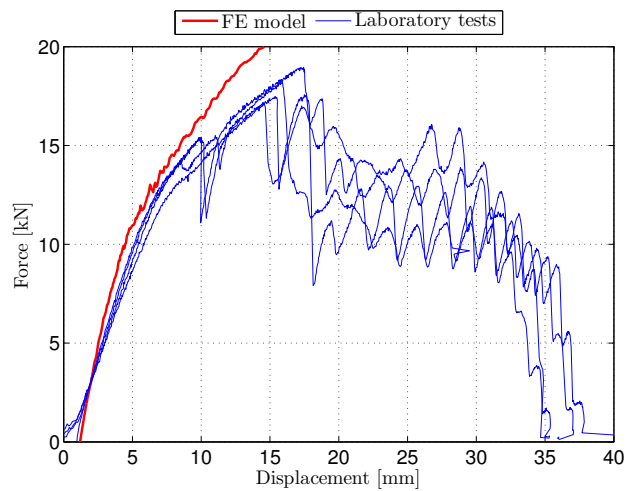


Figure 8.3: Force-displacement comparison of the test results and the initial finite element model in the 15° configuration

In the 15° configuration the finite element model results were not as close to the laboratory test results as in the 0° configuration. The finite element model had a stiffer response than the laboratory tests, and the stiffness of the finite element model did not decline in the same manner as the laboratory tests as more displacement was applied.

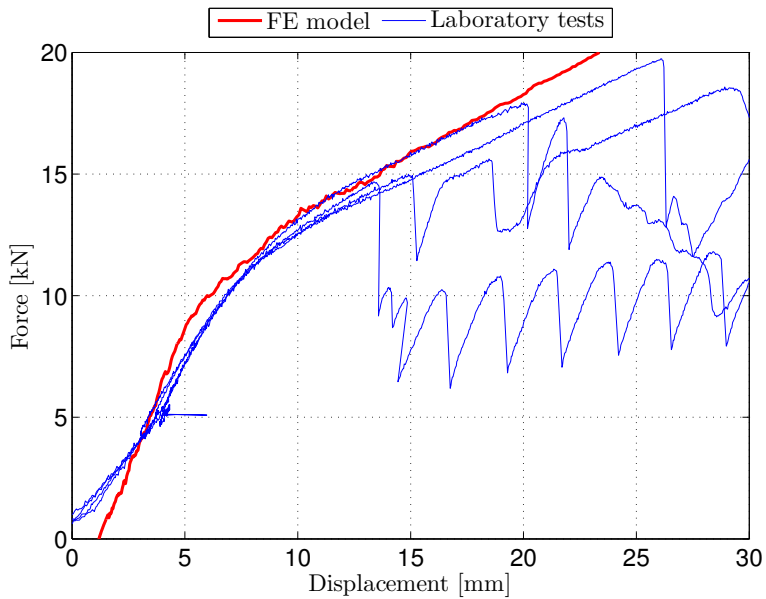


Figure 8.4: Force-displacement comparison of the test results and the initial finite element model in the 30° configuration

In the 30° configuration the finite element model showed a stiffer behaviour than the laboratory tests in the initial part of the analysis, while the stiffness was more or less the same after the onset of yielding.

8.3 Results of the finite element threads stripping model

The behaviour of the bolt in thread stripping was simulated for the three load configurations 0° , 15° and 30° using a finite element model. This was done by extracting relative displacement of the bolt and nut in the initial model and applying the displacements to the bolt in the finite element thread stripping model. Two analyses were made for each load configuration: one with a rigid and one with a deformable nut. A mistake was made in the finite element models of the bolt with the deformable nut, where the bolt was not initially set in contact with the nut. This resulted in the bolt having to displace freely until contact with the nut was established. This free displacement has been adjusted for in the force-displacement plots and the plots are shown from the onset of contact between the bolt and the nut for each mode. Since the bolt is prescribed with the same displacements for the models with the rigid and the deformable nut, it appears as if the analyses with the deformable nut have not displaced as far as the rigid nut. It was decided that since the main focus of the analyses is the maximum capacity of the threads, and due to the models being computationally expensive, to not correct the mistake in the models. The resulting force-displacement curves of the analyses are shown and discussed next.

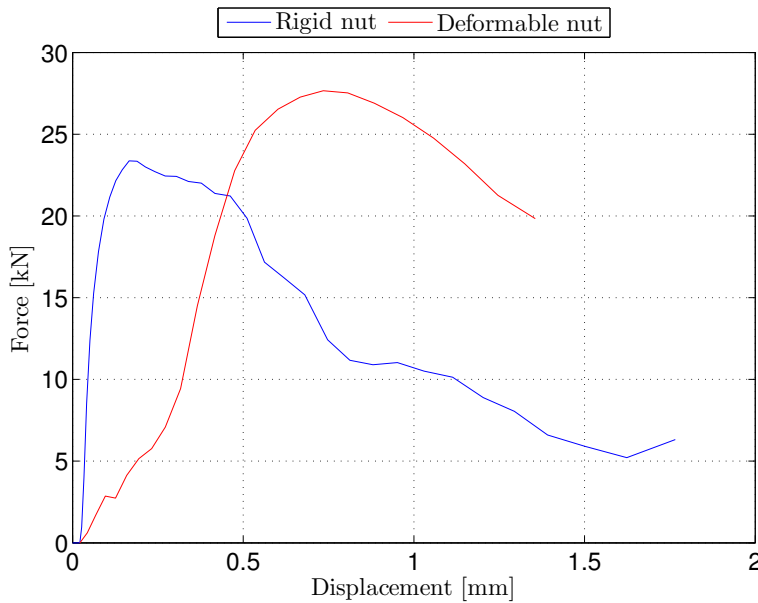


Figure 8.5: Force-displacement of the thread stripping model in the 0° configuration

The force-displacement curves of the finite element thread stripping model analyses in the 0° configuration are shown in figure 8.5, while the evolution of the threads during the analyses is shown in figure 8.6. It can be seen that the model with the rigid nut has a much stiffer behaviour than the model with the deformable nut, but also experiences a lower peak force. The difference in stiffness in the models is expected; When the nut is allowed to deform the model becomes less stiff. There is also some noise in the beginning of the force-displacement curve of the deformable nut, which could be due to the establishment of initial contact between the bolt and the nut. The analysis with the rigid nut shows more clear signs of thread stripping, where several locations of the curve have sudden changes in stiffness indicating thread stripping.

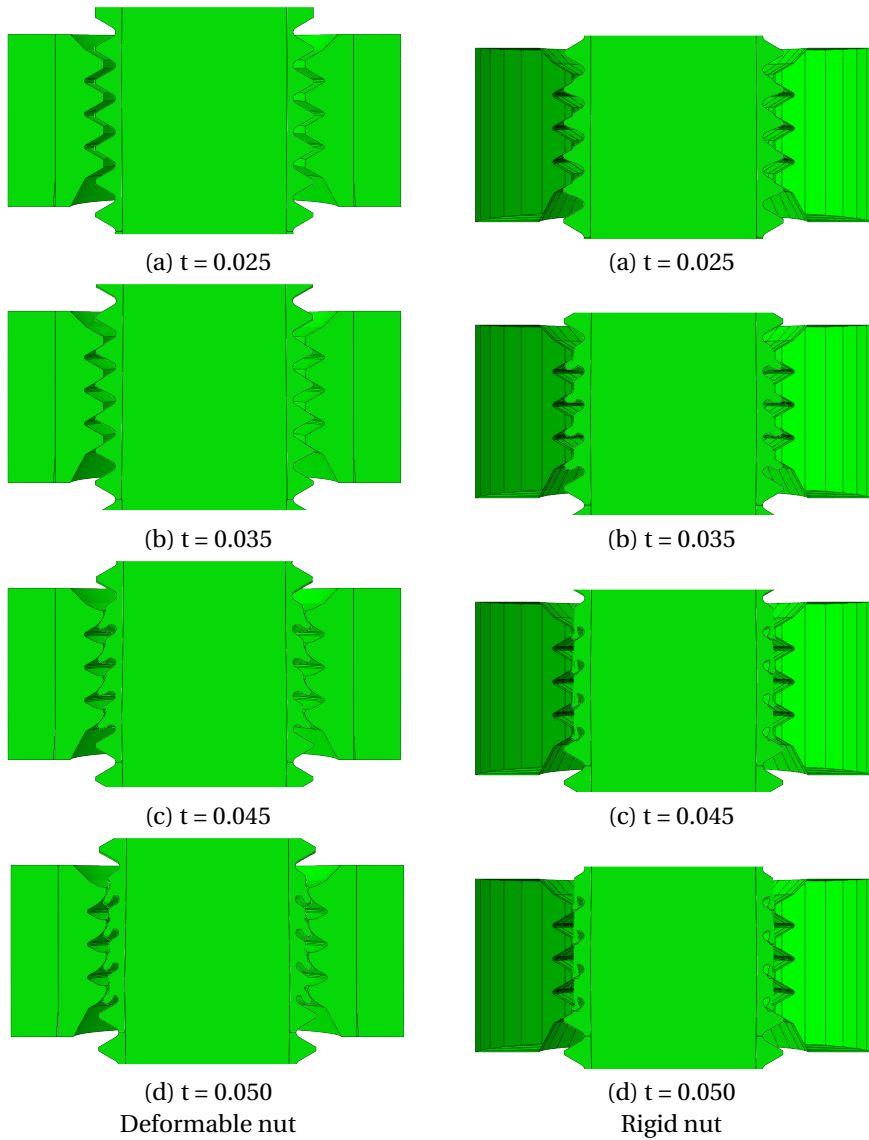


Figure 8.6: Evolution of the bolt threads in the 0° configuration

It was discovered in the late stage of the thesis that the displacements applied to the finite element thread stripping model in the 15° and 30° were inaccurate. The coordinate system in the initial model which the displacement data were extracted from did not match that of the finite element thread stripping model. The results from the finite element thread stripping model in the 15° and 30° configuration are therefore not representative. There are however some general observations regarding the finite element thread stripping model which can be made.

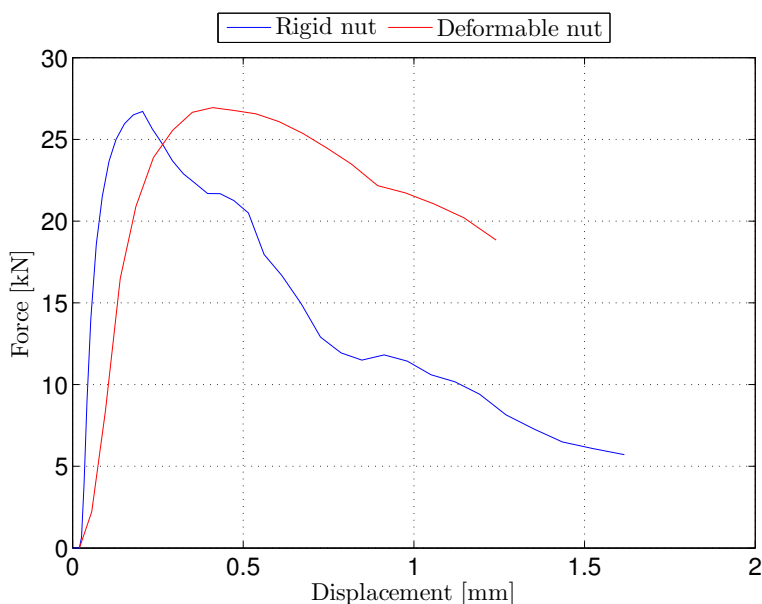


Figure 8.7: Force-displacement of the thread stripping model in the 15° configuration

The force-displacement curves of the finite element thread stripping model analyses in the 15° configuration are shown in figure 8.7, while the evolution of the threads during the analyses is shown in figure 8.8. Again the analysis with the rigid nut is more stiff, as expected. There is however less difference in the peak force. Clear signs of thread stripping are present for the analysis with the rigid nut, although it is also somewhat evident in the force-displacement curve of the deformable nut.

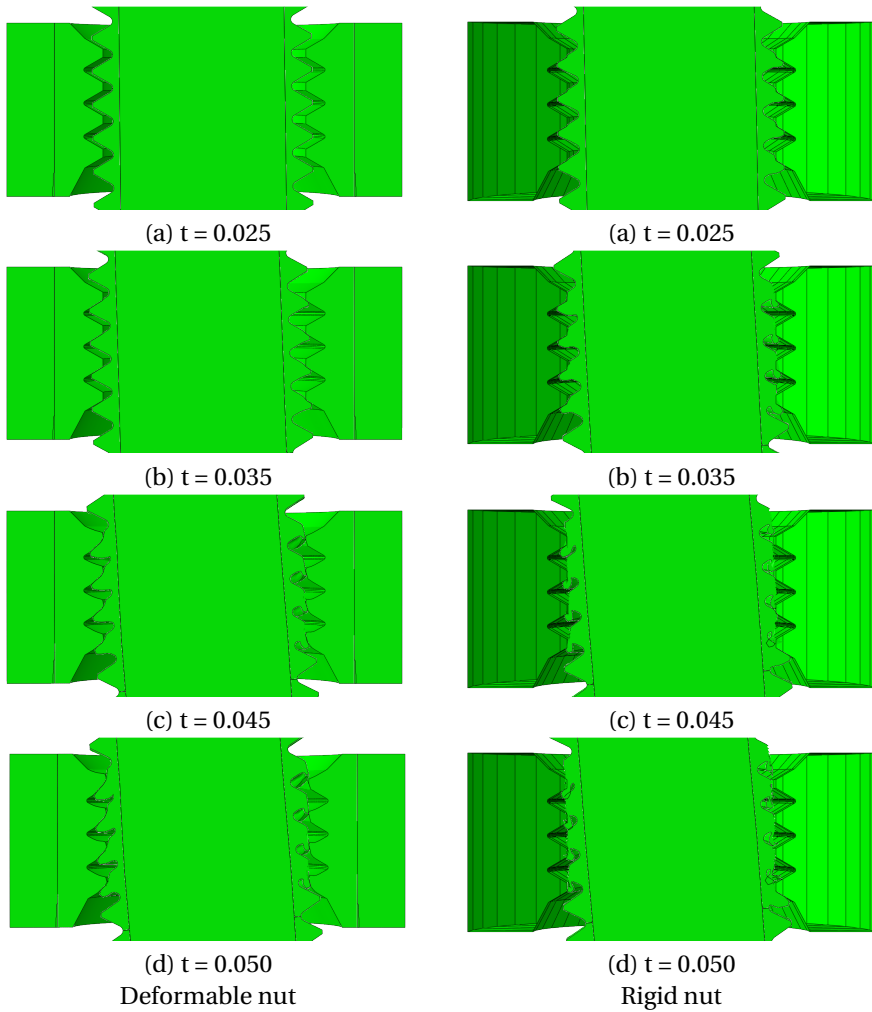


Figure 8.8: Evolution of the bolt threads in the 15° configuration

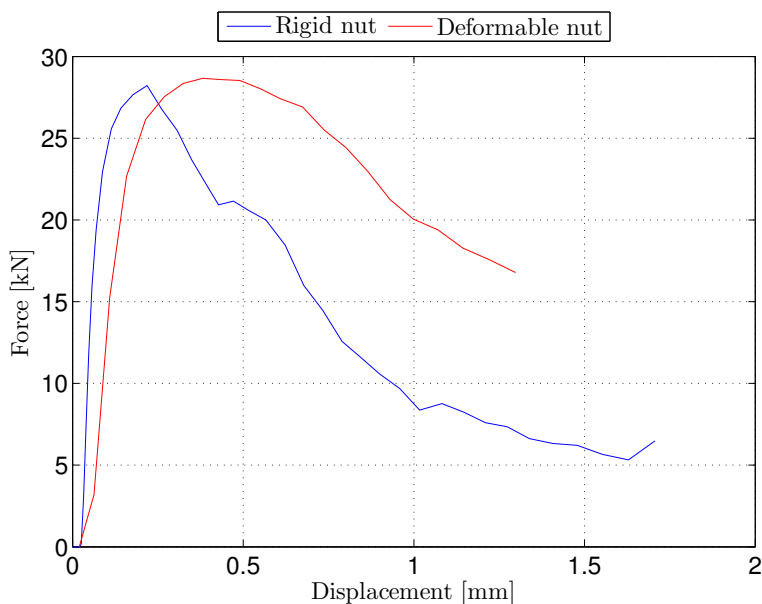


Figure 8.9: Force-displacement of the thread stripping model in the 30° configuration

The force-displacement curves of the finite element thread stripping model analyses in the 30° configuration are shown in figure 8.9, while the evolution of the threads during the analyses is shown in figure 8.10. The results for the 30° configuration are similar to those in the 15° configuration, and similar observations can be made. The peak force from each analysis is summarized in table 8.2.

Table 8.2: Peak forces from the finite element bolt thread stripping models

	$F_u - 0^\circ$ [kN]	$F_u - 15^\circ$ [kN]	$F_u - 30^\circ$ [kN]
Rigid nut	23.4	26.7	28.7
Deformable nut	27.7	26.9	28.7

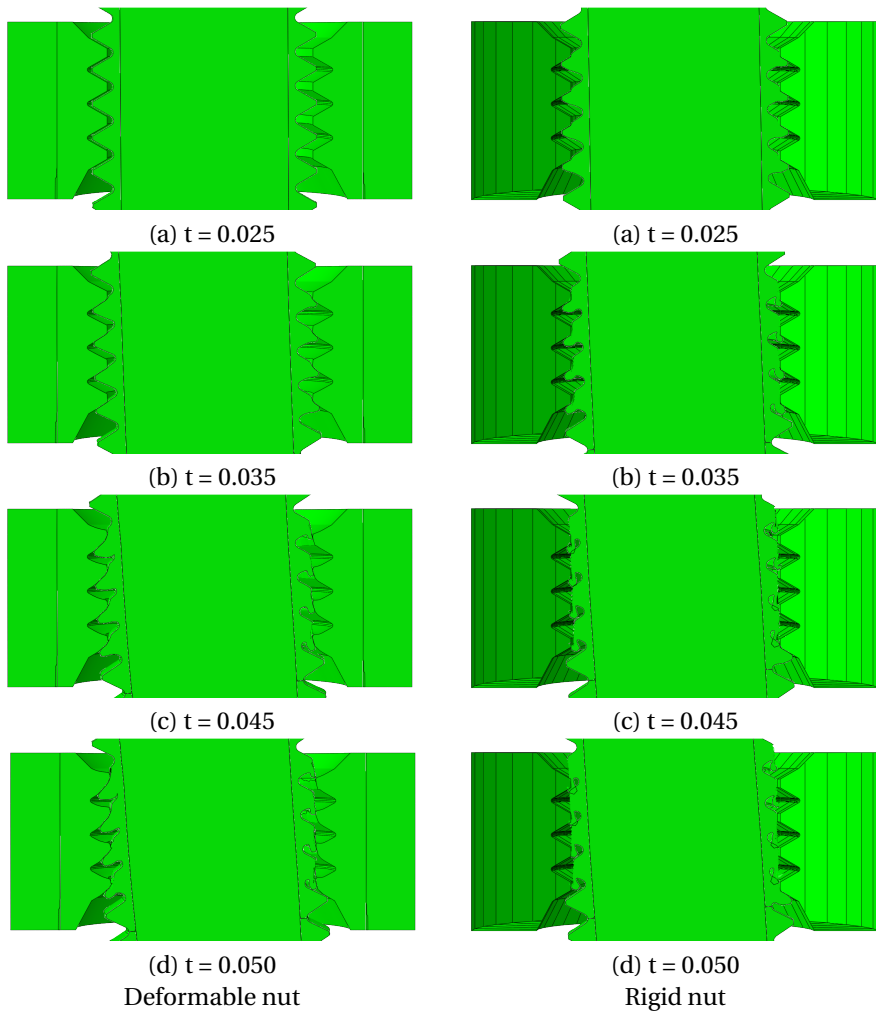


Figure 8.10: Evolution of the bolt threads in the 30° configuration

8.4 Results of the full finite element model

Two versions of the full finite element model were analysed: one with the nut as a rigid body, and one with the nut as a deformable body using the same material in the nut as in the bolt. All the analysis exited with errors, due to some elements being excessively distorted. Thread stripping was observed in all the models, though some of the models exited before the peak load was reached. The results are presented in figure 8.11, 8.12 and 8.14 for the 0°, 15° and 30° configurations respectively.

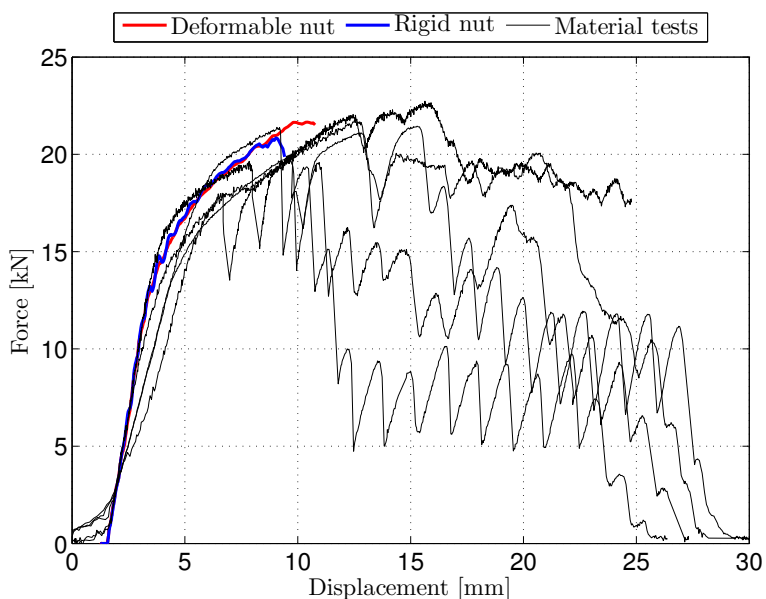


Figure 8.11: Full model force-displacement curves in the 0° configuration

In table 8.3 the maximum load for all configurations are presented. It should be noted that the ultimate load might be higher in both the 15° and 30° configuration since the threads were not fully stripped when the analysis exited with errors.

Table 8.3: Termination loads for the full model

	$F_u - 0^\circ$ [kN]	$F_u - 15^\circ$ [kN]	$F_u - 30^\circ$ [kN]
Rigid nut	20.8	20.1	16.8
Deformable nut	21.7	21.5	18.9

In the 0° configuration both the model with the deformable nut and the one with the rigid nut showed a response very similar to laboratory tests. Both the stiffness and the failure load in the models are in approximately the same region as in the laboratory tests. The model with the deformable nut did not fail before the analysis exited with errors, however it appears that the peak load was reached as the curve plateaued at the end. There is no significant difference in stiffness between the models, but the one with the rigid nut failed before the one with the deformable one. This is expected since the deformation of the threads in the deformable allow for better stress distribution between the bolt and nut threads, resulting in a higher load capacity. This in turn results in greater displacements prior to failure.

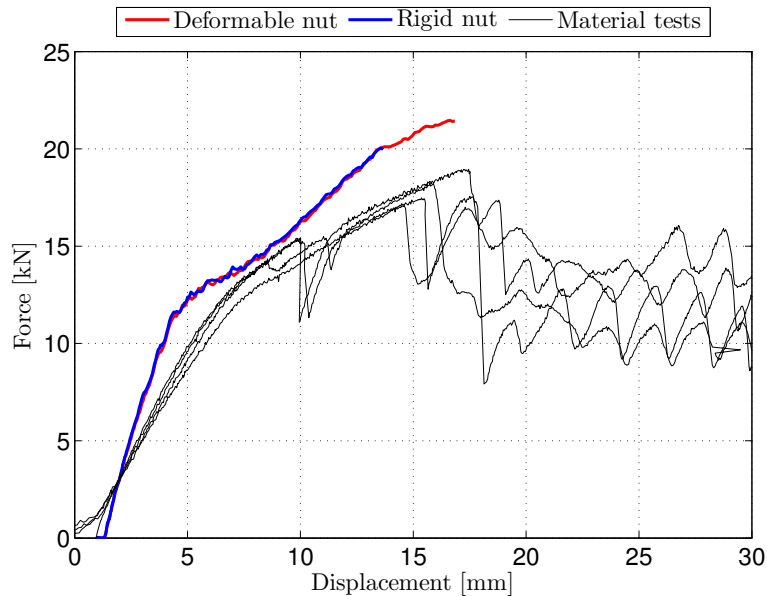


Figure 8.12: Full model force-displacement curves in the 15° configuration

In the 15° configuration much of the same behaviour was seen in the full model as in the initial model. The behaviour was in general too stiff. What could be the onset of yield in the finite element model is followed by an increase in stiffness not seen in the laboratory tests. Neither the analysis with the deformable nut nor the one with the rigid nut reached its peak load, but as seen in figure 8.13 the threads were severely deformed. This indicates that thread stripping was imminent and that the peak load was likely to be close to the force level at the end of the simulation.

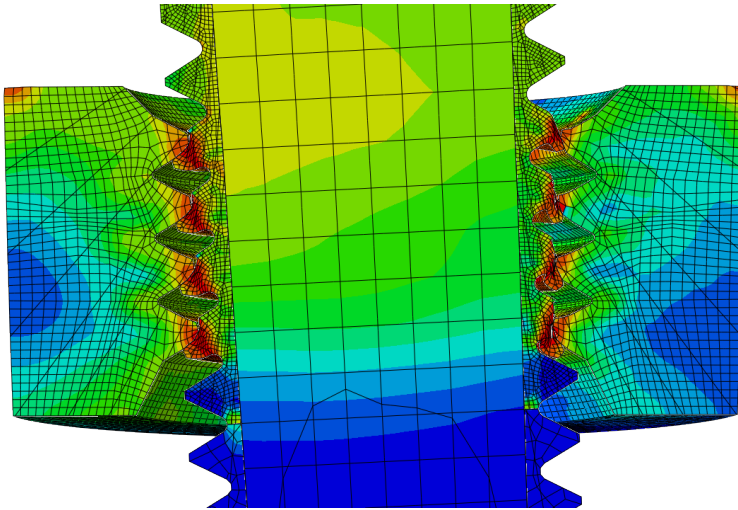


Figure 8.13: Thread stripping in 15° configuration

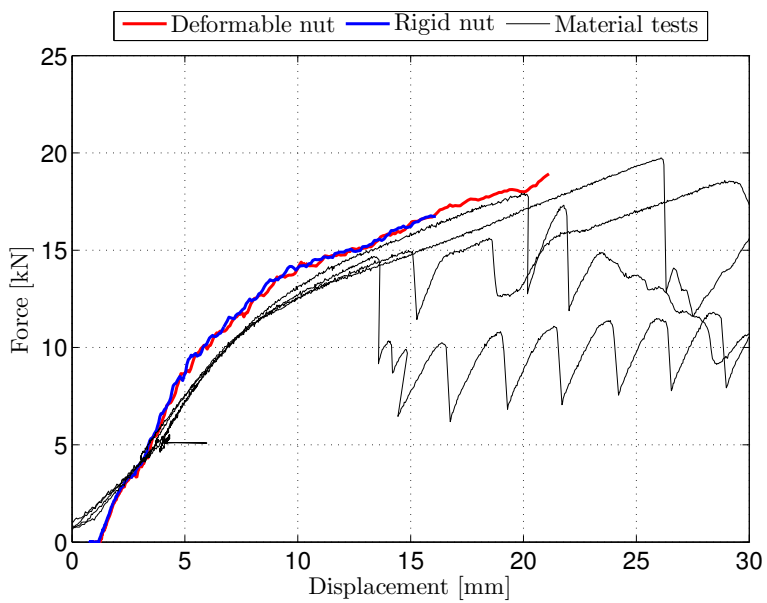


Figure 8.14: Full model force-displacement curves in 30° configuration

The response of the full model in the 30° configuration was also very similar to the one in the initial model. As with the 15 ° configuration neither analysis reached its peak load, but the as seen in figure 8.15 thread stripping was imminent.

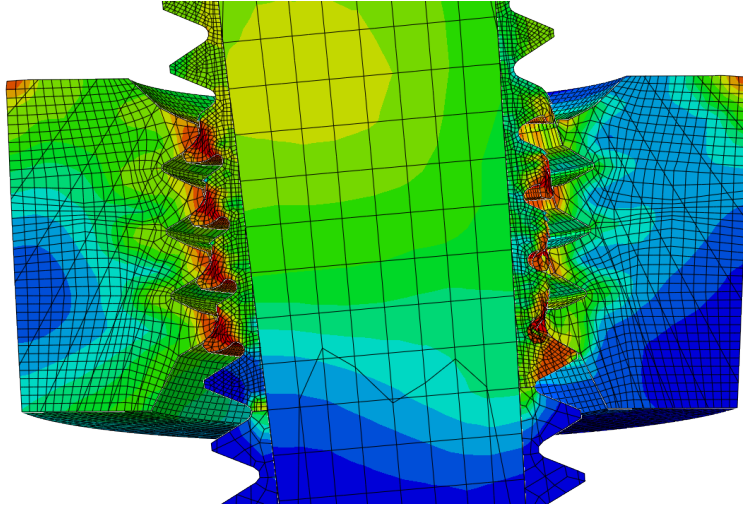


Figure 8.15: Thread stripping in 30° configuration

9 Discussion

In this chapter the results of the laboratory tests and finite element models will be compared and discussed. Possible causes of inaccuracy in the assumptions made and models produced in this thesis will be highlighted.

9.1 Laboratory results

The bolted connection in the road safety barrier is found to be the crucial component in the road safety barrier assembly, given the loading scenarios which have been investigated in this thesis. Laboratory tests on the road safety barrier with the bolted connection all experienced thread stripping as the failure mode, as seen in section 4.5. The failure mode of thread stripping experienced in the laboratory is consistent with results found in other literature. The ultimate load experienced in the laboratory tests are compared with tests on thread stripping of the bolt performed by Bakken-Berg and Iversen[9], as well as the analytical computations according to Alexander[11], in table 9.1.

Table 9.1: Average ultimate thread stripping load

	$F_u - 0^\circ$ [kN]	$F_u - 15^\circ$ [kN]	$F_u - 30^\circ$ [kN]
Alexander	22.2	-	-
Bakken-Berg & Iversen	21.8	-	-
Tests	21.4	18.0	17.7

Comparisons in table 9.1 show close similarities between the analytical load capacity of the threads to what was found in the laboratory tests of Bakken-Berg and Iversen, and the laboratory tests of this thesis. This indicates that the ultimate failure load is controlled by the bolt failure, and that the influence of the other parts of the road safety

barrier on the ultimate capacity of the connection is negligible. Laboratory tests show a drop in the capacity in the bolted connection when loaded in a combination of tension and shear. The average ultimate load experienced in the 15° and 30° configuration is very similar. Any trend in the reduction of ultimate capacity with increased load angle can therefore not be established. The decrease in the ultimate load in the 15° and 30° configuration, and the failure mode of thread stripping, are inconsistent with the results experienced by Shakir-Khalil and Ho[7]. They experienced trouble with thread stripping when loading the bolt in pure tension at 0° and up to a combination of tension and shear at 15°. That thread stripping persists in loading above 15° is inconsistent with what was found by Shakir-Khalil and Ho.

The laboratory results produced by Bakken-Berg and Iversen show that thread stripping in the M10 bolt is a more unpredictable failure mode than conventional failure in the bolt cross-section. Tests on thread stripping experience larger differences in ultimate capacity than failure in pure tension or shear. The deviations in the ultimate failure load in the different failure modes are summarized in table 9.2.

Table 9.2: Deviation in the ultimate failure loads by failure mode[9]

	$F_{u,max}$ [kN]	$F_{u,min}$ [kN]	$F_{u,avg}$ [kN]	$Diff_{max}$ [%]	$Diff_{avg}$ [%]
Tension	31.6	28.6	29.2	9.5	8.2
Shear	20.6	17.9	19.0	13.1	8.4
Threads	24.5	16.2	21.6	33.9	25.0

The unpredictability of thread stripping failure in the bolt could possibly be due to geometrical imperfections in the bolts. The threads in the bolt are relatively fine compared to the rest of the bolt material, and could be more susceptible to geometrical imperfections. Slight deviations in the thread geometry could cause uneven stress distributions which are difficult to predict. This same effect is compounded in the threads of the nut. Deviations in the diameter of the bolt and nut might also cause deviations in the behaviour of the threaded assembly. The fit of the bolt threads in the nut determine the shear area of the threads, which could cause large variations in the bolt capacity in thread stripping. Differences in the material properties of the bolt in the cross-section might also cause variations in the behaviour. A Vickers hardness test on a bolt from the batch used in the laboratory tests showed that the hardness of the bolt material varied in the cross-section. The threaded area had in some measurement points reduced hardness compared to the center of the bolt, but no concise conclusions

can be made based on the relatively small differences in hardness observed in the test.

9.2 Accuracy of the finite element models

9.2.1 The initial model

The initial finite element model of the road safety barrier fits the elastic, and to some extent plastic, behaviour of the road safety barrier tested in the laboratory. It is modelled using a simplified bolt and does not include a fracture criteria, which causes the fit to diverge as the test data reaches plasticity and subsequent failure. This initial fit with subsequent divergence indicates that the elastic and initial plastic behaviour of the road safety barrier is dominated by the W-beam and Σ -post, while the failure is dominated by the bolted connection. The initial model is consistently more stiff than the test results, which is expected in a valid finite element model. A refinement of the mesh will cause the finite element model to converge toward the real behaviour of the road safety barrier, given that accurate geometries and material models are used.

9.2.2 The thread stripping model

The finite element model of the bolt and nut with threads was able to successfully simulate thread stripping, as seen in section 8.3. The results of the model in the 15° and 30° configuration are however inaccurate due to an error in the prescribed displacements, as discussed in section 8.3. The ultimate load in the finite element model is compared to the ultimate load in the laboratory test in table 9.3.

Table 9.3: Ultimate load in the laboratory tests and bolt FE model

	F_u [kN] - 0°	F_u [kN] - 15°	F_u [kN] - 30°
Laboratory tests	21.4	18.0	17.7
FEM - Rigid nut	23.4	26.7	28.7
FEM - Deformable nut	27.7	26.9	28.7

It is evident that the finite element thread stripping model has too high a capacity to accurately simulate the failure mode in the laboratory tests. The results of the model in the 0° configuration with the rigid nut are close to those of the laboratory tests, but not necessarily representative for the behaviour of the model in the 15° and 30° configuration. The model with the deformable nut had significantly higher failure load

in the 0° configuration. This is likely a result of an improved stress distribution as the nut is deformed, as the effective shear area is increased due to the threads in the nut and bolt "sticking" together. The following discussion of the finite element thread stripping model is mainly concerned with the model in the 0° configuration.

There are several possible reasons for the discrepancies observed between the laboratory tests and the finite element bolt stripping model. The most potent source of errors is the bolt material model. While the material model is a good fit to the bolt material test data from test by D'Angelo, it is suspected that the bolt material properties vary considerably dependent on production batches. Bakken-Berg and Iversen performed capacity tests on the M10 bolt used in the road safety barrier and found ultimate forces of the bolt in thread stripping similar to the ultimate force experienced in the laboratory tests of this thesis. The material certificate for the bolts tested in the thesis by Bakken-Berg and Iversen report an ultimate tensile strength of 430 MPa. The ultimate tensile strength of the material reported by D'Angelo is ~ 650 MPa.

To investigate this further a finite element thread stripping model was created where the material in the threads was modified. The yield stress was reduced with 200 MPa and the fracture criteria equivalently reduced. A mesh size of 0.2 mm and a rigid nut was used to reduce computational time. The resulting force-displacement relationship is plotted with the results for the original bolt thread stripping models at 0° in figure 9.1.

The ultimate force experienced in the modified finite element thread stripping model was 20.4 kN. This is similar to those found in laboratory tests in this thesis and by Bakken-Berg and Iversen. Visual inspection of the force displacement curves in figure 2.4c and figure 9.1 also show similar behaviour in the force-displacement curves from the finite element model and laboratory tests. More extensive analyses with the reduced material model were unfortunately not performed due to time constraints. The results of the one modified model does however contribute to the suspicion that the material properties of the bolt vary considerably, and that the properties of the bolts in the batch tested in this thesis are different from those tested by D'Angelo.

Another possible explanation of the discrepancies observed in the material of the bolt is that the material properties of the bolt are not uniformly distributed in the bolt cross-section. To investigate this possibility a Vickers hardness test was performed on an undeformed bolt from the same batch as those used in the laboratory tests. While the results show some variation in the hardness of the material in the cross-section, the differences in hardness are too small, and the test sample too small, to say anything conclusively about the bolt material.

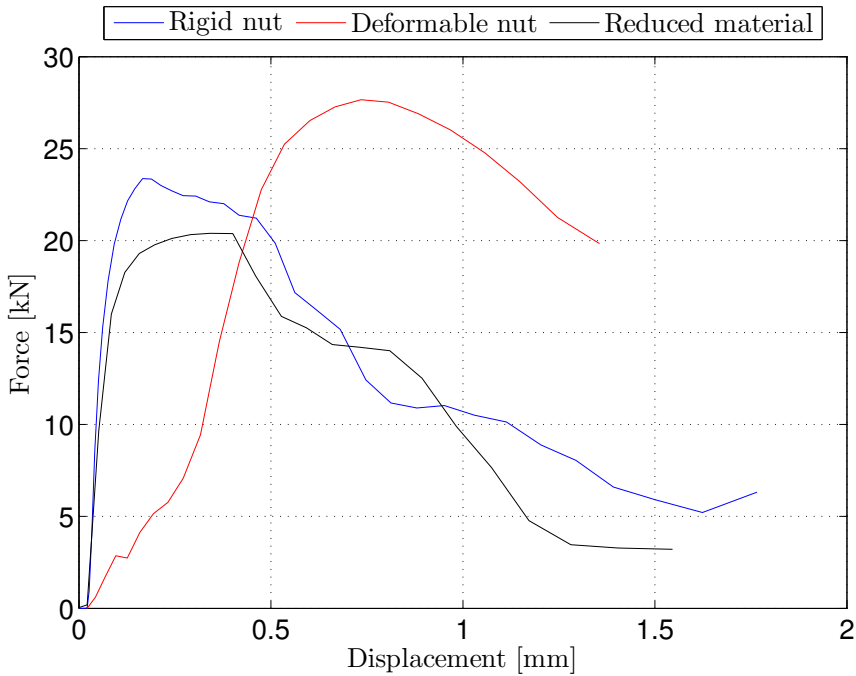


Figure 9.1: Force-displacement relationship of the bolt stripping model with the modified material

The geometry of the bolt and nut in the finite element model is not exact and based on some assumptions. The threads in the real bolt and nut are helical while the threads in the finite element model are circular. This will affect the effective contact area between the bolt and the nut and might have a significant influence on the response. If the circular threads provide more contact area, the ultimate force will consequently be higher than with helical threads. The number of threads in the nut determines the possible contact area between the threads in the nut and bolt. It was observed that more threads "fit" into the nut when using circular rather than helical threads. This unrealistic increase in thread contact area will probably contribute to the increased ultimate force in the finite element thread stripping model. There is also an assumption involved in determining the minor diameter of the threads in the nut. The diameter is based on the diameter of the test bolts after thread stripping. It is suspected that the minor diameter of the nut in reality is less than the diameter of 9.15 mm which was used in the model. The nut will have experienced dilation during testing and therefore increased in diameter during the tests, consequently allowing a deformed bolt with a wider diameter than the original nut

diameter to pass through. The larger diameter will result in a reduced fit between the bolt and the nut, reducing the effective shear area of the threads.

There are several arguments as to why the behaviour of the finite element thread stripping model deviates from the behaviour experienced in the laboratory. The real properties of the M10 bolt with the nut is probably found in a combination of the arguments discussed previously.

9.2.3 The full road safety barrier model

The finite element model of the bolt and nut with threads was inserted into the initial model in order to create a full model of the road safety barrier. The resulting model is very detailed and computationally expensive. All the models terminated due to excessively distorted elements during the analyses, resulting in incomplete data sets. It was not possible to create more robust versions of the model due to time constraints in writing this thesis. There are however several observations to be made on the data available from the incomplete analyses. An analysis of the full model in the 0° configuration simulates the road safety barrier up to failure of the bolt. It can be seen that the finite element model fails at a similar loading level compared to results found in the laboratory tests. The failure load of the FE model in the 0° configuration are shown in table 9.4.

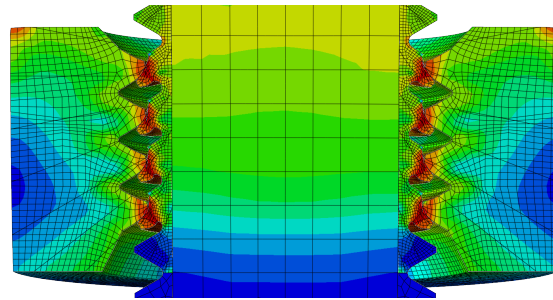
Table 9.4: Ultimate load in the 0° configuration of the full finite element model

	Tests	FEM - Rigid nut	FEM - Deformable nut
F_u [kN]	21.4	20.8	21.7
Diff [%]	-	2.7	1.1

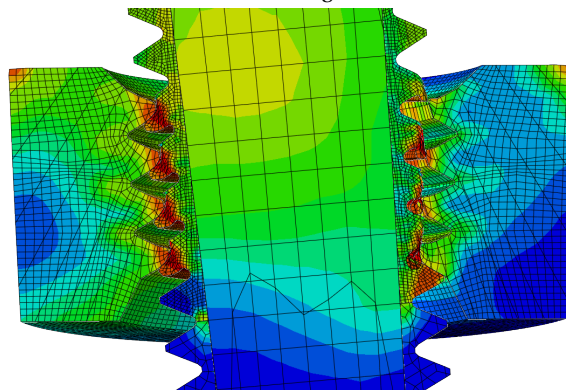
It can be seen that the experienced ultimate loads of the analysis are very similar to those experienced in the lab, suggesting that the model is realistic. There is however no evidence of the individual threads failing, causing momentary drops in the force, as was observed in the laboratory testing. The behaviour of the full finite element model prior to failure is similar to the behaviour exhibited in the laboratory tests as well. This same behaviour was seen in the initial model, which supports the argument that the behaviour of the road safety barrier prior to failure in the bolt is essentially dependent on the W-beam and Σ -post.

Due the early termination of the analyses in the 15° and 30° configuration it is more difficult to make conclusions about the accuracy of the full finite element model in these configurations. The full finite element model in the 15° configuration has the largest

deviation from the the laboratory results. As observed for the initial model in the same configuration, the deviation in stiffness is much greater in the 15° configuration than for 0° and 30°. This supports the possibility that the finite element model in the 15° is less valid. A possible failure of the full finite element model in the 15° configuration is reached at $F_u = 21.47$ kN for the model with the deformable nut, and $F_u = 20.06$ kN in the model with the rigid nut. The behaviour of the full finite element model in the 30° configuration is close to the corresponding laboratory results. As in the initial model the fit prior to failure is close. Similar elastic behaviour are achieved and the loss of stiffness due to plasticity is the same as in the laboratory tests. The analyses terminated before any failure was evident. However, visual inspection of the finite element models gives indications of the behaviour of the model up to failure. Figure 9.2 compares the threads in the finite element models in the 0° and 30° configurations with the deformable nut.



(a) The 0° configuration



(b) The 30° configuration

Figure 9.2: Comparison of the threads in the full model

The thread engagement in the 0° configuration is equally distributed on all sides of the threads, while in the 30° configuration the threads on one side are massively deformed. The increased loading angle results in a rotation of the bolt and subsequently uneven contact of the bolt threads with the nut. The shear area of the threads on one side is reduced, resulting in earlier thread stripping than in the 0° configuration. Observing figure 9.2b it is possible that the threads on the right are at the point of failure, indicating that the model should fail at an ultimate force of 18.9 kN. This is close to the average ultimate load experienced in the laboratory for loading at 30° .

9.3 Validity of the laboratory test versus the real road safety barrier

The purpose of the laboratory tests performed in this thesis is to investigate the behaviour of the bolted connection in the road safety barrier. A section of the road safety barrier centered about the bolted connection between the W-beam and Σ -post was tested in quasi-static loading in different combinations of tension and shear. This is an idealized test setup designed to study the behaviour of the bolted connection in a controlled and reproducible manner. The real road safety barrier subjected to a vehicular impact will obviously experience a different type of loading. A vehicular impact is a dynamic process with high loads in a short period in time, involving high strain rates in the road safety barrier. Literature on the effect of increased strain rate in the components of the road safety barrier, and notably bolts, has shown that it has an effect on their behaviour. Such effects are not accounted for in the laboratory tests in this thesis or in the finite element models produced. This limits the ability to extrapolate accurate information from the results of this thesis to the real behaviour of the road safety barrier.

10 Conclusion

Laboratory tests on the road safety barrier with the bolted connection have all consistently experience stripping of the bolt threads as the failure mode. Stripping of the threads has a demonstrably lower capacity than conventional failure of the bolt material, and should be accounted for in designs with threaded bolts. The deformation of the road safety barrier prior to failure occurs in the vicinity of the bolted connection; mainly in the W-beam, Σ -post and washers. It is possible to simulate the force-displacement behavior of the laboratory tests, using finite element models, to an acceptable degree. Although the general behaviour can be recreated, individual behavior of each test, such as the number of threads stripped prior reaching ultimate capacity, is not accounted for in the finite element models. Based on these observations, some concluding remarks can be made.

10.1 Concluding remarks

The laboratory tests on the road safety barrier with the bolted connection have consistently shown that the threaded bolt is the critical component in the connection. The failure mode observed during testing was in all tests stripping of the bolt threads. The bolt experiences different degrees of thread stripping prior to failure, and subsequent local force peaks were observed as the remaining threads on the bolt were engaged and stripped. This failure mode is also found in related literature on the behaviour of threaded bolts subjected to loading in tension, and combinations of tension and shear.

Stripping of the threads is dependent on the threaded engagement between the bolt and nut. Studies by Bakken-Berg and Iversen[9] and the laboratory tests performed in this thesis show that the combination of bolt and nut specified by the Norwegian Public Roads Administration for the N2 steel road safety barrier will experience thread stripping when dominantly loaded in tension.

The initial finite element model is able to describe the elastic, and initial plastic, behaviour of the road safety barrier section with an acceptable degree of accuracy. It is concluded, based on the results of the initial model, that the behaviour of the road safety barrier section prior to failure is primarily controlled by the elastic and plastic deformations in the W-beam, Σ -post and washers. This again indicates that the behaviour at the onset of, and after, failure is determined by the bolt and nut.

A realistic finite element model of the bolt with threads is required in order to properly model the failure mode of thread stripping, and consequently the failure of the full-scale road safety barrier. This requires accurate knowledge of the geometry of the bolt and nut, as well as a material model capable of reproducing the proper material behaviour.

The finite element model of the threaded bolt and nut established in this thesis has shown that the material model of the bolt has a significant impact on the resulting capacity. Material parameters of the bolt from the theses of Bakken-Berg and Iversen, and D'Angelo, vary by up to 220 MPa. The road safety barrier is designed to have an upper and lower capacity in the bolted connection, and the large variation in bolt material properties may result in dangerous errors in the design. It is important to have an accurate knowledge of the material properties of the bolt used in the road safety barrier.

The full finite element model experienced excessively distorted elements during analyses, which caused it to terminate prematurely. However, the full finite element model is able to model the road safety barrier section in all load configurations except 15°, to an acceptable degree of accuracy. The close results in the initial model are retained in the 0° and 30° configuration in the full model. The inclusion of the threaded bolt and nut with a failure criteria provides a similar failure load and displacement as seen in the laboratory tests. In the 0° configuration the obtained load capacity deviates from the laboratory tests by only 1.1 to 2.7 percent.

All finite element models which included the threaded bolt and nut were able to simulate the correct failure mode of thread stripping.

10.2 Suggestions for further work

1. The quasi-static load configurations applied to the road safety barrier section during the laboratory tests are highly idealized. The load experienced by a road safety barrier during vehicular impact is dynamic, and applied at a much higher loading rate. The literature study conducted in this thesis show that the behaviour

of the components in the road safety barrier is susceptible to strain rates. The strain rates that will occur in a vehicular impact will be highly different from the strain rates tested in the laboratory tests on the road safety barrier section. Further tests should be performed on the road safety barrier section where the effects of higher strain rates are investigated.

2. The finite element models established in this thesis are able to simulate the behaviour of the bolted connection in a road safety barrier, subjected to loading conditions in combinations of tension and shear, to a reasonable degree of accuracy. However, further investigations should be made into the instability experienced in the full finite element model. Self-contact in the deformed threads of the bolt might be a possible source of the premature termination experienced in the analyses, and should be investigated. In general, more robust finite element models of the road safety barrier, and the bolted connection, need to be established.
3. Stripping of the bolt threads is the critical failure mode for the road safety barrier with the bolted connection. Efforts should be made to improve the finite element models of the bolt and nut in simulating thread stripping. The effect of modelling the bolt and nut using exact geometry, such as helical threads, should be investigated. The presence of the W-beam, Σ -post and washers in the connection should also be included in the model. In addition, a full parameter study on the bolt thread stripping model should be conducted.
4. The finite element models simulating thread stripping in the bolted connection are very computationally expensive. The analysis time reached more than 24 hours for some configurations of the models. Further work should be done on improving the efficiency of the model, and investigations made into introducing cheaper alternatives for modelling the bolted connection.

Bibliography

- [1] World Health Organization et al. *WHO global status report on road safety 2013: supporting a decade of action*. World Health Organization, 2013. Accessed: 25 May, 2014.
- [2] Statistics Norway. Road traffic accidents involving personal injury in 2012, May 2013. website:<http://ssb.no/en/transport-og-reiseliv/statistikker/vtu/aar>. Accessed: May 2014.
- [3] Trond Åge Langeland. *Language and Change: An Inter-Organisational Study of the Zero Vision in the Road Safety Campaign*. PhD thesis, University of Stavanger, 2009.
- [4] Alena Høye. Trafikksikkerhetshåndboken. Website:<http://tsh.toi.no/doc631.htm>, Accessed: May 2014, 2012.
- [5] Statens Vegvesen. *Manual 231 E: Vehicle Restraint Systems and Roadside Areas*. Statens Vegvesen, December 2001.
- [6] Statens Vegvesen. *Håndbok 267 Standard Vegrekkverk*. Statens Vegvesen, 2006.
- [7] H Shakir-Khalil and CM Ho. Black bolts under combined tension and shear. *STRUCTURAL ENGINEER-PART B*, 57(4):69–76, 1979.
- [8] A.P Mouritz. Failure mechanisms of mild steel bolts under different tensile loading rates. *International journal of impact engineering*, 15(3):311–324, 1994.
- [9] Hans Olav Bakken-Berg and Håkon Iversen. Computational analysis of a deformable safety barrier. Master's thesis, Norwegian University of Science and Technology, 2007.

- [10] H Fransplass, M Langseth, and OS Hopperstad. Tensile behaviour of threaded steel fasteners at elevated rates of strain. *International Journal of Mechanical Sciences*, 53(11):946–957, 2011.
- [11] EM Alexander. Analysis and design of threaded assemblies. *Detroit: SAE, Paper*, 770420:4–28, 1977.
- [12] Luca D’Angelo. Development of an arcan test setup for characterization of road restraint system. Master’s thesis, Norwegian University of Science and Technology, 2012.
- [13] NS-EN 10025-2: Hot rolled products of structural steels - part 2: Technical delivery conditions for non-alloy structural steels, May 2005.
- [14] Eurocode 3: Design of steel structures - part 1-8: Design of joints, May 2005.
- [15] E Fagerholt. *Field Measurements in Mechanical Testing Using Close-Range Photogrammetry and Digital Image Analysis*. PhD thesis, Norwegian University of Science and Technology, 2011.
- [16] Aase Reyes. *Oblique loading of aluminum crash components*. PhD thesis, Norwegian University of Science and Technology, 2002.
- [17] Eurocode 3: Design of steel structures - part 1-1: General rules and rules for buildings, May 2005.
- [18] Hagbart S Alsos, Jørgen Amdahl, and Odd S Hopperstad. On the resistance to penetration of stiffened plates, part ii: Numerical analysis. *International Journal of Impact Engineering*, 36(7):875–887, 2009.
- [19] SIMLab. *Theory Manual: SIMLab Metal Model*, May 2014.
- [20] Unknown. Engineer’s handbook. Website: <http://www.engineershandbook.com/Tables/frictioncoefficients.htm>, Accessed: April 2014, April 2014.
- [21] K.M Mathisen. Tkt4197 nonlinear finite element analysis, lecture 11: Solution methods for contact problems, 2013. Norwegian University of Science and Technology, Institute of Structural Mechanics.
- [22] Simulia Dassault Systems. Abaqus theory manual: 6.12 getting started with abaqus. <http://ivt-abaqusdoc.ivt.ntnu.no:2080/v6.12/books/gsk/default.htm>.

A Geometry

A.1 Geometry of the W-beam

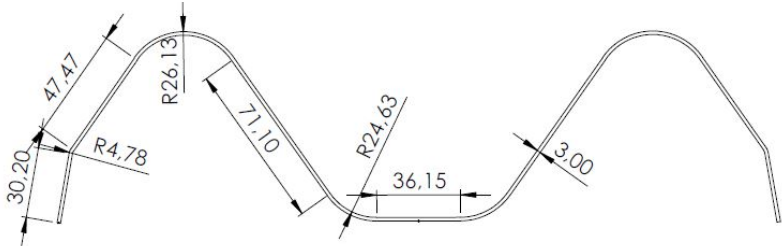


Figure A.1: Cross-section view of the W-beam with dimensions

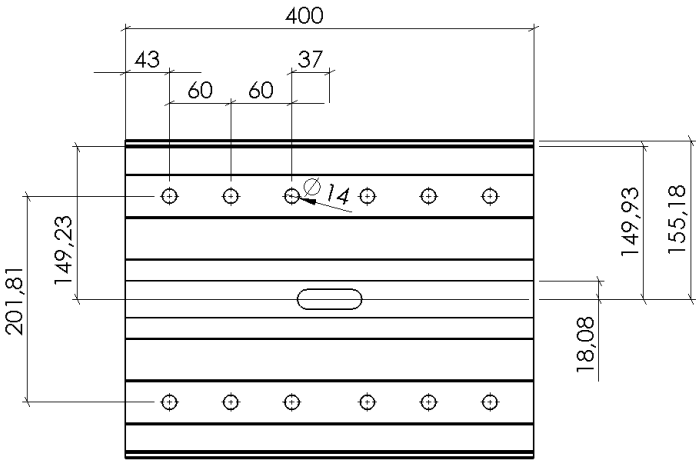


Figure A.2: Top view of the W-beam with dimensions

A.2 Geometry of the Σ -post

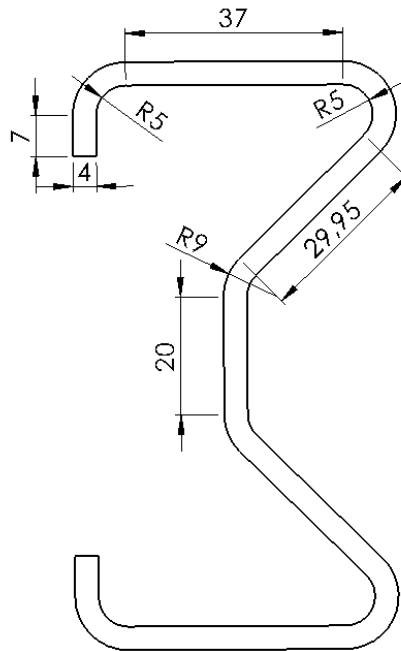


Figure A.3: Cross-section view of the Σ -post with dimension

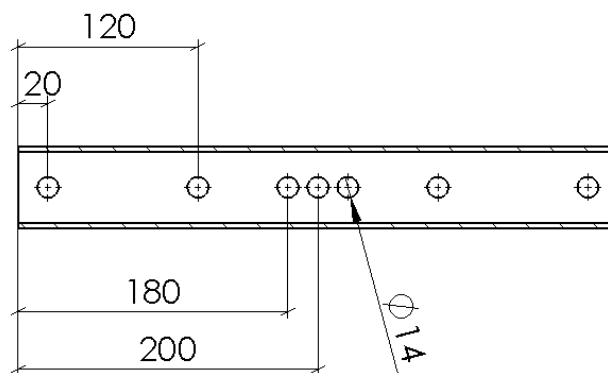


Figure A.4: Underside view of the Σ -post with dimension

A.3 Geometry of the washers

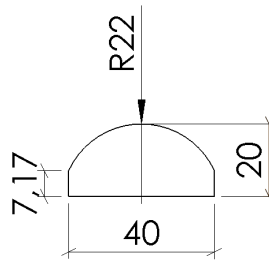


Figure A.5: Cross-section view of the longitudinal washers of the W-beam with dimensions

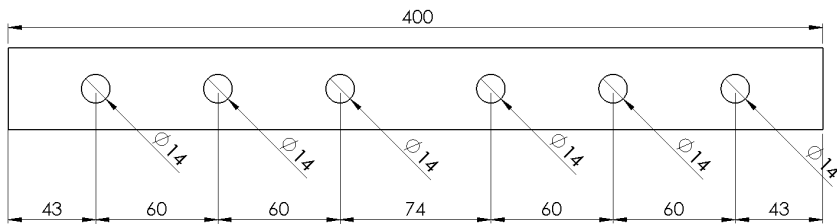


Figure A.6: Top view of the the longitudinal washer of the W-beam with dimensions

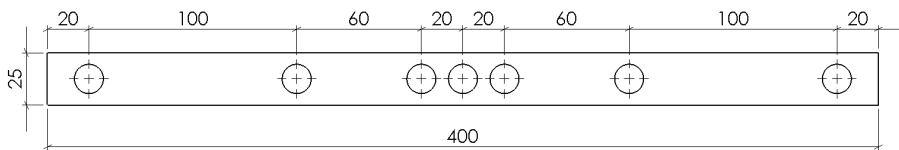


Figure A.7: Top view of the longitudinal washer of the Σ -post with dimensions

The thickness of the Σ -post washer is $t = 10$ mm.

A.4 Geometry of the loading clamp

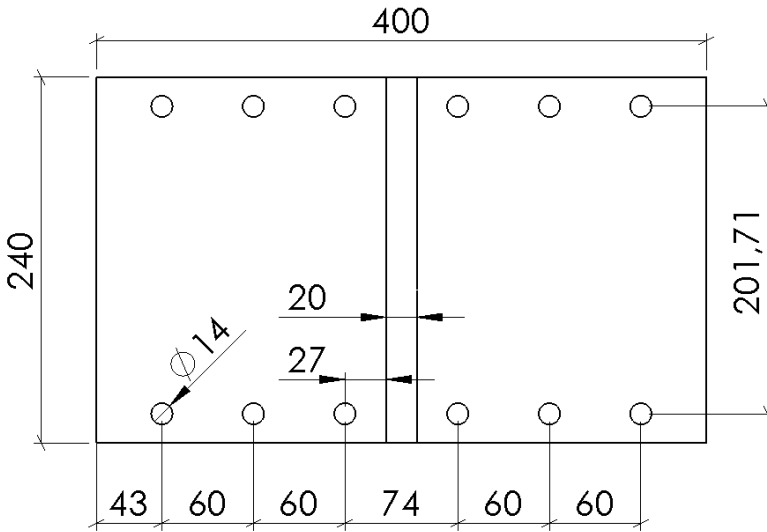


Figure A.8: Top view of the loading clamp with dimensions

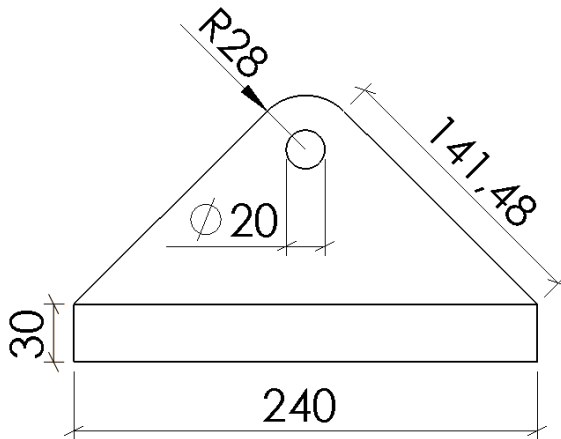


Figure A.9: Side view of the loading clamp with dimensions

A.5 Geometry of the cradle

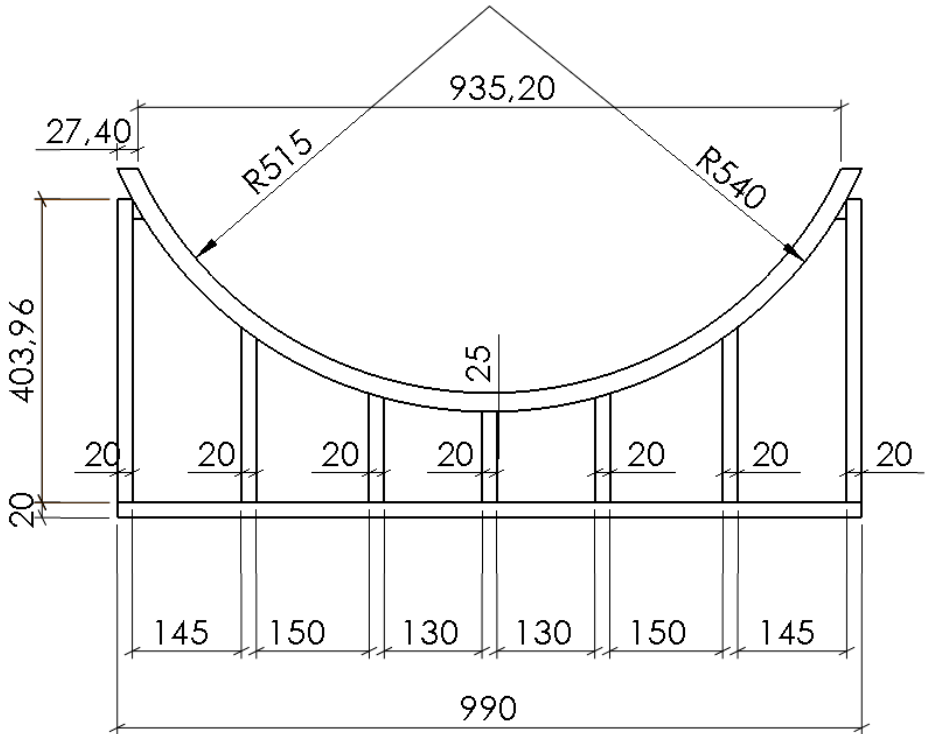


Figure A.10: Front view of the cradle with dimensions

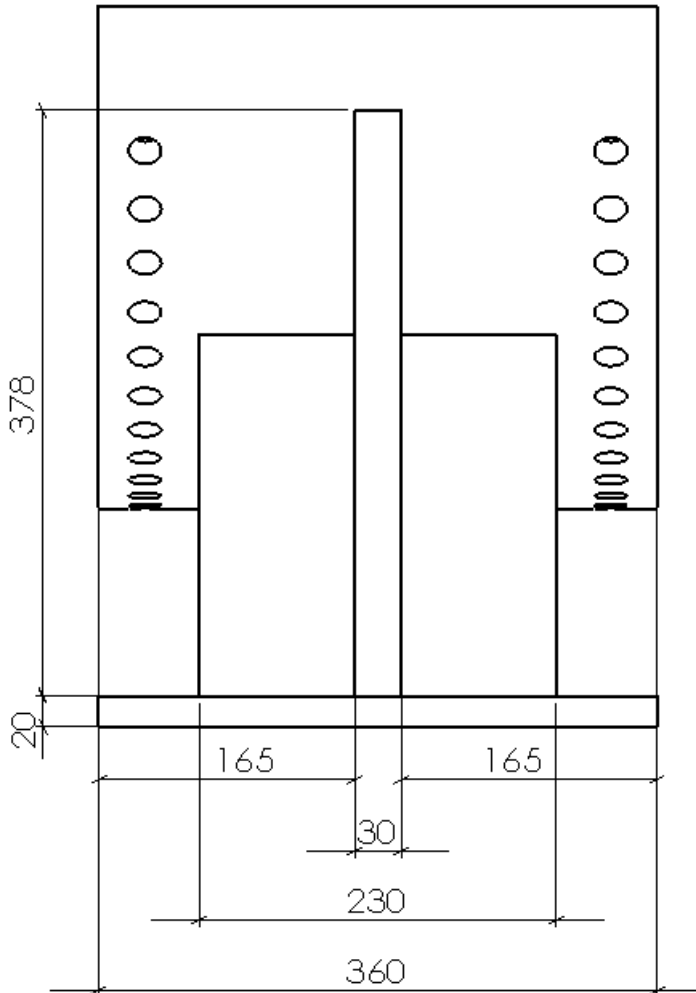


Figure A.11: Side view of the cradle with dimension

A.6 Geometry of the M10 bolt and nut

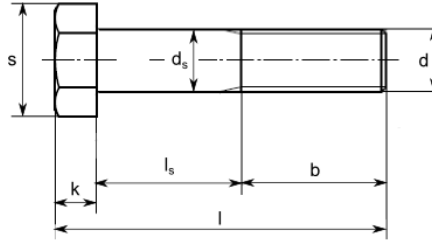


Figure A.12: Nominal Geometry of the DIN 601 M10 bolt

Table A.1: Bolt geometric parameters

s	= 17 mm,	Width across flats
k	= 6.4 mm,	Height of the bolt head
l	= 45 mm,	Bolt length
l_s	= 12.6 mm,	Shank section length
b	= 26 mm,	Thread section length
d_s	= 9,9 mm,	Shank diameter
d	= 9.9 mm,	Thread major diameter

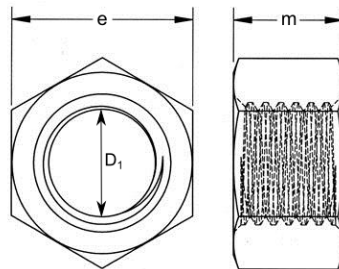


Figure A.13: Geometry of the M10 nut

Table A.2: Nut geometric parameters

e	= 17mm,	Width across flats
m	= 7.8 mm,	Height of the nut
D_1	= 9.15 mm,	Threads minor diameter

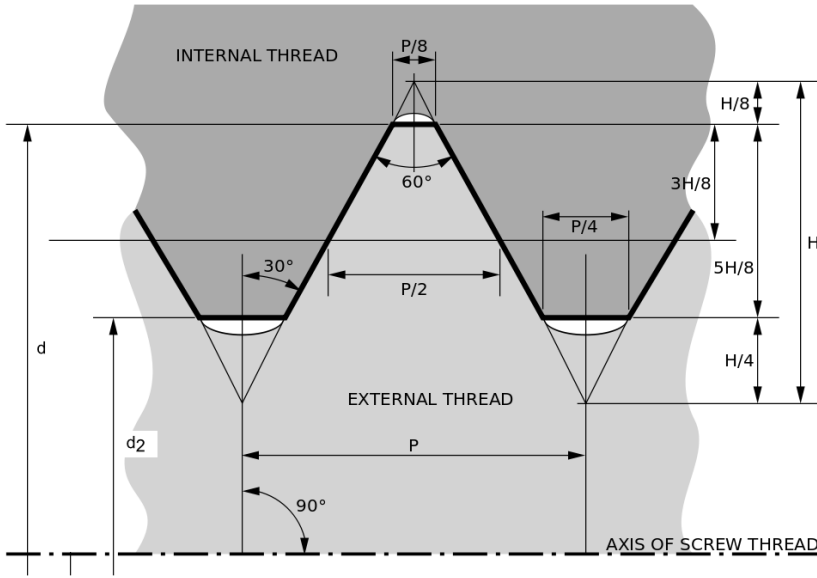


Figure A.14: Geometry of the threads

Table A.3: Thread geometric parameters

P	=	1.5mm,	Thread pitch
d	=	9.9 mm,	Thread major diameter
H	=	$\cos(30^\circ) \times P,$	Thread height
d ₂	=	$d - \frac{5H}{8},$	Thread minor diameter

B Laboratory Tests Assembly

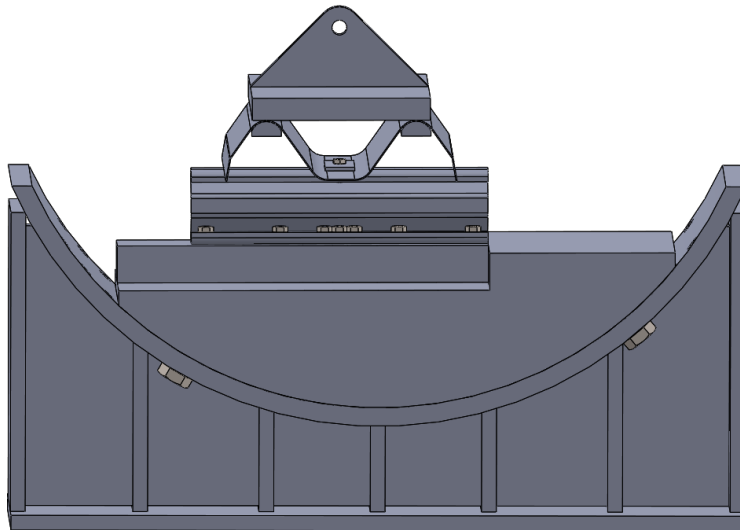


Figure B.1: Model of the test assembly

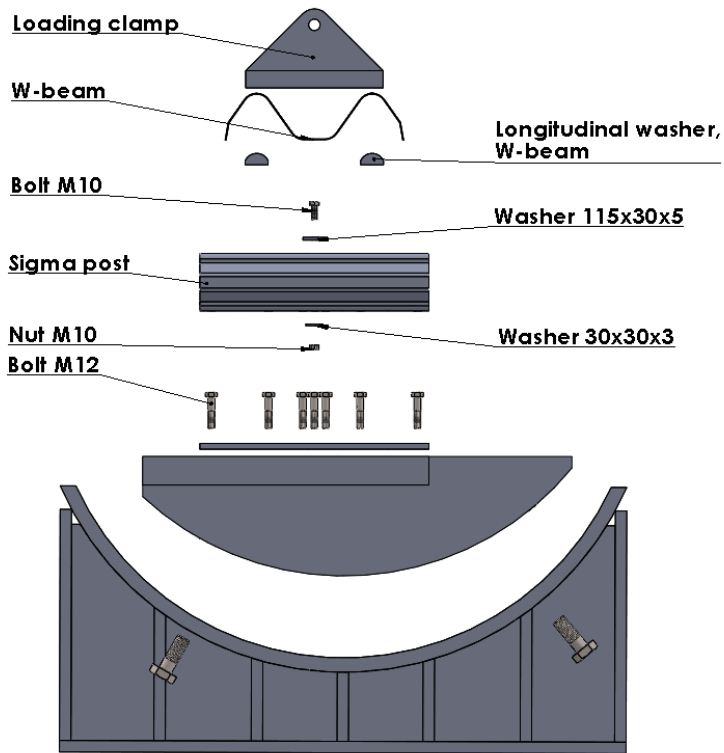


Figure B.2: Exploded model of the test assembly

C Geometrical Measurements

In this Appendix the cross-section thickness measurements of the W-beam, Σ -posts, washers and bolts used in the laboratory tests are listed. All measurements were made using a micrometer and are reported in mm. Measurements were made at specific positions in the cross-section at each end of the W-beam and Σ -posts, while for the washers and the bolts the average thickness and diameter are reported. Figure C.1 explains the points of measurements of the W-beam, while figure C.2 explains the Σ -post.

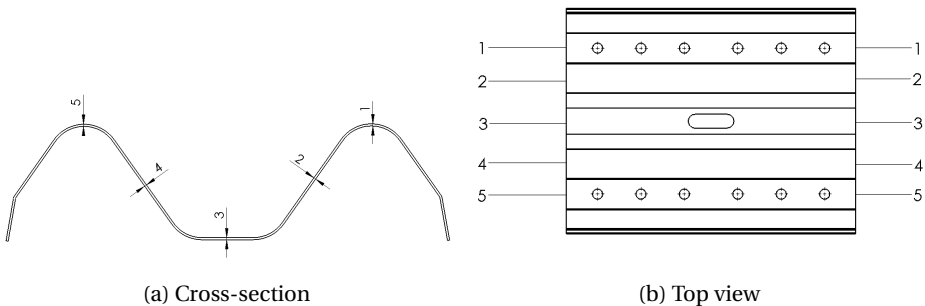


Figure C.1: Thickness measurement points of the W-beam

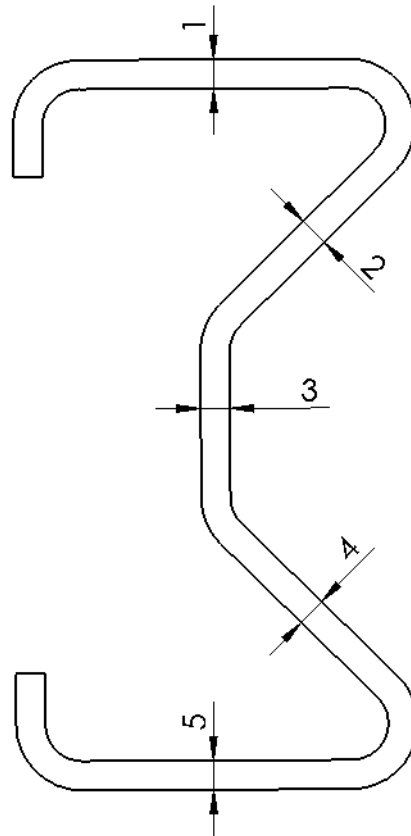


Figure C.2: Thickness measurement points of the Σ -post

The Σ -post has an open and a closed side. The end to the left of the open side is referred to as *end 1*, while the end to the right is referred to as *end 2*.

Table C.1: Geometric data of the W-beam

Test	End	W-beam			
		Average ¹	Diff-norm ²	Int-diff ³	Ext-diff ⁴
Test 1-0°	End 1	3.05	0.09	0.06	0.11
	End 2	3.08	0.15	0.14	
Test 2-0°	End 1	3.19	0.39	0.32	0.17
	End 2	3.19	0.40	0.36	
Test 3-0°	End 1	3.09	0.22	0.27	0.16
	End 2	3.02	0.10	0.14	
Test 5-0°	End 1	3.08	0.23	0.25	0.20
	End 2	3.02	0.10	0.14	
Test 1-15°	End 1	3.19	0.35	0.29	0.20
	End 2	3.14	0.23	0.13	
Test 2-15°	End 1	3.09	0.19	0.16	0.05
	End 2	3.10	0.18	0.11	
Test 3-15°	End 1	3.06	0.26	0.33	0.16
	End 2	3.04	0.30	0.39	
Test 4-15°	End 1	2.96	0.09	0.12	0.03
	End 2	2.97	0.09	0.12	
Test 1-30°	End 1	2.96	0.11	0.20	0.16
	End 2	2.96	0.06	0.06	
Test 2-30°	End 1	3.30	0.98	1.02	1.01
	End 2	3.01	0.11	0.16	
Test 3-30°	End 1	2.95	0.08	0.10	0.12
	End 2	3.01	0.07	0.12	
Test 4-30°	End 1	3.09	0.23	0.24	0.13
	End 2	3.04	0.10	0.12	

1) Average thickness of the cross-section

2) Largest difference from the nominal thickness 3 mm

3) Largest internal difference

4) Largest thickness difference between the two ends

Table C.2: Geometric data of the Σ -post

Test	End	Σ -post			
		Average ¹	Diff-norm ²	Int-diff ³	Ext-diff ⁴
Test 1-0°	End 1	4.23	0.32	0.16	0.20
	End 2	4.16	0.20	0.08	
Test 2-0°	End 1	4.35	0.48	0.20	0.26
	End 2	4.27	0.42	0.24	
Test 3-0°	End 1	4.24	0.34	0.20	0.10
	End 2	4.27	0.32	0.08	
Test 5-0°	End 1	4.22	0.33	0.17	0.02
	End 2	4.21	0.30	0.13	
Test 1-15°	End 1	4.23	0.29	0.12	0.01
	End 2	4.22	0.28	0.10	
Test 2-15°	End 1	4.16	0.23	0.09	0.01
	End 2	4.17	0.22	0.09	
Test 3-15°	End 1	4.21	0.26	0.09	0.10
	End 2	4.27	0.37	0.19	
Test 4-15°	End 1	4.18	0.22	0.08	0.02
	End 2	4.18	0.22	0.07	
Test 1-30°	End 1	4.22	0.26	0.08	0.12
	End 2	4.24	0.38	0.23	
Test 2-30°	End 1	4.18	0.23	0.08	0.03
	End 2	4.17	0.22	0.09	
Test 3-30°	End 1	4.22	0.29	0.13	0.02
	End 2	4.20	0.29	0.14	
Test 4-30°	End 1	4.24	0.44	0.28	0.05
	End 2	4.24	0.33	0.13	

1) Average thickness of the cross-section

2) Largest difference from the nominal thickness 4 mm

3) Largest internal difference

4) Largest thickness difference between the two ends

Table C.3: Thickness of the washers

	30×30×3 mm washer	115×40×5 mm washer
Test 2-0°	4.75	2.60
Test 3-0°	4.40	2.37
Test 4-0°	4.70	2.85
Test 5-0°	4.15	2.60
Test 6-0°	4.45	2.35
Test 1-15°	4.40	2.85
Test 2-15°	4.50	2.40
Test 3-15°	4.10	2.60
Test 4-15°	4.60	2.35
Test 1-30°	4.65	2.40
Test 2-30°	4.50	2.80
Test 3-30°	4.25	2.75
Test 4-30°	4.30	2.40
Average	4.44	2.56
Minimum	4.10	2.35
Maximum	4.75	2.85

Table C.4: Diameter of the bolts

	Diameter, undeformed	Diameter, stripped
Ref 1	10.08	-
Ref 2	10.06	-
Ref 3	9.84	-
Ref 4	9.85	-
Ref 5	9.86	-
Average	9.90	-
Test 2-0°	9.81	9.18
Test 3-0°	9.83	9.13
Test 4-0°	9.85	9.24
Test 5-0°	9.76	9.05
Test 6-0°	9.80	9.15
Average	9.81	9.15
Test 1-15°	9.71	9.24
Test 2-15°	9.76	9.10
Test 3-15°	9.76	9.20
Test 4-15°	9.78	9.15
Average	9.75	9.17
Test 1-30°	9.68	9.20
Test 2-30°	9.84	9.00
Test 3-30°	9.64	9.06
Test 4-30°	9.82	8.96
Average	9.75	9.06

D Calculations of the Bolt Stripping Load

In this Appendix the calculations of the bolt stripping loads are presented. All formulas used along with the measured dimensions are presented. The basis for this calculation is presented in the work of Alexander[11].

$$F_{bb} = \sigma_s \cdot A_{si} \quad (\text{D.1a})$$

$$F_{bs} = \sigma_s \cdot A_{si} \cdot C_1 \cdot C_2 \cdot 0.6 \quad (\text{D.1b})$$

$$C_1 = \left(-\left(\frac{s}{D}\right)^2 + 3.8\left(\frac{s}{D}\right) - 2.61 \right) \quad (\text{D.1c})$$

$$C_2 = \begin{cases} 5.594 - 13.682R_s + 14.107R_s^2 - 6.057R_s^3 + 0.9353R_s^4, & 1 < R_s < 2.2 \\ 0.897, & R_s \leq 1 \end{cases} \quad (\text{D.1d})$$

$$LE = m - (D_c - D_1 - T_{D1}) \cdot 0.6 \quad (\text{D.1e})$$

$$AS_s = \frac{LE}{P} \cdot \pi \cdot D_1 \left(\frac{P}{2} + (d_2 - D_1) \cdot \frac{1}{\sqrt{3}} \right) \quad (\text{D.1f})$$

$$H = \frac{\sqrt{3}}{2} \cdot P \quad (\text{D.1g})$$

$$D = D_1 + 2 \cdot \frac{5}{8} \cdot H \quad (\text{D.1h})$$

$$d_2 = d - 2 \cdot \frac{3}{8} \cdot H \quad (\text{D.1i})$$

The parameters in table D.2 were measured from the bolt and nut respectively. The basic major diameter, D , of the nut was assumed to be equivalent to the mean diameter

Table D.1: Symbols

P	=	Pitch
m	=	Nut height
H	=	Thread height
LE	=	Length of thread engagement
AS_s	=	Shear area of external threads
D	=	Basic major diameter, internal
D_1	=	Basic minor diameter, internal
d	=	Basic major diameter, external
d_2	=	Basic pitch diameter, external
D_c	=	Design countersink diameter
T_{D1}	=	Tolerance for basic minor diameter, internal
s	=	Width across flats
σ_s	=	Ultimate tensile strength of bolt material
C_1	=	Nut dilation factor
C_2	=	Strength reduction factor, external threads

Table D.2: Parameters used for calculating bolt stripping load

d	=	9.9 mm	D	=	9.15 mm
P	=	1.5 mm	s	=	17 mm
m	=	7.8 mm	R_S	=	2.2
T_{D1}	=	0.475 mm	σ_s	=	400 MPa
D_c	=	11.3 mm			

of the stripped part of the bolt. Both s and P was taken as the design parameters of the bolt. T_{D1} was taken from ISO-965-1 assuming the nut was in tolerance grade 8.

E Design Calculations on the Loading Clamp According to EC3

Shear capacity of the bolt, EC3-1-8, Table 3.10

Assuming the capacity of the bolt to be equal to 50 kN the necessary cross-section area of the bolt is calculated.

$$F_{v,Rd} = \frac{0.6 A_s f_{up}}{\gamma_{M0}} \geq F_{v,Ed} \quad (E.1)$$
$$A_s \geq \frac{1.25 \times 50 \times 10^3 N}{0.6 \times 400 MPa} = 260.4 mm^2$$

This area is then used to calculate the necessary diameter of the bolt.

$$A_s = \frac{\pi D^2}{4}$$
$$D = \sqrt{\frac{4}{\pi} A} \quad (E.2)$$
$$D = \sqrt{\frac{4}{\pi} \times 260.4 mm^2}$$
$$= 18.2 mm \approx 20 mm$$

Moment capacity of the bolt, EC3-1-8, Table 3.10

The moment capacity of the bolt is given as

$$M_{Rd} = \frac{1.5 W_{el} f_{yp}}{\gamma_{M0}} \geq M_{Ed} \quad (\text{E.3})$$

$$M_{Rd} = \frac{1.5 \times 1570.8 \text{ mm}^3 \times 240 \text{ MPa}}{1.05} = 0.539 \text{ kNm}$$

where

$$W_{el} = \frac{1}{16} \pi D^3 \quad (\text{E.4})$$

$$W_{el} = \frac{1}{16} \times \pi \times (10 \text{ mm})^3 = 1570.8 \text{ mm}^3$$

The active moment of the loading force of 50 kN is calculated as

$$M_{Ed} = \frac{F_{Ed}}{8} (b + 4c + 2a)$$

$$M_{Ed} = \frac{50 \times 10^3 \text{ N}}{8} (10 \text{ mm} + 4 \times 1 \text{ mm} + 2 \times 8 \text{ mm}) \quad (\text{E.5})$$

$$= 0.188 \text{ kNm}$$

Noting that $M_{Rd} \geq M_{Ed}$, the moment capacity of the bolt should be sufficient.

Shear and moment interaction capacity of the bolt, EC3-1-8, Table 3.10

Interaction capacity of the bolt is given as

$$\left(\frac{M_{Ed}}{M_{Rd}} \right)^2 + \left(\frac{F_{v,Ed}}{F_{v,Rd}} \right)^2 \leq 1 \quad (\text{E.6})$$

$$\left(\frac{0.188 \text{ kNm}}{0.359 \text{ kNm}} \right)^2 + \left(\frac{50 \text{ kN}}{60.32 \text{ kN}} \right)^2 = 0.96 \leq 1$$

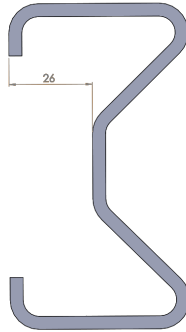


Figure E.1: Eccentricity

where

$$F_{v,Rd} = \frac{0.6 A_s f_{up}}{\gamma_{M2}} \quad (E.7)$$

$$F_{v,Rd} = \frac{0.6 \times \pi \times (20 \text{ mm})^2 \times 400 \text{ MPa}}{1.25 \times 4} = 60.32 \text{ kN}$$

Moment capacity of the vertical plate

The loading clamp is at risk for moment about the weak axis of the loading clamp. This is due to the unsymmetrical shape of the sigma post cross-section. This can be seen in figure E.1, where the largest eccentricity is measured to 26 mm.

$$M_{Ed} = 50 \times 1^3 \text{ N} \times 26 \text{ mm} = 1.3 \text{ kNm}$$

$$M_{Rd} = \frac{W_{el} f_y}{\gamma_{M0}} = \frac{14666.7 \text{ mm}^3 \times 240 \text{ MPa}}{1.05} = 3.352 \text{ kNm}$$

$$M_{Ed} \leq M_{Rd}, \text{ the capacity is satisfactory.}$$

Necessary material of the vertical plate, EC3-1-8, Table 3.9

The distance from the pin hole to the end of the vertical plate must be no more than 20 mm for the pin to fit. This affects the necessary thickness of the vertical plate. The Eurocode offers rules for the geometry of the pin connection which determines the thickness of the vertical plate, see figure E.2.

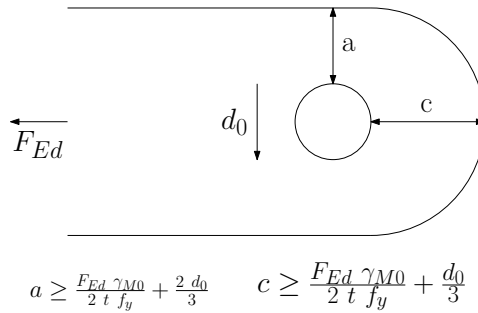


Figure E.2: EC3-1-8, Table 3.9

$$a = \frac{F_{v,Ed} \gamma_{M0}}{2 t f_y} + \frac{2 d_0}{3} \leq 20 \text{ mm}$$

$$t \geq \frac{\left(\frac{F_{v,Ed} \gamma_{M0}}{2} \right)}{20 \text{ mm} - \frac{2 d_0}{3}} \quad (\text{E.8})$$

$$t \geq \frac{\left(\frac{50 \times 10^3 \text{ N}}{2} \frac{1.05}{240 \text{ MPa}} \right)}{20 \text{ mm} - \frac{2 \times 20 \text{ mm}}{3}} = 16.4 \text{ mm}$$

The thickness of the vertical plate is rounded up to 20 mm in a conservative effort.

Capacity of the weld between the vertical and horizontal plate, EC3-1-8, 4.5.3.3

The load from the pin is assumed transferred through the vertical plate in an area of 45°, see figure E.3 . The figure shows the loading clamp from the short end with the effective weld length to transfer the load to the horizontal plate being $2 \times 180 \text{ mm}$.

The shear force the weld needs to transfer is

$$q_w = \frac{50 \text{ kN}}{2 \times 180 \text{ mm}} = 139.9 \frac{\text{N}}{\text{mm}}$$

The shear capacity of the weld is determined as

$$f_{w,d} = \frac{f_u}{\sqrt{3} \beta_w \gamma_{M2}} \times a \quad (\text{E.9})$$

$$f_{w,d} = \frac{240 \text{ MPa}}{\sqrt{3} \times 1.0 \times 1.25} \times 3 \text{ mm} = 332.6 \frac{\text{N}}{\text{mm}}$$

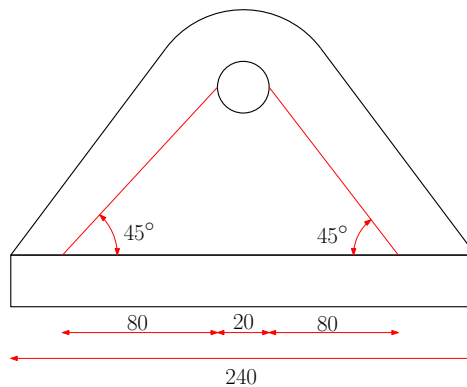


Figure E.3: Estimated effective weld area

The shear capacity f_{wd} exceeds the load q_w and the capacity is adequate.

Capacity of the loading clamp bolts, EC3-1-8, Table 3.4

The loading clamp is connected to the W-beam using M12 bolts and washers. The bolts need to have enough capacity to transfer the 50 kN load. Assuming the forces are distributed 45° through the horizontal plate, the bolts within a distance of 30 mm from the vertical plate must carry the load, see figure A.8. The four bolts closest to the vertical plate are within this threshold. The bolts have to carry the load when in pure tension but also when rotated up to 30°. Calculations for the capacity of the bolts have therefore been made.

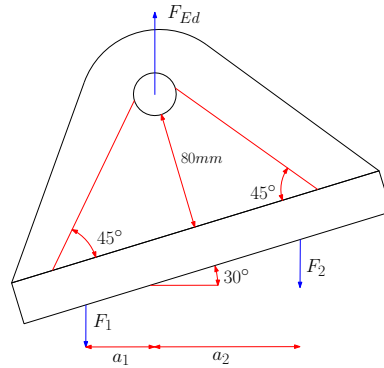


Figure E.4: Bolt forces at 30° rotation

The rotation of the clamp causes an uneven distribution of the load on the bolts, see figure E.4. The bolt forces F_1 and F_2 are calculated.

$$a_1 = \frac{\cos(30) \times 200 \text{ mm}}{2} - \sin(30) \times 80 \text{ mm} = 46.6 \text{ mm}$$

$$a_2 = \frac{\cos(30) \times 200 \text{ mm}}{2} + \sin(30) \times 80 \text{ mm} = 126.6 \text{ mm}$$

$$F_2 = \frac{F_{Ed} a_1}{a_1 + a_2} = \frac{50 \text{ kN} \times 46.6 \text{ mm}}{126.6 \text{ mm} + 46.6 \text{ mm}} = 13.5 \text{ kN}$$

$$F_1 = F_{Ed} - F_2 = 50 \text{ kN} - 13.5 \text{ kN} = 36.5 \text{ kN}$$

The loads F_1 and F_2 are distributed on two bolts on each side of the vertical plate. The load on each bolt consists of a component in tension and one in shear.

$$F_{\parallel} = 0.5 \cos(30) F_1 = 0.5 \times \cos(30) \times 36.5 \text{ kN} = 15.8 \text{ kN}$$

$$f_{\perp} = \sin(30) F_1 = \sin(30) \times 36.5 \text{ kN} = 9.1 \text{ kN}$$

The Eurocode provides rules for calculating the capacity of a bolt in tension and shear:

$$F_{v,Rd} = \frac{\alpha_v f_{ub} A}{\gamma_{M2}} = \frac{0.6 \times 400 \text{ MPa} \times \pi \times (6 \text{ mm})^2}{1.25} = 21.7 \text{ kN}$$

$$F_{t,Rd} = \frac{k_2 f_{ub} A_s}{1.25} = \frac{0.9 \times 400 \text{ MPa} \times 84 \text{ mm}^2}{1.25} = 24.2 \text{ kN}$$

$$\begin{aligned}\frac{F_{v,Ed}}{F_{v,Rd}} + \frac{F_{t,Ed}}{1.4 F_{t,Rd}} &\leq 1.0 \\ \frac{F_{\perp}}{F_{v,Ed}} + \frac{F_{\parallel}}{1.4 F_{t,Rd}} &\leq 1.0 \\ \frac{9.1 \text{ kN}}{21.7 \text{ kN}} + \frac{15.8 \text{ kN}}{1.4 \times 24.2 \text{ kN}} &= 0.89 \leq 1.0\end{aligned}\tag{E.10}$$

The capacity of the bolt is adequate.